

Distribution of shallow-water sediments founded in the records of deep-sea drilling and sea-level rise since the Jurassic period

Masahiro Shiba

Museum of Natural and Environmental History, Shizuoka

shiba@dino.or.jp

Abstract. Hoshino (1991) argued that the sea-level in the Jurassic period was at the present depth of 6,000 m, and that the sea-level rise was caused by the uplift of the sea floor including the volcanic activity of flood basalts as well as the uplift of the crust after the Jurassic period. In order to provide evidence for Hoshino's sea-level rise theory, this paper investigates the sites where shallow-water sediments and volcanic rocks of subaerial eruption were found in the drilling records from DSDP to ODP. As a result, 256 sites were recovered with sediments and rocks indicating such shallow-water or land. Based on their distribution and assuming that they did not subsident we can estimate that the sea-level was about 6,000 m in the Late Jurassic period, 5,200 m in Barremian, 4,100 m at the end of Albian, 3,800 m in Early Eocene, 3,400 m in Late Oligocene, 3,400 m in Middle Miocene, and 3,000 m lower at the end of Miocene, or even lower in respectively. This supports the Hoshino's sea-level rise theory. However, the thickness of the coral reef limestone at each period suggests that the sea-level position at each period was lower than the past sea-level position estimated from the results of deep-sea drilling. Therefore, a sea-level rise curve was created by accumulating the amount of coastal onlap in the Haq's curve and assuming that the sea-level was 3,000 m lower than the present sea-level at the end of Miocene epoch. According to the new sea-level rise curve proposed in this paper, the position of the sea-level at the end of the Jurassic period may have been considerably lower, about 12 km below present sea-level. In other words, the sea-level may have risen by 12 km since the Jurassic period.

Based on the drilling records and the geological structure of each area, the deep-sea floor of the Atlantic and Indian Oceans is thought to have been composed of the Proterozoic and Hercynian basement rocks until the end of the Paleozoic Era, submerged by sea-level rise due to flood basalts since Triassic, and deepened by large-scale sea-level rise since Cretaceous. On the other hand, the base of the deep-sea floor of the Pacific Ocean is likely to be composed of the Archean basements, which were submerged more than 6,000 m by volcanic activity of basaltic lava of the Large Igneous Provinces (LIPs) mainly after the Late Jurassic period.

Keywords: DSDP, ODP, shallow-water limestone, subaerial erupted basalt, Atlantic Ocean, Indian Ocean, Pacific Ocean

Introduction

The Deep-sea Drilling Project (DSDP) began in 1968, followed by the International Ocean Drilling Program (ODP) from 1985 to 2002, the Integrated International Ocean Drilling Program (IODP) from 2003 to 2013 and the International Ocean Discovery Program (IODP) from 2013.

This paper identifies sites in the entire drilling record from DSDP Leg. 1, Site 1 (The SSP, 1969a) to ODP Leg 210, Site 1277 (SSP, 2004a), where shallow-water sediments, volcanic rocks erupted from shallow water or onshore, basement rocks consisting of plutonic and metamorphic rocks and onshore erosional unconformities were found. The evidence of shallow-water indicator that show the location of these past sea-level provides an overview of the geological history of these areas and the changes in sea-level through geological time on a global scale. Based on the results, the post-Jurassic sea-level rise proposed by Hoshino (1962, 1970, 1991) is reviewed and discussed. The term SSP in the references cited is an abbreviation for "Shipboard Scientific Party".

Geological age and depth of the shallow-water indicating rocks

The shallow-water indicating rocks recovered during deep-sea drilling are 108 sites in the Atlantic Ocean (Fig. 1), 62 sites in the Indian Ocean (Fig. 2) and 86 sites in the Pacific Ocean (Fig. 3), for a total of 256 sites. A list of the location (latitude, longitude), bathymetry, depth of excavation, shallow-water indicating rocks and unconformities, depth below sea-level, age and description of each of these sites, in order of site number, is given in the Supplementary table.

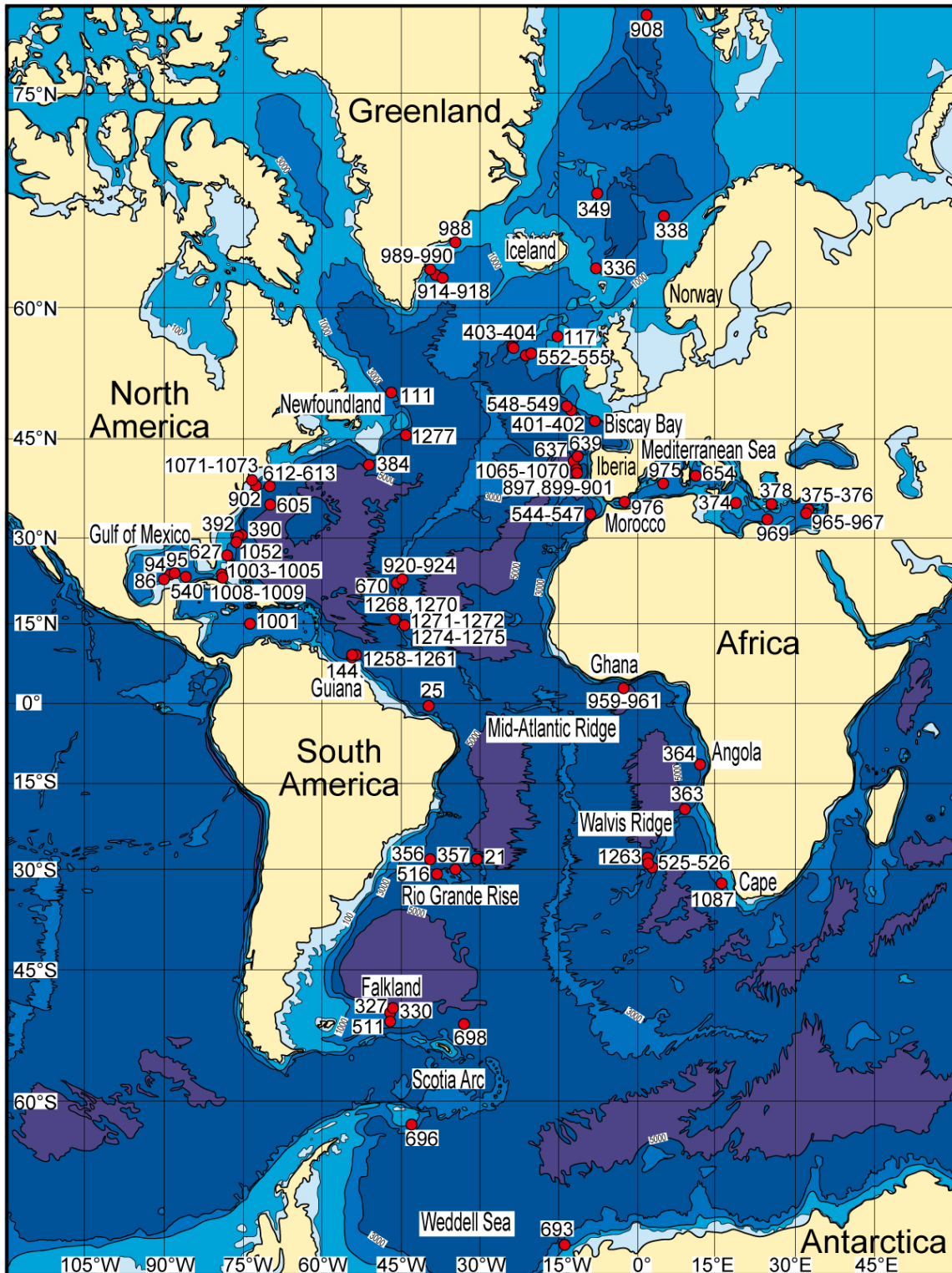


Fig. 1 Sites in the Atlantic Ocean where shallow-water sediments and subaerial erupted lavas have been recovered by DSDP and ODP. The red circle is the site location and the number is the site number. Bathymetric map from Bathymetric Data Viewer of NOAA on <https://www.ncei.noaa.gov/maps/bathymetry/>

In the Atlantic Ocean, the distribution is in 12 regions: the Gulf of Mexico-the Greater Bahamas Reef, the North American Continental Rise-Newfoundland, the southeastern Greenland margin, Iceland-the Norwegian continental margin, the western Iberian margin-the Biscay margin-the Galician Bank, the western Morocco-Ghana-the Angola continental margin, the Walvis

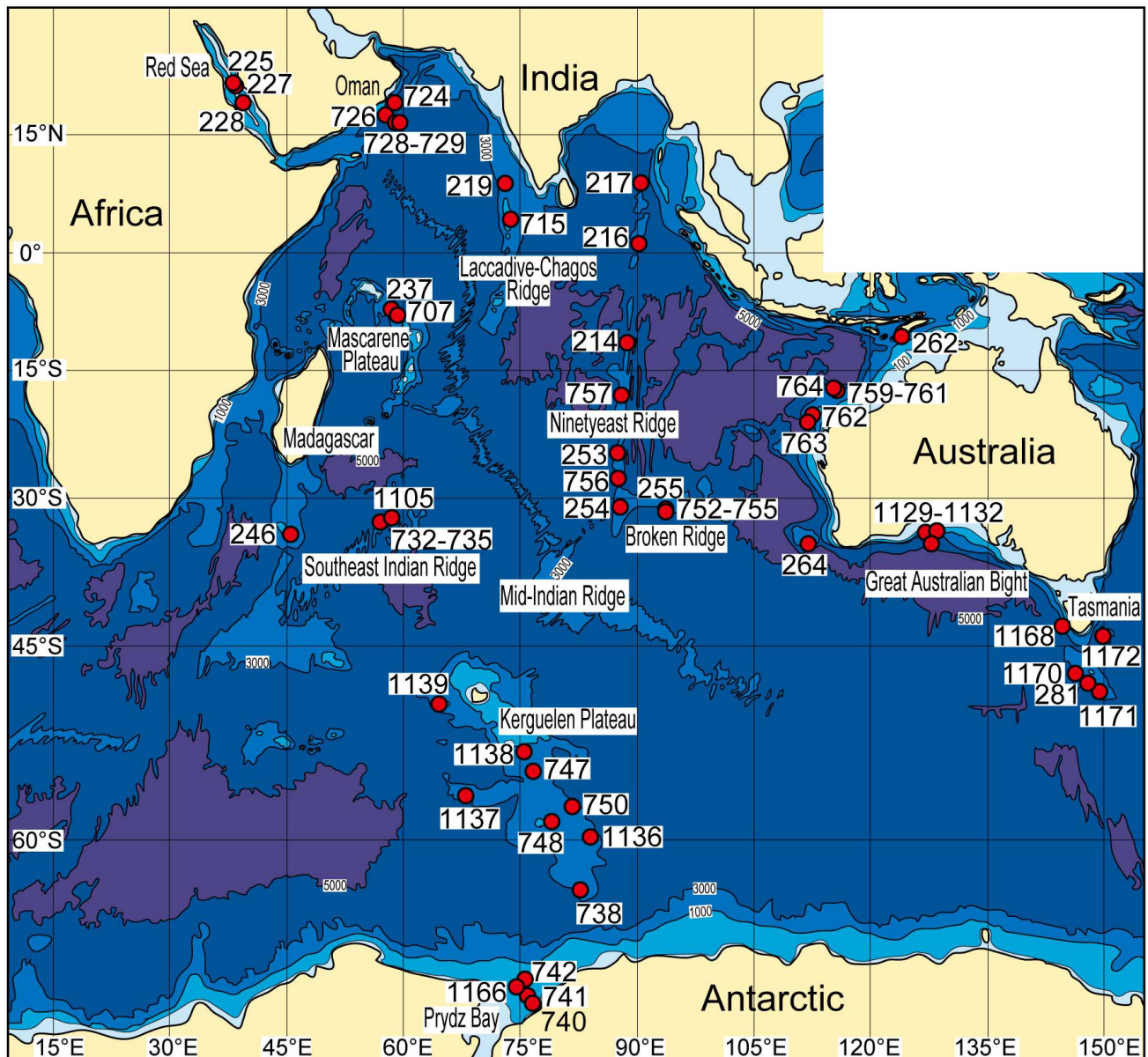


Fig. 2 Sites in the Indian Ocean where shallow-water sediments and subaerial erupted lavas have been recovered by DSDP and ODP. The red circle is the site location and the number is the site number. Bathymetric map from Bathymetric Data Viewer of NOAA on <https://www.ncei.noaa.gov/maps/bathymetry/>

Ridge-the Cape Basin, the Demerara Rise off Guiana, the Brazilian coast-the Rio Grande Rise, the Falklands Rise, the Mid-Atlantic Ridge and the Mediterranean Sea. In the Indian Ocean, it is distributed in 7 regions: the Red Sea, the Ninetyeast Ridge and the Broken Ridge, the Southwest Indian Ridge and the Kerguelen Ridge, the Mascarene Ridge and the Oman continental margin, the western Australian margin, the Great Australian Bight and the Tasmanian Rise, and the Antarctic Ocean. In the Pacific Ocean, they are distributed in 11 regions: guyots on the Mid-Pacific Mountains and the Emperor Seamounts, the Large Ocean Rise, the eastern margin of Australia and the southwest of New Zealand, Papua New Guinea and the Vanuatu Island Arc, the Palau-Kyushu Ridge, the Izu-Ogasawara Trench, the Mariana Ridge, the Japan Trench and the Sea of Japan, the Middle American Trench, and the Peru Trench.

Fig. 4 shows that the geological ages from which the shallow-water indicating rocks were recovered are mostly from Late Jurassic, Early Cretaceous, Eocene, Miocene and Pliocene. The following section will therefore be divided into four sections: the pre-Jurassic and Jurassic periods, the Cretaceous period, the Paleogene period and the Neogene and Quaternary period. In Fig. 5, the depths at which shallow-water indicating rocks were recovered (distance from the present sea-level) tended to become

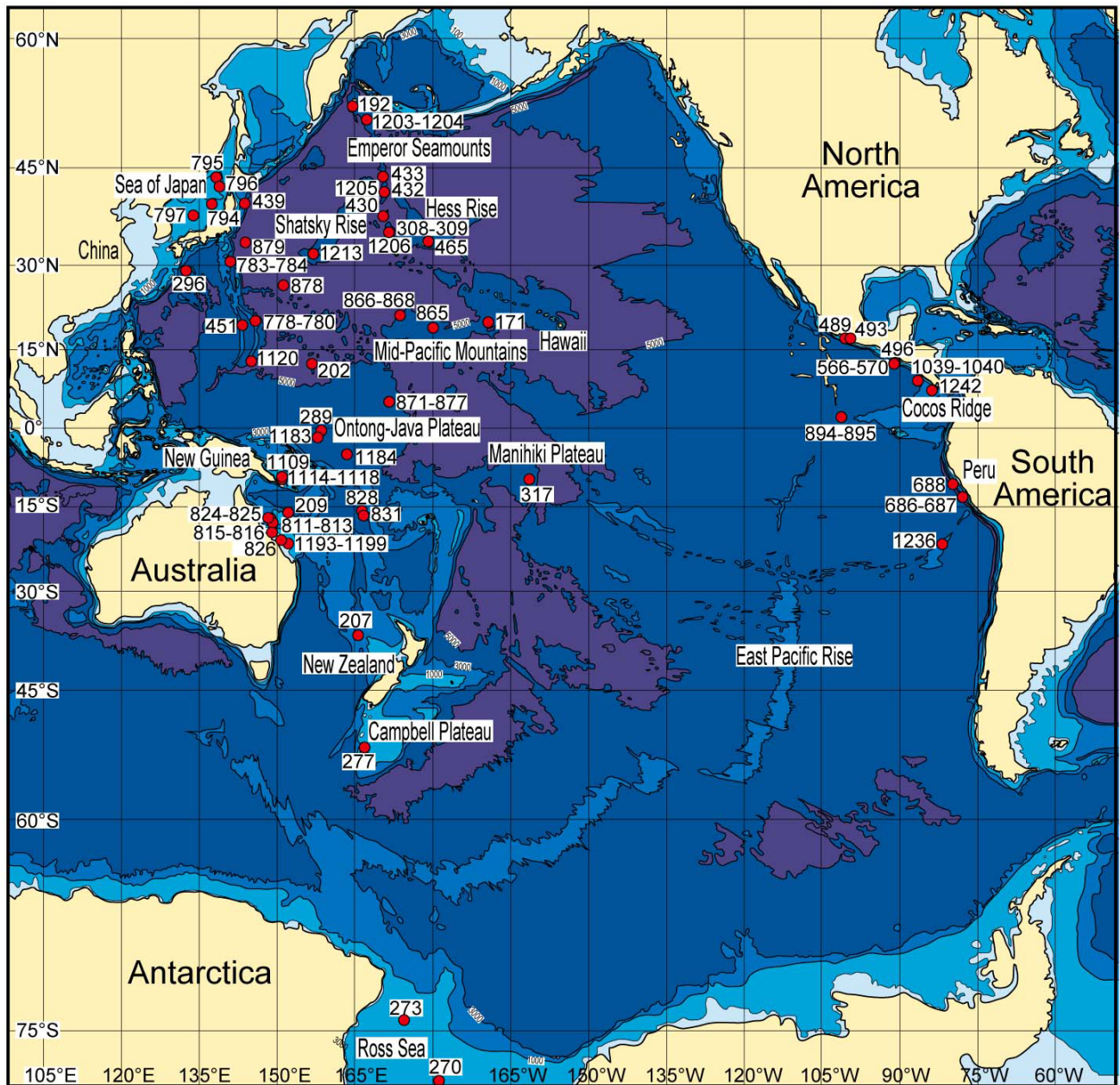


Fig. 3 Sites in the Pacific Ocean where shallow-water sediments and subaerial erupted lavas have been recovered by DSDP and ODP. The red circle is the site location and the number is the site number. Bathymetric map from Bathymetric Data Viewer of NOAA on <https://www.ncei.noaa.gov/maps/bathymetry/>

shallower from the oldest to the present for each period, with a dotted line showing the maximum depths, except for Site 374.

The pre-Jurassic and Jurassic periods

The presence of Jurassic salt domes in the Gulf of Mexico in the Atlantic Ocean as the Jurassic shallow-water indicating rocks, was strongly suggested (The SSP, 1969b). According to Mullins and Lynts (1977), pre-Triassic continental crust underlying the Gulf of Mexico-the Greater Bahamas Reef area formed horsts and grabens in Late Triassic-Early Jurassic and continued to subside after the Jurassic period, continuing this structure. Sheridan et al. (1981) also noted the boundary between Aptian-Albian shallow-water limestones and post-Cenomanian pelagic sediments, and stated that the previously homogeneous large carbonate reef platform (Megabank) was subsided from Late Cretaceous (Fig. 6). Note that Mullins and Lynts (1977) and Sheridan et al. (1981) assumed a basal depth of about 9 km and 12 km, respectively, for the Jurassic evaporite layer.

At the Goban Spur (Site 548: SSP, 1985a; Site 549: SSP, 1985b), west of the Britain, Devonian arkose sandstones comprising

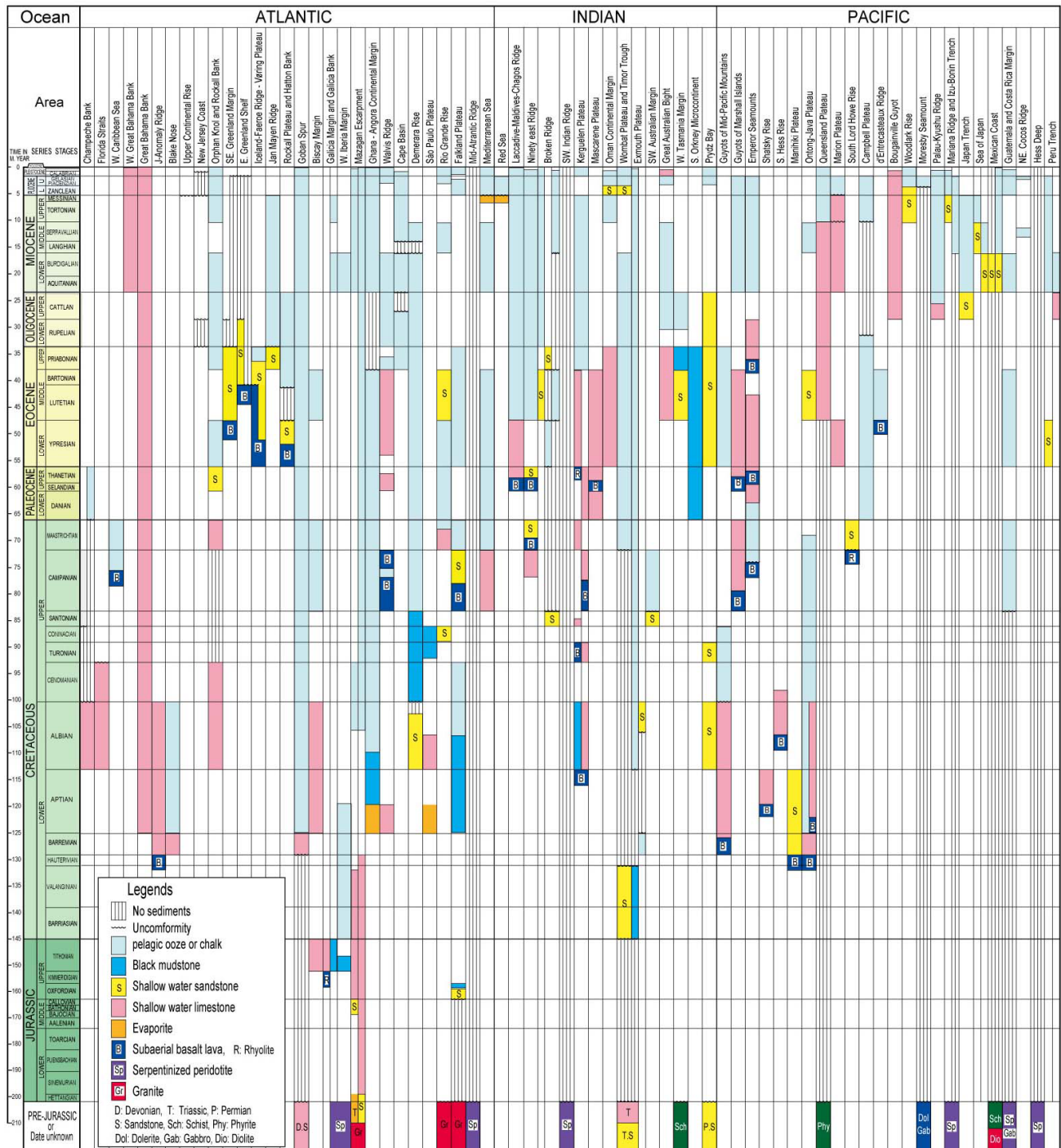


Fig. 4 Lithology and age range of shallow-water sediments and subaerial erupted lavas recovered by deep-sea drilling. The recovered rocks of Shatsky Rise show the results of Site U1349 of the IODP (Sager et al., 2010).

the Hercynian Orogenic (=Variscan Orogenic: Middle Devonian-Carboniferous) belt are present at 1,791.5 m and 3,497.5 m below sea-level (Fig. 7).

In the northern part of the Biscay margin, Jurassic Tithonian biogenic clastic limestones are present at 2,803 m below sea-level (Site 401: The SSP et al., 1979). On the Galician margin, Tithonian shallow-limestone is at 4,949.8 m below sea-level and the basement consists of rhyolitic volcanic rocks or volcanoclastic rocks (Site 639: SSP, 1987a). In the south-western part of the Galicia Bank, conglomerates consisting of claystone and limestone gravels deposited on the inner shelf during Middle to Late Jurassic are present at 5,078.9 m (Site 1065: SSP, 1998a) and 5,942.6 m (Site 1069: SSP, 1998b) below sea-level, while serpentinite or serpentinised plagioclase peridotite at 5,700-6,000 m below sea-level (Site 1068: SSP, 1998c; Site 1070: SSP, 1998d).

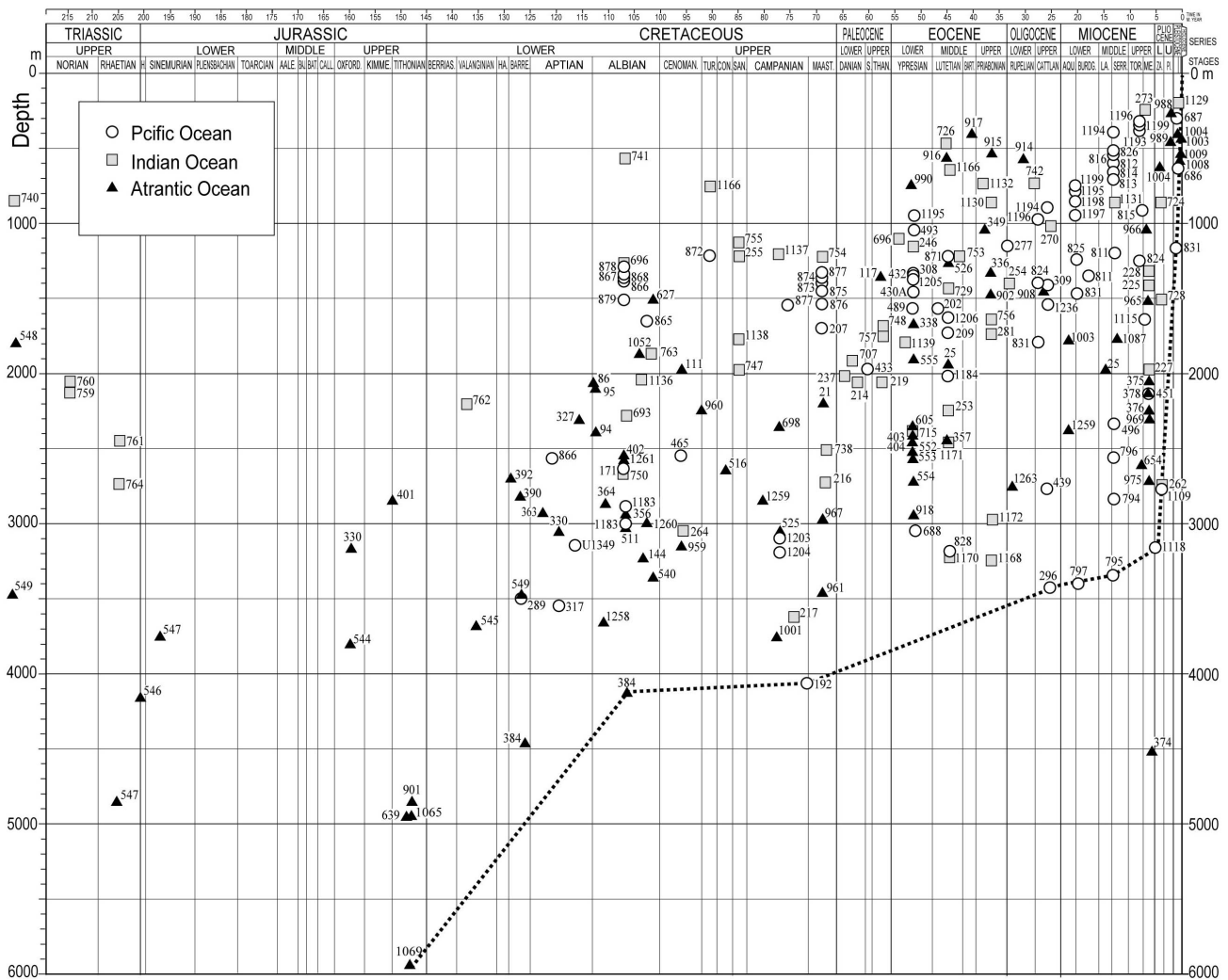


Fig. 5 Age and depth of shallow-water sediments and subaerial erupted lavas recovered by deep-sea drilling Number shows site number. The dotted line is the estimated position of the sea-level for each age from the deepest depth at which the shallow-water indicator rocks were recovered, except for Site 374.

According to Pinheiro et al. (1996), the western Iberian margin is composed of the basement blocks of the Hercynian Orogenic belt, and sedimentary basins developed during the Mesozoic-Cenozoic Era, reflecting the NNW-SSE substructure of the Hercynian basement (Fig. 8). The serpentinite or serpentinised plagioclase peridotite at 5,700-6,000 m below sea-level on the western Iberian margin-the Biscay margin is inferred to belong to the Hercynian Orogenic belt. To the south, in the Mazagan Escarpment (Sites 544-547: SSP, 1984a-1984d) in the western Morocco, Jurassic shallow-limestones are present at 3,700-4,900 m below sea-level, with Triassic-Jurassic alluvial fan deposits, rock salt beds and granite gneiss basement below.

In the Rio Grande Rise in the eastern South America, deep-sea drilling has not revealed any pre-Jurassic rocks, but the submersible ‘Shinkai 6500’ discovered exposed granite (Kitasato, 2014) and Santos et al. (2019) dredged 2207-541 million years old plutonic and metamorphic rocks. This indicates that the

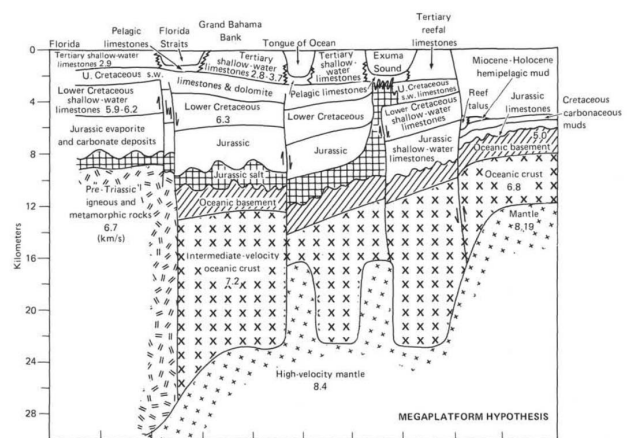


Fig. 6 The origin and evolution of the Bahamas (after Sheridan et al., 1981).

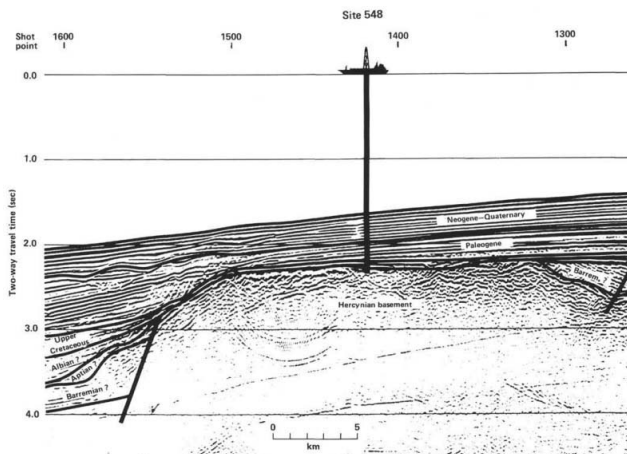


Fig. 7 Segment of multichannel seismic reflection profile OC 202 across Site 548 (after SSP, 1985a).

Proterozoic granites and metamorphic rocks form the basement. On the Falklands Plateau, there is a Proterozoic basement consisting of gneissic pegmatites at about 3,100 m below sea-level at Site 330 (The SSP et al., 1977), with unconformably Oxfordian fluvial deposits immediately above it, and Oxfordian and Aptian sapropelic claystone layers to 3,061 m below sea-level.

In the Indian Ocean, Late Triassic swamp to lagoon-bearing shallow-water coral reef complex is present at 2,054.6-2,748.2 m below sea-level at the south-eastern foot of the Wombat Plateau (Site 760: SSP, 1990a) in the western Australia. In the southern part of the Tasman Rise (Site 281: The SSP and Wilson, 1975) in the southeastern Australia, the basement rocks composed of quartz biotite schist are present at 1,751 m below sea-level, and the southern part of the Tasman Rise is a continental submarine uplift (Ovenshine et al., 1975), which is seen as a southern extension of the Hercynian Orogenic belt in the eastern Australia (Udintsev, 1987). At Site 740 (SSP, 1989a), the Prydz Bay in the eastern Antarctica, fluvial red sandstone formation of possible the Permian period is present at 864.1 m below sea-level.

The oldest pre-Jurassic sediments of definite age are the Devonian arkose sandstone recovered from 1,791.5 m (Site 548: SSP 1985a) and 3,497.5 m (Site 549: SSP, 1985b) below sea-level at the Goban Spur, which constitute the Hercynian Orogenic belt. For the rocks of the Hercynian Orogenic belt, serpentinite and serpentinitised plagioclase peridotite were also recovered from 5,700-6,000 m below sea-level from the western Iberian margin-the Biscay margin (Site 1067: SSP, 1998e; Site 1068: SSP, 1998c; Site 1070: SSP, 1998d), although the age is unknown in pre-Cretaceous.

The deepest Late Jurassic shallow-water deposits are the conglomerate beds consisting of Late Jurassic (Tithonian?) limestone gravels at 5,942.6 m below sea-level in the Galicia Bank (Site 1069: SSP, 1998b). The next deepest is also claystone of Middle to Late Jurassic (Tithonian) deposited at 5,078.9 m below sea-level in the Galicia Bank (Site 1065: SSP, 1998a). Others exist at shallower depths. Assuming that these Late Jurassic shallow-water sediments were not subsided, the Late Jurassic sea-level position would have been about 6,000 m or more below the present sea-level.

The Cretaceous period

Shallow-water Albian reef limestones in the Atlantic Ocean are widely distributed 2,071-2,428 m below sea-level in the Champeche Bank of the Gulf of Mexico (Site 86: The SSP, 1973a; Site 94: The SSP, 1973b; Site 95: The SSP, 1973c). In the

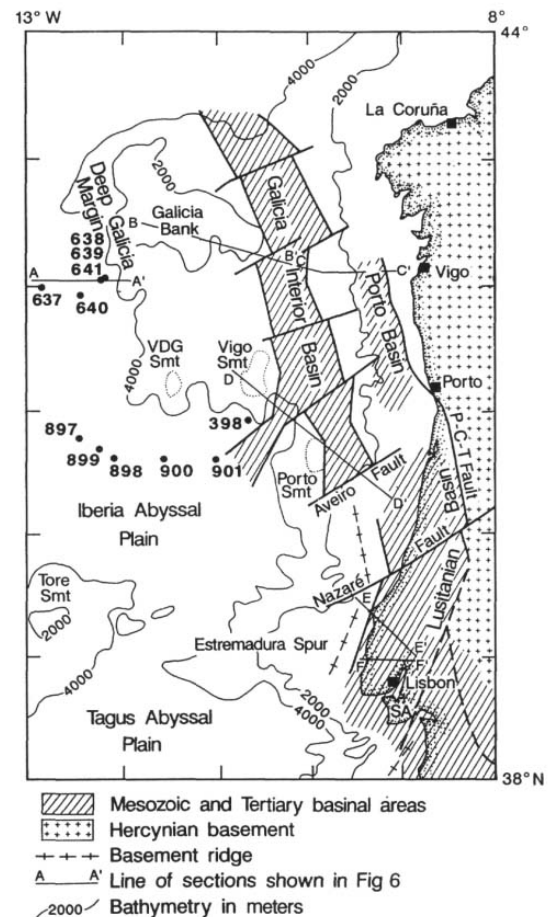


Fig. 8 Sketch map showing the distribution of marginal sedimentary basins along the west Iberian margin (after Pinheiro et al., 1996). SA: Serra de Arrábida, P-C-T: Porto-Coimbra-Tomar, VDG Smt: Vasco de Gama Seamount.

western Florida Straits (Site 540: SSP, 1984e), Albian-Cenomanian reef limestone is 3,357.5 m below sea-level and has an extensive the Middle Cretaceous unconformity (MCU) with its upper layers. Paulus (1972), based on the results of drilling at the Andros Island and the New Providence Island, concluded that the Great Bahama Reef is a growth of reefs from Cretaceous to the present, with the base of the reefs being Early Cretaceous limestone at depths greater than 3,000 m below present sea-level (Fig. 9). The Gulf of Mexico-the Greater Bahama Reef area is thought to have been submerged after Jurassic, with large-scale carbonate reefs developing in Early Cretaceous, especially in Albian, coral reefs developing in areas that were subsequently uplifted, forming the present-day peninsulas and islands, while other areas with less uplift were submerged, forming deep-sea floor such as the Gulf of Mexico and the Florida Strait.

On the Continental Rise of the east coast of North America, Late Barremian-Aptian/Albian shallow-water biogenic limestones are below 4,121 m below sea-level at the J-Anomaly Ridge (Site 384: The SSP, 1979) and Barremian shallow-marine limestones are at 2, 817.9 m below sea-level at the northern margin of Blake Nose (Site 390: SSP, 1978a), and Albian-Cenomanian limestone sandstone and shell limestone are at 1,986 m below sea-level at the Orphan Knoll in Newfoundland (Site 111: The SSP et al., 1972).

Aptian-Albian shallow-water limestones are present at 2,530 m below sea-level on the continental margin of the northern Biscay Bay in the East Atlantic (Site 402: The SSP and Mann, 1979). Clastic dolomitic limestones formed in shallow-water during Late Jurassic-Neocomian? at 3,690.7 m below sea-level at the Mazagan Escarpment (Site 545: SSP, 1984b) in the western Morocco. In the Angolan margin, Late Aptian-Early Albian dolomitic limestones and sapropel shales are 2,800-3,200 m below sea-level at Site 364 (The SSP, 1978a) just above Aptian evaporites formations (Roberts, 1975). Late Albian shallow-water sandstones are 3,172.4 m below sea-level at Site 959 (SSP, 1996a) in the northern part of the Cote d'Ivoire-Ghana Marginal Ridge on the Ghanaian continental margin. To the south of this, there are Early Aptian shallow-water limestones at 2,943 m below sea-level at Site 363 (The SSP, 1978b) of the Walvis Ridge, and Campanian subaerial weathered basalt lava at 3,053.9 m below sea-level.

In the Demerara Rise off Guiana of the western Atlantic (Site 144: The SSP, 1972; Sites 1258-1261: SSP, 2004c-2004g), Early-Middle Albian quartz sandstone and mudstone deposited in shallow-water at 2,500-3,000 m below sea-level overlie the unconformity and are overlain by Cenomanian-Turonian black shale deposited in a closed sea floor environment. On the Brazilian margin, as on the west coast of Africa, Early Cretaceous Aptian evaporites occur on the sea floor at 4,000 m depth (Roberts, 1975), and at Site 21 (The SSP, 1970) of the Rio Grande Rise, Maastrichtian coquina deposited on the continental shelf at 2,305.9 m below the sea-level and Coniacian well-selected shallow-water calcareous sandstones at 2,576.5 m below sea-level. At Site 330 (The SSP et al., 1977a) on the Falklands Plateau, Aptian sapropel mudstone layer is 3,061 m below sea-level, while at Site 698 (SSP, 1988a), subaerial erupted basalt lava is present below Campanian sandy mud at about 2,300 m below sea-level. At Site 967 (SSP, 1996b), the Eratosthenes Seamount, the south of the Cyprus Island in the Mediterranean Sea, there are Late Cretaceous shallow-water limestones at 2,979.7 m below sea-level.

On the eastern flank of the Ninetyeast Ridge of the Indian Ocean at Site 217 (The SSP, 1974a), there are shallow-water dolomite with Late Campanian shells at 3,620 m below sea-level and Late Maastrichtian shallow-water chalk at 2,704 m below sea-level. At Site 748 (SSP, 1989b) in the southern part of the Kerguelen Plateau, Late Albian-Turonian reef limestones are present at 1,679.6 m below sea-level, with basaltic lava subaerial erupted below. Claystone deposited at 200-500 m depth in Berriasian-Early Valanginian is present at 2,208.5 m below sea-level in the Wombat Plateau (Site 761: SSP, 1990b) of the western margin of Australia, and in the central part of the Exmouth Plateau (Site 762: SSP, 1990c; Site 763: SSP, 1990d), there are siltstones deposited

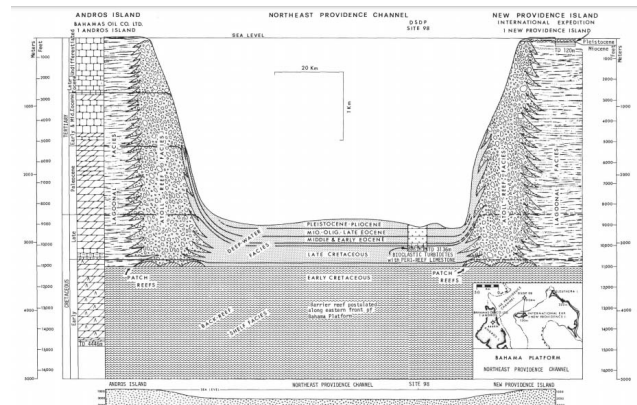


Figure 9. Cross-section of a portion of the Bahama Platform through Site 98 from Andros Island to the New Providence Island showing the relationships of shallow-water bank and shelf growth and the deep-water channel decline (after Paulus, 1972). Time lines are based on ages from the Andros Island well and the Site 98 core hole (Paulus, 1972).

Fig. 9 Cross-section of a portion of the Bahama Platform through Site 98 from the Andros Island to the New Providence Island showing the relationships of shallow-water bank and shelf growth and the deep-water channel decline (after Paulus, 1972). Time lines are based on ages from the Andros Island well and the Site 98 core hole (Paulus, 1972).

on the outer continental shelf in Early Valanginian-Early Berriasian at 1,938-2,209 m below sea-level (Fig. 10). At Site 264 (The SSP, 1975a), the Naturaliste Plateau of the Southwestern tip of Australia, the unconformably Cenomanian-Santonian chalk overlies pre-Cenomanian volcanoclastic conglomerate. In other words, the western margin of Australia was terrestrial or shallow-water during Late Triassic (Carnian-Rhaetian), continued shallow water environment until Early Cretaceous Berriasian (partly Late Albian), and then deepened. In the West Antarctica, the Weddell Sea, there are Middle Albian clayey mudstones deposited at a depth of around 500 m below sea-level at 2,768 m. At Site 741 (SSP, 1989c) in the Prydz Bay, sandstones interbedded with carbonized plant fragments and gravel beds deposited in Albian rivers or coastal plains at 575.5 m below sea-level and at Site 742 (SSP, 1989d) are Turonian charcoal clays deposited in a lagoonal environment at 751.8 m below sea-level.

Many of the Pacific guyots have Aptian-Albian shallow-water reef limestones on their flat summits, with the maximum thickness of Aptian-Albian reef limestone on the summit of guyot being at 1,183.8 m at the Resolution Guyot (Site 866: SSP, 1993a). According to Winterer and Metzler (1984), in the Mid-Pacific Mountains, seismic sections at several guyots have revealed with reef thicknesses of up to 1,000 m (Fig. 11). The Wodejebato Guyot (Sites 873-877: SSP, 1993b-1993e) in the Marshall Islands has reef limestones in Late Campanian-Maastrichtian. Aptian-Cenomanian coral reef limestone have been obtained at the southern end of the Japan Trench at the Dai-Ichi Kashima Seamount at a depth of about 4,000 m (Dai-Ichi Kashima Seamount Research Group, 1976; Shiba, 1988, 1993) and at the northern end at the Erimo (Sysoev) seamount, where Cretaceous or Late Cretaceous reef limestones were also obtained at a depth of about 4,000 m (Tsuchi and Kagami, 1967).

Aptian-Cenomanian biogenic reef limestones have been reported by Hamilton (1956) at the Hess Guyot and the Cape Johnson Guyot in the Mid-Pacific Mountains. Heezen et al. (1973) and Matthews et al. (1974) are reported many guyots of Cretaceous reef in the Mid-Pacific Mountains and the Japanese Seamounts: Aptian reef limestones from the Winterer Guyot and the Seiko Guyot (Takuyo II seamount), Aptian-Cenomanian reef limestones from the Isakov Guyot, Cretaceous or Late Cretaceous reef limestones from the Shepard Guyot, the Menard Guyot, the Jacqueline Guyot, the Makarov Guyot, the T. Washington Guyot and the Eiko Guyot. Other Aptian-Cenomanian or Cretaceous reef limestones from Guyots are the Yabe Guyot (Shiba, 1979) and the Broken-top Guyot (Konishi, 1985) in the Bonin Plateau and the Darwin Guyot of the Mid-Pacific Mountains (Ladd et al. al., 1974). At the Meiji Guyot (Site 192: The SSP, 1973d) and the Detroit Seamount (Site 1203: SSP, 2002a; Site 1204: SSP, 2002b) in the Emperor Seamounts, Late Maastrichtian and Campanian chalk and alkaline basalt erupted in shallow-water or subaerial have been recovered at 4,058 m and 3,061.9 m below sea-level, respectively.

Shallow-water sediments have not been recovered by the DSDP and ODP in the Shatsky Rise, but pre-Albian shallow-water limestones were recovered at 3,300.7 m below the sea floor in IODP drilling site U1349 at the top of the Ori Massif, with subaerial weathered basalt lava and pyroclastic rocks below the limestone (Sager et al., 2010). Relatively shallow-water basalts were recovered from 3,523 m below sea-level at Site 317 (The SSP, 1976) in the Manihiki Plateau. Aptian or pre-Aptian basalt lava is

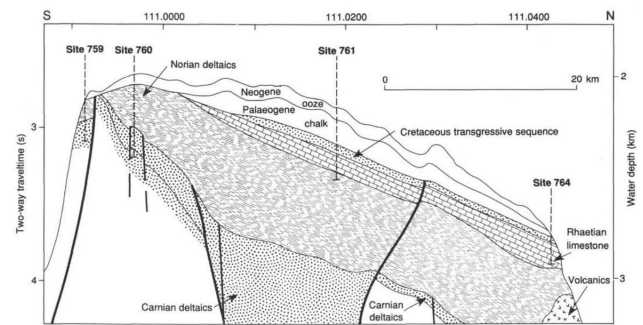


Fig. 10 Structural N-S cross section of the Wombat Plateau (after SSP, 1990a). The Cretaceous transgressive sequence overlay the Triassic (Carnian-Rhaetian) basements, which was deepened in the Paleogene and then tilted to the north.

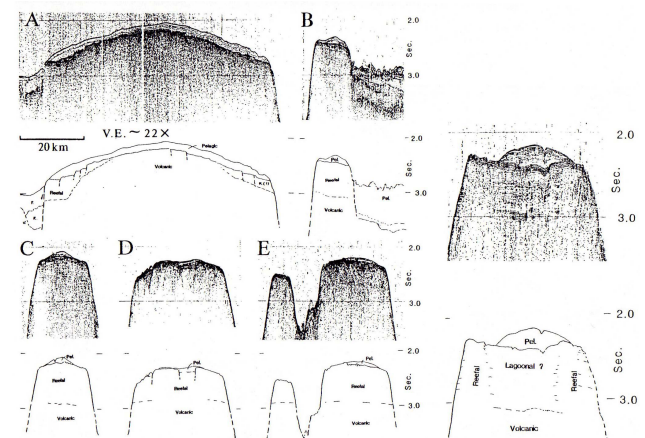


Fig. 11 Topographic sections and seismic profiles of the Mid-Pacific Mountains (after Winterer and Metzler, 1984). A: Horizon Guyot, B: Lenard Guyot, C: Shepard Guyot, D: Jacqueline Guyot, E: Stedson Guyot, F: Alison Guyot.

in the northern part (Site 289: The SSP, 1975b) and main ridge (Site 1183: SSP, 2001a) of the Ontong-Java Plateau, with Aptian-Albian limestones 2,894-3,486 m below sea-level above them. These large-scale rises and guyots are thought to have been formed by coral reefs from Aptian to Albian on top of islands formed by pre-Aptian or pre-Albian basaltic volcanism, which have since been submerged. There was also shallow-water volcanism on the northern ridge of the eastern branch of the Ontong-Java Plateau (Site 1184: SSP, 2001b) during Middle Eocene, and the islands on the margins of this Plateau, such as the Manihiki Island, the Danger Island and the Suvarow Island, rose and formed atolls as sea-level rose (SSP, 2001b). In the South Lord Howe Rise (Site 207: The SSP et al., 1973), the southeast Australia, Maastrichtian glauconite sandstones are present at 1,746 m below sea-level, with subaerial erupted rhyolite beneath.

The main Cretaceous shallow-water sediments are Aptian-Cenomanian coral reef limestones and evaporites widespread along the Atlantic continental margin and at the top of the guyots in the Pacific Ocean. They are overlain by Late Cretaceous pelagic sediments. This suggests that the Aptian-Cenomanian coral reefs and evaporites were interrupted in their upward growth by rapid submergence during Cenomanian or Turonian. The almost simultaneity of this rapid submergence in early Late Cretaceous suggests that the cause of this submergence was not regional subsidence, as Hamilton (1956) inferred for the guyot formation, but a rapid sea-level rise that submerged all these reefs almost simultaneously (Shiba, 1988, 1993).

The maximum thickness of coral reefs during the Aptian and Albian epochs at guyot in the Pacific is 1,183.8 m at the Resolution Guyot (Site 866: SSP, 1993a). As the amount of upward growth of a coral reef indicates the amount of subsidence of that reef or the global sea-level rise, it is thought that sea-level rose by more than 1,100 m during Aptian-Albian, assuming that the reef did not subside. The formation of the massive Aptian-Albian carbonate reefs, more than 1,100 m thick, and the subsequent rapid sea-level rise are thought to be closely related to the formation of the Large Igneous Provinces (LIPs) that formed the large-scale rise and seamount groups in the Pacific, which occurred at about the same time.

The distance of the tops of these guyot reef-bearing limestones from the present sea-level varies from 1,352 m (Site 867: SSP, 1993f) to about 4,121 m (Site 384: The SSP, 1979), the deepest being Late Barremian-Aptian/Albian shallow-water limestone of the J-Anomaly Ridge at Site 384. This suggests that the sea-level at the end of Albian was about 4,100 m or lower, assuming that they did not subside, which is in agreement with the value given by Hoshino (1970). If sea-level rose by more than 1,100 m during the Aptian-Albian period, as inferred from the thickness of the guyot reef limestone, the position of the Barremian sea-level would have been about 5,200 m or more lower than the present sea-level.

The Aptian-Albian shallow-water sediments are at different depths in each region. This may be due to the different amounts of post-Cenomanian uplift in each region after the submergence of the guyots (Fig. 12). The thickness of the reef limestone in Late Campanian-Maastrichtian is 125-183 m at the Wodejebato Guyot, which suggests that the sea-level rise in Late Campanian-Maastrichtian is more than 183 m.

On the landward upper slope of the west coast of Mexico in the Central American Trench (Site 489: SSP, 1982a; Site 493: SSP, 1982b), at 1,040-1,566.5 m below sea-level, there is a basement composed of pre-Cenozoic biotite schist and diorite. On the

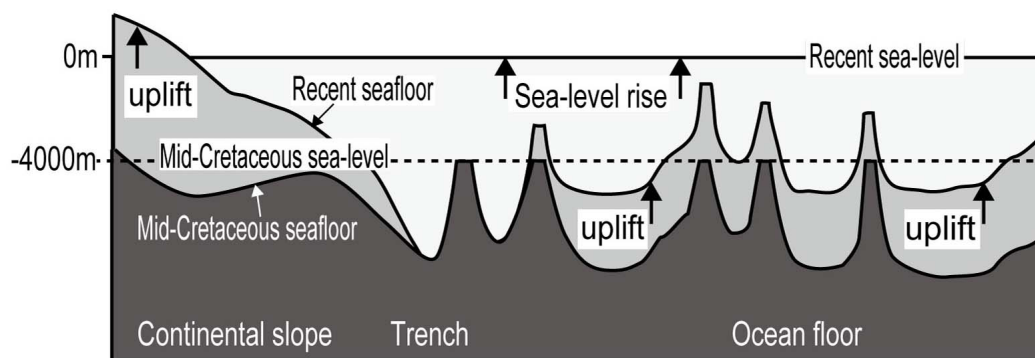


Fig. 12 Middle Cretaceous and present-day modelled topographic sections from the Japan Trench to the Pacific floor (after Shiba, 1988). The uplift of the island arc and the ocean floor has caused sea-level rise, resulting in the Middle Cretaceous coral reefs of Guyots being topped at various depth.

Guatemala margin (Sites 566-570: SSP, 1985c-1985f) and the Costa Rica margin (Site 1039: SSP, 1997a; Site 1040: SSP, 1997b) trench floors and their landward slopes, there are an ophiolitic complexes composed of basalt, diorite, gabbro, peridotite and serpentinite at 2,092.2-5,897 m below sea-level (Fig. 13), and these basement rocks are similar to the terrestrial geology and are considered to be extensions of igneous zone belonging to the Laramie Orogeny (Late Cretaceous-Early Paleogene) that form the continent of Central America (SSP, 1985f). On the Santa Elena Peninsula, Costa Rica, an ophiolite complex and Late Cretaceous pelagic limestone unconformity, identical onshore and at the trench floor, suggest that the onshore one was uplifted more than 6,000 m (SSP, 1985f).

The Paleogene period

At the western foot of the Rockall Bank in Newfoundland, the Northwest Atlantic Ocean (Site 117), there are Late Eocene basaltic sandstones deposited in shallow-water or nearshore environments at 1,341 m below sea-level, gradually deepening to about 600 m in Early Eocene. In the eastern Greenland margin (Sites 914-917: SSP, 1994b-1994e; Sites 988-990: SSP, 1996c-1996e) or the southeast (Site 918: SSP, 1994e), there is subaerial weathered basalt lava at 272.6-3,026.1 m below sea-level or late Early Eocene-Late Eocene shallow-water volcanoclastic sandstones and sandy siltstones deposited on the slope. There is also an unconformity between the middle Eocene and the upper Oligocene at 2,976.4 m below sea-level.

According to SSP (1994f), in the Irminger Basin of the Greenland Shelf, marine shales were deposited during Paleocene, uplifted by west-trending faults, flattened by subaerial erosion, erupted subaerial basalt, then eroded and trended eastwards during Early Eocene, with seaward relatively subsided and covered by marine formation, the Irminger Basin was subsided during Middle Eocene from a water depth of 75-200 m to a sea floor of 200-600 m (Fig. 14). In the eastern part of the Greenland Shelf (Site 918: SSP, 1994e), massive sandstones or sandy siltstones of Late Eocene-Early Oligocene were deposited at a depth of 100-250 m below sea-level at 617.9-720.4 m below sea-level, beneath Quaternary sandy silts. The geological section of the southeast Greenland margin (Fig. 15) shows that the continental margin strata and continental basement, including basaltic layer, are continuous to the sea floor, with the continental and ocean crusts distinguished at the slope margin. Larsen et al. (1994) show on a map of the North Atlantic Ocean from the Greenland to the North Sea (Fig. 16) the same basalt and seaward dipping strata as on the east coast of the Greenland.

Belousov and Milanovsky (1977) noted that the crust of Iceland is 50 km thick, indicating that there is continental crust there. Bott (1968) also states that the Fellows Islands have continental crust among the submarine mountain ranges between the Greenland and the Shetland Islands. Fig. 16 shows that the uplifted areas in the North Atlantic, including Iceland, appear to be composed of the same combinations of strata and rocks, and that the continental crust is thought to underlie them. If the geological section in Fig. 15, which is considered to be ocean crust, is directly continental crust continuous with the deep-sea floor, then what has been considered the Atlantic

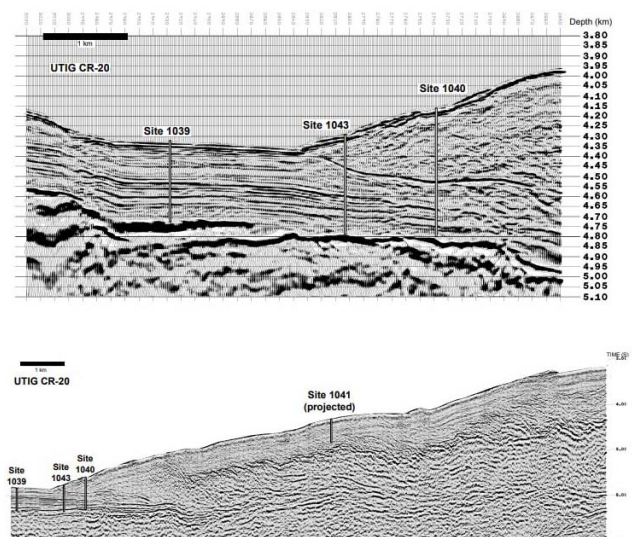


Fig. 13 Seismic profiles and Site locations of the Middle America Trench on the Costa Rica margin (after SSP, 1997c).

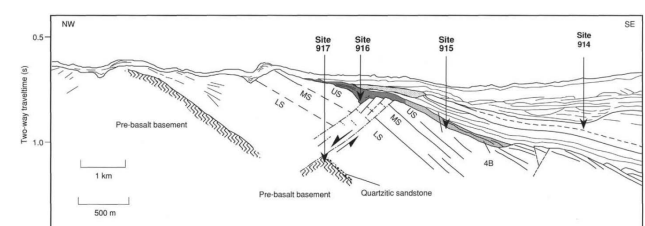


Fig. 14 A reconstruction of the position of the three-lava series established in Hole 917A within the innermost part of the seaward dipping reflector sequences on the southeast Greenland Margin (after SSP, 1994f). LS: Lower Series, MS: Middle Series, US: Upper Series. The boundary may represent the time of the final rupture of the continent. Drilling at Site 917 probably penetrated the southeastern fault block at the crest of the pre-basaltic basement, implying that only part of the sediments at the breakup unconformity was recovered. About 300 to 400 m of the oldest lavas has not been drilled. Note that the dips are exaggerated; the true dip of the lavas and main normal fault is about 20° to 30°.

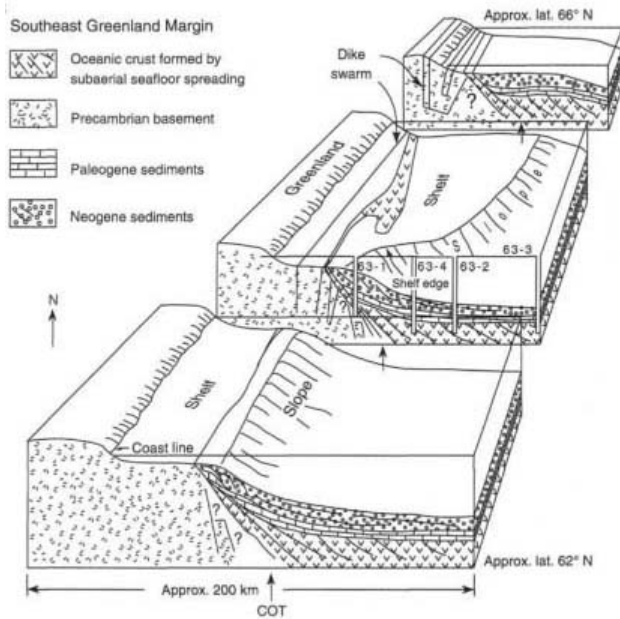


Fig. 15 Main geological features of the southeast Greenland margin (after Larsen et al., 1994). COT: continent/ocean transition. If the COT did not exist and was continuous with the continent, then the deep ocean floor of the Atlantic Ocean would contain continental crust.

oceanic crust may be basalt-covered continental crust.

In the Iceland-Faeroe Ridge (Site 336: The SSP et al., 1976a) and the Vøring Plateau Escarpment (Site 338: The SSP et al., 1976b), 1,315 m and 1,700 m below sea-level respectively, there are subaerial erupted basalt lava during Early or Middle Eocene and have been continuously submerged since Late Eocene. At the Jan Mayen Ridge (Site 349: The SSP et al., 1976c), Late Eocene terrigenous sandstones and conglomeratic mudstones overlie unconformably Oligocene to Middle Miocene sediments at 1,047 m below the sea-level. On the western Iberian margin-the Biscay margin, the environment became pelagic after Late Cretaceous and deepened further during Oligocene, but during Late Eocene? -Early Oligocene, the sea floor became near the Carbonate Compensation Depth (CCD), whereas it had previously been below the CCD.

At Site 526, the Walvis Ridge, shallow-water limestones of Late Oligocene to Middle Eocene are present at 1,287.1 m below sea-level and the lower Oligocene and the Miocene unconformity is present at 2,767.1 m below sea-level. The Demerara Rise off the coast of Guiana is believed to have experienced significant and rapid global warming (5° - 7° C at the poles) at the Eocene/Paleocene boundary, mass extinction of marine microorganisms and widespread shallowing of the CCD (SSP, 2004e). However, this widespread shallowing of the CCD is interpreted as a deepening of the sea floor due to sea-level rise, rather than a shallowing of the CCD.

In Site 357 (The SSP, 1997) of the Rio Grande Rise, volcanic breccia and shallow-water fossil fragments of Middle Eocene are present at 2,444 m below sea-level, subsided during Paleocene to be the middle bathyal zone, uplifted into a dome with igneous activity during Eocene, and the top of this Rise was flattened by subaerial erosion and then submerged (Fioravanti, 2020). Shallow-water sediments and other materials of this period have not been obtained from the Falklands Plateau, but drilling results from Site 702 (SSP, 1988b) suggest that the area became rapidly colder from Middle Eocene, suggesting that the Circumpolar Current formed during Middle Eocene (SSP, 1988c).

At Site 214 (The SSP, 1974b) on the top of the Ninetyeast Ridge in the Indian Ocean, Site 219 (The SSP et al., 1974a) on the

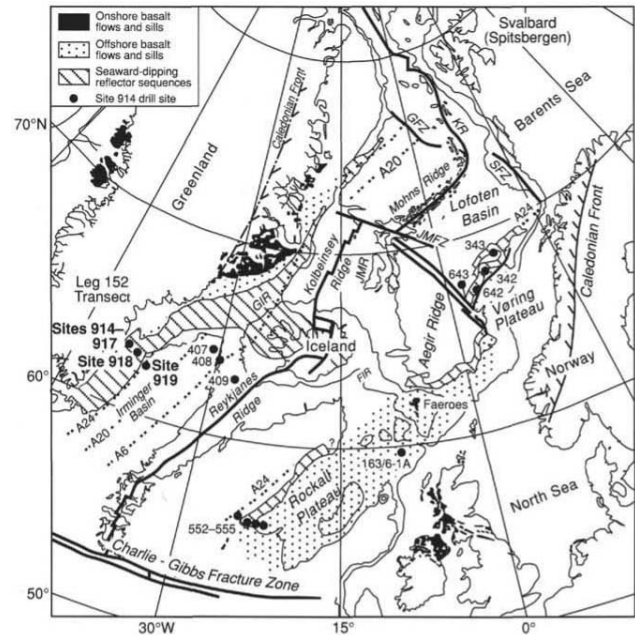


Fig. 16 Map of the Northeast Atlantic Ocean showing the main physiographic features of the region, previous DSDP and ODP drill sites (after Larsen et al., 1994). The location of the main major early Tertiary basalt outcrop and subcrop, and the broad division into Caledonian and pre-Caledonian crustal blocks (in Greenland and Scandinavia). Abbreviations, from north to south; KR: Knipovich Ridge, GFZ: Greenland Fracture Zone, SFZ: Senja Fracture Zone, JMFZ: Jan Mayen Fracture Zone, JMR: Jan Mayen Ridge, GIR: Greenland-Iceland Ridge, FIR: Faeroes-Iceland Ridge.

Laccadive-Chagos Ridge and Site 253 on the top of the Broken Ridge, there were subaerial erupted volcanoes at 1,500-2,700 m below sea-level in Late Eocene, which became an inner shelf in Middle Eocene and submerged, pelagic environment from Late Eocene. At the Maldives Ridge (Site 715: SSP, 1988d), subaerial erupted peridotite-basalt lava is present below Early Eocene reef-bearing limestone. In the northern part of the Kerguelen Plateau (Site 1139: SSP, 2000a), there are basaltic lava and rhyolite volcanoclastic rocks that erupted in Eocene or older terrestrial or shallow-water at 1,800-2,700 m below sea-level. At the top of the Broken Ridge (Sites 752-755: SSP, 1989e-1989h), approximately 1,200 m below sea-level, there is a nearly horizontal wave erosion unconformity between Late Cretaceous chalk and Middle Miocene or Middle to Late Eocene calcareous soft mud (Fig. 17).

In the Mascarene Plateau (Site 237: The SSP, 1974c; Site 707: SSP, 1988e) and the Madagascar Ridge (Site 246: The SSP, 1974d) in the eastern Africa, shallow-water calcareous mudstones and reef limestones of Early Paleocene to Middle Eocene were deposited in shallow-water environment between 1,155 and 2,377 m below sea-level. Eocene reef-bearing limestones with *Nummulites* are present at 471-1,432 m below sea-level on the Oman continental margin (Site 724: SSP, 1989i; Site 726: SSP, 1989j; Site 728: SSP, 1989k and Site 729: SSP, 1989l).

Shallow-water limestones or calcareous sandstones of Middle to Late Eocene are present at 736-858 m below sea-level at Site 1130 (SSP, 2000b) and Site 1132 (SSP, 2000c) in the Great Australian Bight. On the western margin of Tasmania (Site 1168: SSP, 2001c) and the west of the South Tasman Rise (Site 1770: SSP, 2001d), silty claystone was deposited in shallow to brackish hypoxic environments during Late Eocene at 2,491-3,225 m below sea-level (Fig. 18). These Eocene deposits, as well as those of Sites 280 and 282 to the northwest and the south of them, were deposited in Late Eocene anaerobic environment widespread from the eastern Australia to the Antarctic Bay, where these continental margins underwent an Oligocene transitional phase and were transformed into bathyal zone, oxygen-rich open ocean environment during the Neogene period (SSP, 2001f).

At Site 696 (SSP, 1988f), the South Orkney Microcontinent, the Antarctic Ocean, there are sandy mudstones deposited in an Early Oligocene-Eocene inner shelf environment at 1,256.9 m below sea-level. There are Early Eocene-Oligocene non-marine claystone and sandstones below 720.0 m below sea-level at Site 742 (1989d), in Prydz Bay, the East Antarctica (Fig. 19), and coarse-grained sandstones deposited in an Eocene fan at Site 1166 (SSP, 2001g), 631.9 m below sea-level, suggesting that a terrestrial environment prevailed until Oligocene.

In the Pacific Ocean, at the Limalok Guyot (Site 871: SSP, 1993g), the Marshall Islands, reef limestones of Late Eocene-Middle Eocene are present at about 1,400 m below sea-level, with basalt lava that has subaerial erupted or weathered below the limestone. The shallow-water reef limestone of the Limalok Guyot is 318 m thick. In Cretaceous guyots such as the Resolution Guyot (Site 867: SSP, 1993f), there are phosphatized nannofossil limestones with manganese cover and phosphatized limestones, which are similar to the occurrence of limestones on the top of the Yabe Guyot (Shiba, 1979). In the Wodejebato Guyot (Sites 873-877: SSP, 1993b-1993e), Middle Eocene limestone gravels are cemented by late Middle Eocene phosphatidic pelagic sediments, suggesting that they became phosphatidic after Middle Eocene.

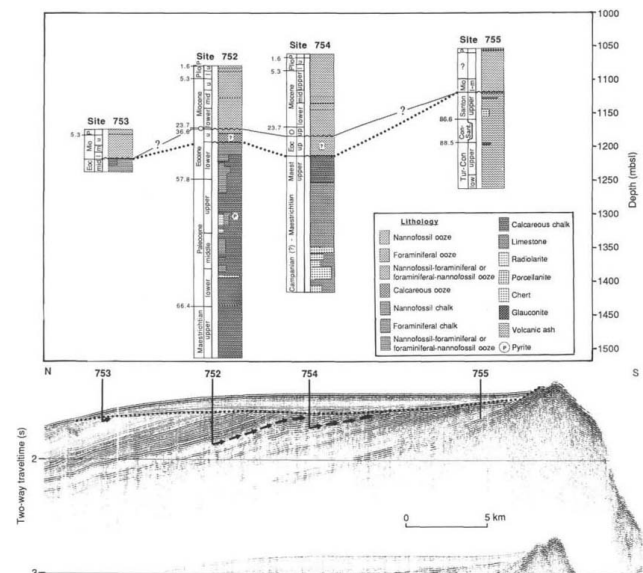


Fig. 17 Correlation of seismic stratigraphy and lithostratigraphy sampled at sites 752, 753, 754, and 755 on the Broken Ridge (after SSP, 1989e). The arrows represent the upward continuation of the deepest horizon penetrated at sites 752, 753, and 754 to the angular unconformity, illustrating the amount of stratigraphic section recovered and the stratigraphic overlap - if any - the sites. The dotted line represents the middle Eocene hiatus and the wavy line denotes the Oligocene hiatus. The two hiatuses coalesce at Sites 753 and 755, but the question marks indicate that the position where they coalesce across the Broken Ridge is not resolved.

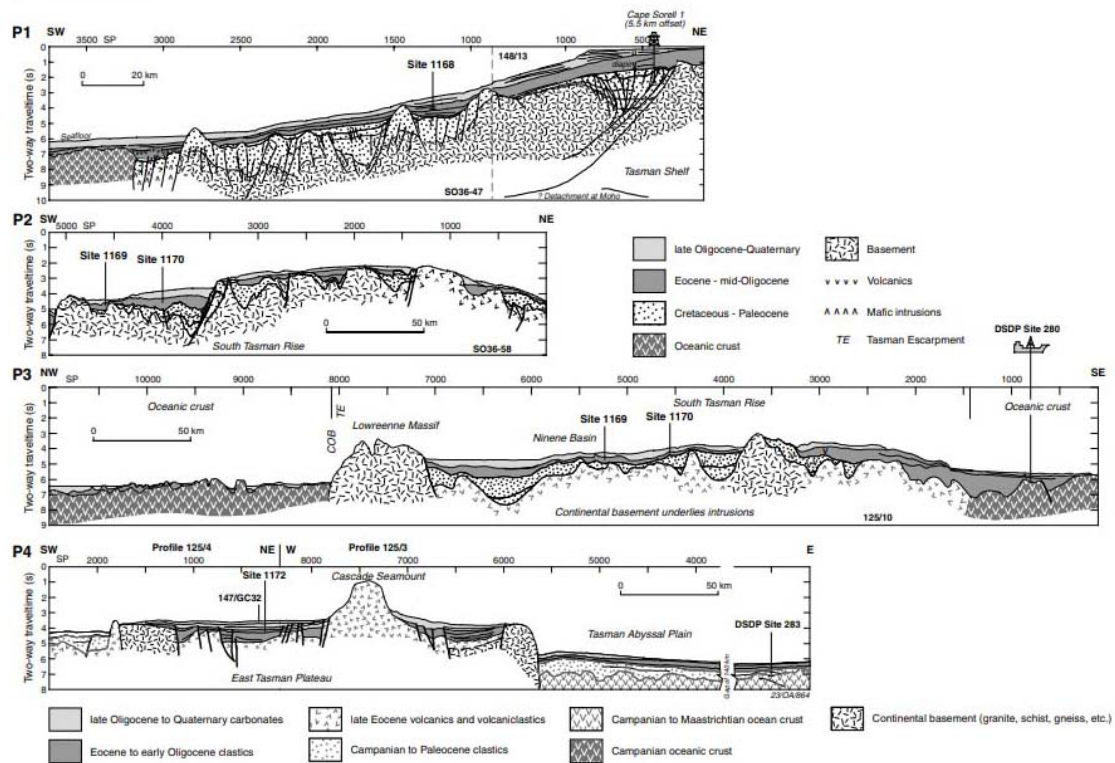


Fig. 18 Pre-drilling cross-sections from seismic profiles across the Tasmania and the South Tasman Rise (after SSP, 2001f). P1: West Tasmania, P2 and P3: South Tasman Rise, and P4: East Tasman Plateau.

Late Oligocene-Early Eocene reef limestones are present at 1,300-2,000 m below sea-level in most of the Emperor Seamounts (Site 192: The SSP, 1973d; Site 202: The SSP, 1973e; Sites 308-309: The SSP, 1975c-1975d; Site 430A: SSP, 1980a; Site 433: SSP, 1980b; Sites 1203-1206: SSP, 2002a-2002d) and are 268 m thick to the lower onshore-erupted basalt lava at the Kōko Guyot (Site 1206: SSP, 2002d). At the Kōko Guyot, after the development of reefs in Early Eocene, the reefs were submerged once but became shallower in Late Oligocene and may have been volcanically active. At the Meiji Guyot (Site 192: The SSP, 1973d) there are alkali basalt and trachyte lava flows erupted in shallow-water or onshore that are older than Late Maastrichtian at 4,058 m below sea-level. At the Detroit Seamount (Site 1203: SSP, 2002a), basalt lava and pyroclastic rocks erupted in shallow-water or on land during Campanian at 3061.9 m below sea-level. The Suiko Seamount (Site 433: SSP, 1980b) was a barrier reef island during Middle Eocene.

Most of the seamounts in the Emperor Seamounts formed as volcanic islands during or before the Paleocene epoch, became shallow reefs during Late Paleocene-Early Eocene and were submerged during Middle Eocene, but the Kōko Seamount, which was continuously volcanically active, remained a reef environment until Early Oligocene. The timing of submergence coincides with Middle Eocene, suggesting that the cause of submergence was a rapid sea-level rise, similar to Cretaceous guyots. This cannot be explained by the story of the northward migration of the Pacific Plate, in which the volcanic islands of the Emperor Seamounts were formed by a hotspot and turned into reefs, which then subsided.

The reefs of the Emperor Seamounts are mainly composed of mosses and calcareous algae, which according to Mckenzie et al.

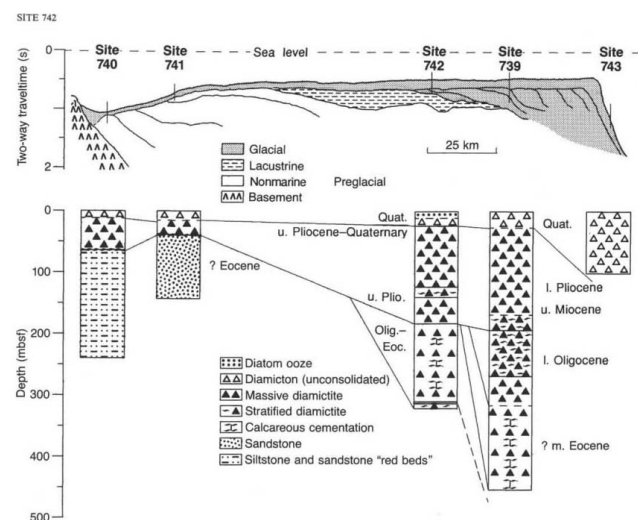


Fig. 19 Representation of the sediment facies recovered from the Prydz Bay during Leg 119, based on the collected seismic and stratigraphic data (after SSP, 1989d).

(1980) are Bryozoan-Algal facies rather than Coral-Algal facies. Schlanger and Konishi (1966) distinguished reef facies into the Coral-Algal facies and the Bryozoan-Algal facies, which corresponded to latitude according to sea surface temperature and solar radiation, with the Bryozoan-Algal facies now distributed at higher latitudes than 23°. Schlanger (1981) questioned the formation of the Emperor Seamounts by a hotspot, as the Suiko Seamount must have formed more than 7° north of the latitude of the present Hawaiian hotspot, based on the Bryozoan-Algal facies found in the Emperor Seamounts.

At the northern ridge of the eastern branch of the Ontong-Java Plateau (Site 1184: SSP, 2001b), there are Middle Eocene volcanic tuff-breccia that were deposited in shallow-water at 1,863 m below sea-level. On the northeastern margin (Site 209: The SSP and Burns, 1973) and the western margin (Site 811: SSP, 1991a) of the Queensland Plateau in the northeastern Australia, shallow-water limestones of Middle Eocene and Middle Eocene-Late Oligocene are present at 1,703-1,345 m below sea-level, with meta-sediments or meta-volcanic rocks of undetermined age lower on the western margin. At Site 828 (SSP, 1992a), north of the d'Entrecasteaux Ridge in the Vanuatu Island arc, angular gravelly basalt and coarse-grained basalt with a soil layer below Middle Eocene? nanofossil chalk at 3,182 m below sea-level. At the Bougainville Guyot (Site 831: SSP, 1992b), Late Oligocene-Early Miocene coral reefs are present from 1,794 to 1,496 m below sea-level.

At Site 296 (The SSP, 1975e) at the western foot of the Palau-Kyushu Ridge, volcanoclastic debris containing shallow-water carbonate rocks of Late Oligocene is present at 3,411 m below sea-level. At Site 439 (SSP, 1980c), the deep-sea plain of the Japan Trench, Late Oligocene terrestrial conglomerates and shallow-water sandstones are recovered at 2,764 m below sea-level, suggesting that the deep-sea plain was on land during Late Oligocene and was submerged after Miocene. On the lower slope of the Peru Trench (Site 688: SSP, 1988g), calcareous mudstones, sandstones and limestones containing plant fragments and pebble gravels of Early Eocene deposited on the sea floor at a depth of 150-1,500 m at 4,514.3 m below sea-level.

In the Paleogene period, Eocene is the epoch during which most shallow-water sediments and terrestrial volcanic ejecta were recovered. The majority of the recovery depths of these Eocene shallow-water indicator is between 1,000-3,411 m. The deepest recovery depth are Early Eocene calcareous mudstones of the lower slope of the Peru Trench at Site 688 (SSP, 1988g), 4,514.3 m below the sea floor, which represent the upper slope (150-1500 m) depositional environment obtained. Alternatively, there are siltstones deposited in shallow-water during Middle Eocene at 3,201.7 m below sea-level in the southern part of the Tasman Rise at Site 1170 (SSP, 2001d). Late Oligocene sediments at 3,411 m below sea-level in the latter Site 296 (The SSP, 1975e) suggest that sea-level in Late Oligocene was about 3,400 m or more below present sea-level.

The thickest Eocene reef limestone is Late Eocene-Middle Eocene reef limestone at the Limalok Guyot at 318 m, and Middle Eocene or Middle Eocene-Late Oligocene shallow-water limestone at the northeastern and western margins of the Queensland Plateau at 358 m. These suggest that sea-level rise during Middle Eocene may have been 310-360 m. The sea-level position during Early Eocene is estimated to have been 3,800 m or lower than at present based on the sea-level position during Late Oligocene and the amount of sea-level rise during Middle Eocene.

On the other hand, the drilling at Eniwetok Atoll, Marshall Islands, Pacific Ocean (Ladd and Schlanger, 1960) recovered Eocene-Miocene coralline limestone to 1,380 m below sea-level and basalt lava below (Fig. 20). There, the Miocene coralline limestone is 630 m thick and the Eocene coralline limestone is 540 m thick. The absence of aragonite in the lower part of the Miocene limestone to the upper part of the Eocene limestone and the recrystallisation of calcite suggest that the top of the atoll was above sea-level and subject to subaerial erosion (Ladd and Schlanger, 1960). The sea-level rise during Miocene

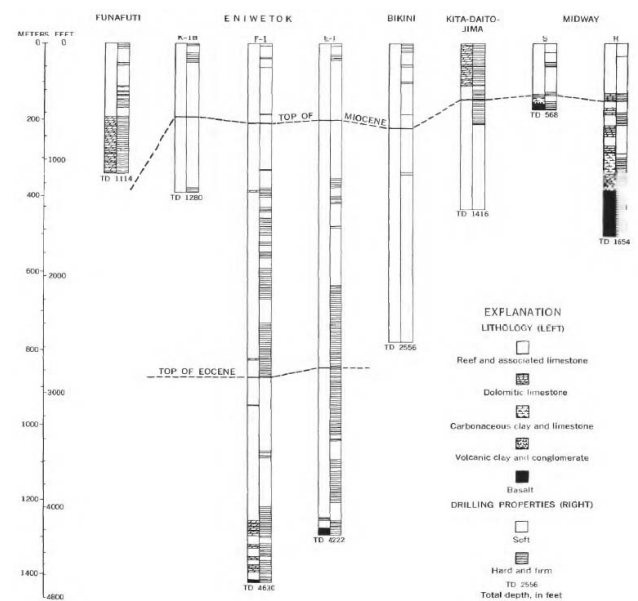


Fig. 20 Summary of results of deep drilling on five atolls in the Pacific Ocean (after Ladd et al., 1970).

and Eocene can be estimated to be 630 m and 540 m or more, respectively, which is greater than the sea-level rise results obtained from deep-sea drilling.

The Neogene and Quaternary periods

In deep-sea drilling, the Neogene and Quaternary systems are mostly pelagic sediments and terrestrial source sediments such as clays, silts and turbidites, and not many shallow-water sediments or terrestrial volcanic ejecta. On the other hand, unconformity and hiatus are observed in some sites. This may be due to the fact that the geographical distribution of the continents and oceans became more or less the same in Neogene as they are today.

In the upper Continental Rise of the Atlantic Ocean (Site 605: SSP, 1987b), an unconformity eroded by the upper Miocene at 2,359 m below sea-level corresponds to the seismic reflection surface AU that develops in this area. On the upper continental slope along the New Jersey coast, an unconformity between the middle Miocene and the upper Pleistocene is found at Sites 902 and 903, 904 and 906, which are also considered important boundaries in seismic reflection analysis (Lorenzo and Hesselbo, 1996). At Site 526 (SSP, 1984c), the Walvis Ridge, the Lower Oligocene-Miocene unconformity lies 2,767.1 m below sea-level, while in the Cape Basin (Site 1087: SSP, 1998f) the Middle Miocene erosional unconformity surface lies about 1,800 m below sea-level and is overlain by late Middle Miocene foraminiferal-nannofossil soft mud.

In the Mediterranean Sea, salt layers consisting of Late Miocene Messinian gypsum and marl were recovered 2,100-2,700 m below sea-level in the Florence Rise west of the Cyprus Island (Sites 375 and 376: The SSP, 1978c), in the North Creta Basin (Site 969: SSP, 1996f), in the Tyrrhenian Sea (Site 654: SSP, 1987c) and in the southern Balearic Margin in the Western Mediterranean (Site 975: SSP, 1996g). In the Messina Abyssal Plain (Site 374: The SSP, 1978d), Messinian gypsum and dolomite layers are present at 4,469.5 m below sea-level, and from 4,524 m below sea-level downwards consist of hard gypsum and salt deposits (Fig. 21).

According to Hsü et al. (1978a), most of today's Mediterranean basins already existed before the salinity crisis (Hsü et al., 1978b), they were basins with water depths of more than 1,000-1,500 m. During the Messinian age, part or all of the basin was aridified multiple times and the eastern and western Mediterranean basins were inundated by continental seawater from the Paratethys. They also stated that in Late Messinian the Balearic and the Tyrrhenian basins were flooded with water from the Atlantic,

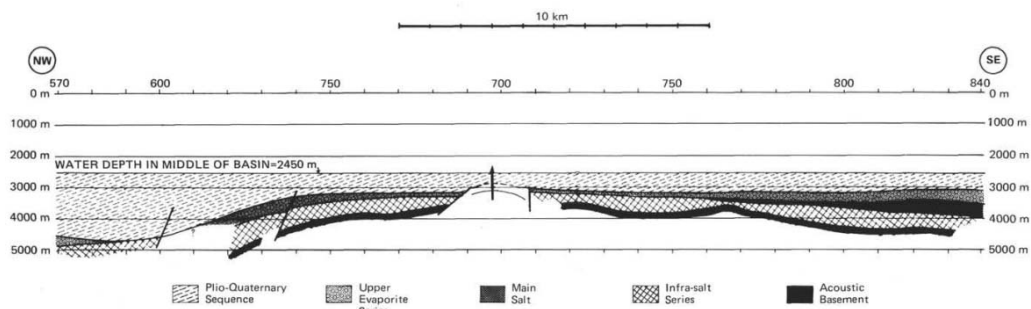


Figure 9. Twofold subdivision of the Mediterranean Evaporite. Note that the Upper Evaporite extends further toward the basin edge than the Lower Evaporite, which includes the main salt deposit. (a) Ligurian Sea near the northwestern corner of the Balearic Basin. The lower evaporite pinches out and the Pliocene/Quaternary sediments thicken toward the Rhone submarine fan area to the northwest. (b) South Balearic Abyssal Plain near Site 371 (location of which is indicated by vertical arrow). Note that both the upper and lower evaporite pinch out toward the top of the submarine high. The lower evaporite (Main Salt) is restricted to the more basinal position under the abyssal plain.

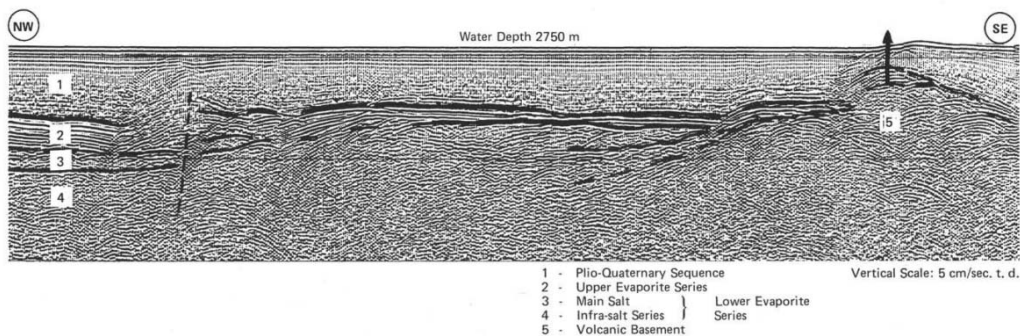


Fig. 21 Sketch section and seismic profile of the Mediterranean Evaporite in the Balearic Basin (after Hsü et al., 1978a).

but that their environment was not fully open oceanic, and that in Early Pliocene all basins in the Mediterranean were again submerged under deep open water, with further subsidence during Pliocene and Quaternary making the basins even deeper. Barber (1981) reported that detailed acoustic surveys of the Nile Delta showed evidence of onshore erosion in the Messinian salinity crisis down to the present depth of 2,500 m. These suggest that the Mediterranean Sea was probably terrestrial in Messinian up to its present depth of 2,500-3,000 m.

At the Atlantis II Deep in the northern Red Sea in the Indian Ocean (Sites 225: The SSP, 1974a; Site 227: The SSP, 1974e; Site 228: The SSP et al., 1974b), the Late Miocene evaporites are 1,400-2,000 m below sea-level and their upper surface corresponds to the seismic reflection surface S in the Red Sea (The SSP, 1974c). The Late Miocene evaporites of the Red Sea are similar to the Messinian evaporites of the Mediterranean Sea and probably were in a continuous or similar geological setting to them. On the continental margin of Oman (Site 724: SSP, 1989i; Site 726: SSP, 1989j; Site 728: SSP, 1989k; Site 729: SSP, 1989l), Early Pliocene clayey silts at 850-1,600 m below sea-level contain shallow-water benthic foraminiferal fossils, which were subsided after 3-4 Ma (Late Pliocene). At Site 262 (The SSP and Erickson, 1974), the Timor Trough on the northwestern margin of Australia, very shallow Pliocene marine dolomite and shell-calcareous sandstone at 2,725 m below sea-level is overlain by shallow marine foraminiferal dolomite and planktonic soft mud of Late Pliocene and Quaternary.

In the western part of the Great Australian Bight (Sites 1129: SSP, 2000d; Site 1131: SSP, 2000e; Site 1132: SSP, 2000c), a widespread Pleistocene zooxanthellate mound complex develops at 202.1-865.3 m below sea-level as a feature of cold-water carbonate deposits (Fig. 22). There is also a large Pliocene/Miocene hiatus or an unconformity at 759-865.3 m below sea-level (SSP, 2000e).

In the Pacific Ocean, Middle or Middle to Late Miocene shallow-water limestones are present at 603-734 m below sea-level in the western and the southern margins of the Queensland Plateau (Sites 812-814: SSP, 1991b-1991d) in the eastern Australia, with a gradual increase in water depth from Pliocene to upper bathyal environments. On the western slope at Site 824 (SSP, 1991e), Middle to Late Miocene biogenic reef limestone is present at 1,244.2 m below sea-level and Late Oligocene-Miocene reef limestone is present up to 1,403.8 m below sea-level.

In the Marion Plateau (Site 824: 1991e; Site 825: SSP, 1991a; Site 826: SSP, 1991f; Site 1193: SSP, 2002e) or the Marion Platform (Site 1194: SSP, 2002f; Site 1195: SSP, 2002g; Sites 1196 and 1199: SSP, 2002h), Early to Late Miocene terrestrial shelf carbonate or dolomitic reef limestones are present at 304-950 m below sea-level, overlying Pliocene semi-pelagic sediments. In some places, karst landforms developed while these Miocene carbonate reefs were exposed onshore during Late Miocene (SSP, 1991g). Lithological changes in the Marion Platform indicate that there was a relative sea-level lowering (uplift) at the boundary between the middle Miocene and the upper Miocene, exposing the carbonate platform; during Late Miocene, sea-level rise caused the carbonate platform to grow; and the last stage of growth exposed the seabed and caused soil formation, depositing the Pliocene in the upper unconformity and upper bathyal environment (SSP, 2002i). The unconformity between the lower Oligocene and the Pliocene and the complete absence of the Miocene in the Campbell Plateau, the southwest of New Zealand, suggests that Site 277 (The SSP, 1975f) in the southern Campbell Plateau may have been terrestrial during the Miocene epoch.

At the Bougainville Guyot (Site 831: SSP, 1992b) in the

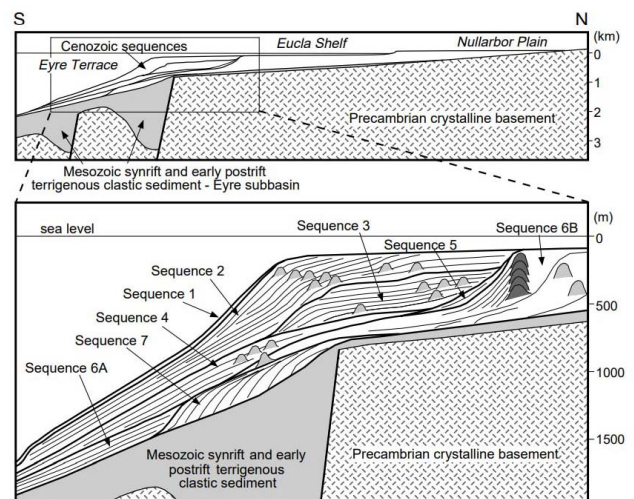


Fig. 22 Schematic north-south diagram from the Nullarbor Plain to the upper continental slope, across the Eyre Terrace (along longitude 128°E) in the Great Australian Bight, showing the distribution and internal relationships of seven Cenozoic sequences defined from seismic data, overlying Mesozoic synrift and early post-rift siliciclastic sequences and Precambrian crystalline basement. Note the distribution of reefs (dark shading) and biogenic mounds (light shading) within many of the Cenozoic sequences (after Feary and James, 1998). Vertical scales are approximate.

Vanuatu Island arc, Late Oligocene-Early Miocene coral reefs were present from 1,794 to 1,496 m below sea-level and continued to form upwards until late Middle Pleistocene, after which they submerged for 1,169 m.

At Sites 1109 (SSP, 2000f) and 1118 (SSP, 2000g) of the Woodlark Rise in the eastern Papua New Guinea, lagoon deposits are 2,883-3,160 m below sea-level and consist of Early to Middle Pliocene shallow-water (<150 m) sandstone and limestone or Early Pliocene or Late Miocene lagoonal limestone in the upper part, and Late Pliocene and later deposits of sandstone and siltstone in the upper bathyal zone. At Site 1115 (SSP, 2000h), Late Miocene inner continental shelf siltstone is located 1,662 m below sea-level and was deepened during Early Pliocene. In other words, the Woodlark Rise was onshore during Late Miocene and submerged for about 3,000 m after Pliocene.

In Site 451 (SSP, 1981) of the western Mariana Ridge, tuffs containing Late Miocene shallow-water fossil fragments are present at 2,106 m below sea-level. In the Yamato Basin of the Sea of Japan (Sites 794: SSP, 1990e and 795: SSP, 1990f), 3,330-3,896 m below sea-level was the middle bathyal zone (500 m in depth) during Middle Miocene, and 3,039 m below sea-level was the middle bathyal zone (500 m in depth) during Middle Miocene at the Okushiri Ridge (Site 796: SSP, 1990g) on the eastern margin of the Japan Sea Basin. In the southern part of the Japan Basin (Site 797: SSP, 1990h), 3,511.5 m below sea-level was the outer land shelf or slope of the delta during Early Miocene, and submerged during Middle Miocene to become the sea floor of the lower middle bathyal zone (1,500-2,000 m water depth). In other words, the deep-sea plain of the Japan Trench was terrestrial in Late Oligocene and the Japan Basin of the Sea of Japan was a land shelf in Early Miocene, both of which subsequently submerged to become the present-day deep-sea floor at a depth of more than 3,000 m. This suggests that both areas are the sea floors submerged by the global sea-level rise since Early Miocene, and that they were not structurally subducted.

On the upper landward slope of the west coast of Mexico (Site 489: SSP, 1982a; Site 493: SSP, 1982b), calcareous sandstones deposited on the outer land shelf during Early Miocene at 1,040-1,566.5 m below sea-level unconformably overlie the underlying biotite schist and diorite, and above which the middle Miocene-the Quaternary or the middle Miocene absent in places. At 2,347 m below sea-level there is a boundary between Early Miocene shallow-marine sediments and Middle Miocene-Quaternary pelagic sedimentary deposits, and this area was submerged after Middle Miocene. At Site 496 (SSP, 1982c) on the landward slope of the Guatemalan margin, there is Middle Miocene gravel layer deposited in shallow-water at 2,347 m below sea-level, with Middle Miocene-Quaternary pelagic sediments overlying it. At the northeastern end of the Cocos Ridge (Site 1242: SSP, 2003a) there is a hiatus between Middle Miocene nannofossil soft mud (12-13 Ma) and Late Pliocene nannofossil clay (0-2.5 Ma). There are also hiatuses lacking sediments between 12-8 Ma at 2,583 m below sea-level at Site 1238 (SSP, 2003b) and 1,894 m at Site 1239 (SSP, 2003c) on the Carnegie Ridge, the southeastern extension of the uplift in this area.

Quaternary diatom mud deposited in an outer continental shelf (50-150 m depth) environment at 421.3-743 m below sea-level on the upper continental slope of the Peru Trench (Site 686: SSP, 1988h; Site 687: SSP, 1988i), becoming an upper bathyal environment towards the top. On the lower continental slope of the Peru Trench (Site 688: SSP, 1988g), Miocene-Pliocene diatomite and mudstone alternation layers, containing benthic foraminiferal fossils, indicate that the lower Miocene (4,429.3-4,391.3 m below sea level) and the upper Miocene (4,240.3-4,286.3 m below sea level) were deposited in the upper-middle bathyal zone (500-1,500 m), which is thought to have been submerged by 500-1,500 m since Pleistocene.

Neogene and Quaternary shallow-water sediments of interest are the shallow-water sediments, including the Late Miocene evaporite beds, the unconformity and hiatus between the upper Miocene and Pliocene, and the deepening from Pliocene. Typical examples of this are the Late Miocene (Messinian) rock salt formations found in the Mediterranean Sea and the Red Sea. The Late Miocene gypsum and marl salt formations are found in the Mediterranean Sea at 4,469.5 m below sea-level in the Messina Abyssal Plain (Site 374), but otherwise between 2,100 and 2,400 m below sea-level in the Mediterranean Sea and 2,100-2,400 m below sea-level in the Red Sea.

For the rock salt layer at 4,469.5 m below sea-level at Site 374 (The SSP, 1978d), the water depth at the bottom of the basin would be 1,500 m, even if Messinian sea-level was at its present depth of 3,000 m. Hsü et al. (1978a) estimated that before the salinity crisis the water depth in the Mediterranean basin today was 1,000-1,500 m or more, and that during the salinity crisis some or all of them became arid. According to Kuroda et al. (2014), rock salt grows rapidly to a thickness of several hundred meters in just a few tens of thousands of years, even with sufficient water depth, without necessarily requiring complete evaporation once

the mother liquor is supersaturated. Based on these considerations, and assuming that the Messinian sea-level was at present-day depths of about 3,000 m, we consider that rock salt formations could form on the sea floor of the Messina Abyssal Plain at a depth of 1,500 m in a closed, arid and specific environment in the Mediterranean Sea.

The deepest Miocene shallow-water sediments are Middle Miocene calcareous claystone thought to have been deposited in the upper part of the upper middle bathyal zone (500 m in depth) at 3,895.7 m below sea-level in the northern Yamato Basin, in the Sea of Japan, Site 795 (SSP, 1990f), and the location of the Middle Miocene sea-level is estimated to be 3,395.7m lower than the present.

There are a number of phenomena such as unconformity and hiatus between the upper Miocene and the overlying Pliocene, or the rapid deepening of Pliocene from shallow-water environment; The unconformity at 2,359 m below sea-level in the upper Atlantic Continental Rise, Early Pliocene shallow-water deposits at 850-1,600 m below sea-level on the continental margin of Oman, the very shallow Pliocene marine dolomites and shell-calcareous sandstones at 2,725 m below sea-level on the western margin of Australia, the large Pliocene/Miocene hiatus or unconformities and shallow-water deposits of Late Miocene in the southern and eastern Australia, the post-Pliocene submergence in the Campbell Plateau and Early Pliocene or Late Miocene reef limestones at 2,883 m below sea-level in the Woodlark Rise, the eastern Papua New Guinea.

In particular, the Woodlark Rise (Site 1109: SSP, 2000f; Site 1118: SSP, 2000g) was terrestrial in Late Miocene and submerged by about 3,000 m since Pliocene, which, together with the distribution of rock salt beds in the Mediterranean, suggests that sea-levels in Late Miocene were about 3,000 m lower than the present. Hoshino (1962) estimated the position of the sea-level at the end of Miocene to have been 2,000 m lower than the present sea-level, based on the alignment of the terminal depths of the present-day submarine canyons and the deep-sea plains to 2,000 m water depth. However, the deep-sea drilling results indicate that the shallow-water sediments and terrestrial strata of Late Miocene are 3,000 m below the present sea-level, which in this paper is estimated to have been 1,000 m lower than the position of Hoshino (1962), or about 3,000 m below the present sea-level. The topography of the terminal bathymetry of present-day submarine canyons and deep-sea plains are, as they are located on continental or island arc margins, considered to have been raised by about 1,000 m or more due to the uplift of the terrestrial margin.

In the Miocene epoch, the sea-level rise was also particularly pronounced during Middle Miocene, with the formation of shallow-water limestones during Middle to Late Miocene and deepening of the sea from Middle Miocene observed in some areas. Sea-level rise since Middle Miocene is thought to have submerged the Sea of Japan by more than about 3,400 m.

For the Quaternary, 1,169 m of subduction occurred after late Middle Pleistocene at the Bougainville Guyot (Site 831: SSP, 1992b) in the Vanuatu Island arc. This phenomenon is considered evidence to support the theory of Shiba (2017, 2021a) that sea-level rise of 1,000 m after 430,000 years ago formed the topography of Suruga Bay and the Japanese Islands. The 1,000 m of sea-level rise after 430,000 years ago submerged land areas on the continental margin and created islands, which may have caused the endemism of animals isolated on these islands (Shiba, 2021b).

Sea-level rise since the Jurassic period

Hanada (1998), who listed the distribution of shallow-water sediments and volcanic rocks erupted in shallow-water and onshore areas from deep-sea drilling until Leg 159, and drew the following conclusions:

(1) There are 117 drilling sites where shallow-water sediments and volcanic rocks erupted in shallow-water and onshore areas from the deep-sea floor have been described, and their distribution is predominant at drilling sites conducted in uplifted terrain areas.

(2) The distribution of sediments and volcanic rocks suggested shallow-water is not clearly related to distance, age or depth from the mid-ocean ridges.

(3) The oldest shallow-water rocks on the deep-sea floor known from deep-sea drilling are from Triassic Norian (Sites 759 and

760) in the Indian Ocean, the Early Jurassic Sinemurian (Site 547) in the Atlantic and Middle Cretaceous Albian (Sites 317, 465, 866, 867, 868, 878 and 879) in the Pacific.

(4) The distribution of shallow-water indicating rocks on the deep-sea floor shows a chronological bias. The Cretaceous period is by far the most common, accounting for 40% of the total. This is followed by the Eocene (23%) and Miocene (17%). The depth distribution of the shallow-water strata in each period is shallow (<4,000 m) in the Cretaceous and becomes shallower in each successive period.

(5) Shallow-water indicating rocks are distributed at various depths. The reason for this is that the depth of their distribution varies in relation to the amount of uplift and sea-level rise in the area.

Regarding (1) of Hanada (1998), the results are similar in this paper: the distribution of drilling sites where shallow-water sediments and volcanic rocks erupted in shallow-water and terrestrial areas are described is predominant in drilling points conducted in uplifted terrain areas. Regarding (2), the relationship between the age and bathymetry of sediments and volcanic rocks suggestive of shallow-water sediments and measured at a distance from the mid-ocean ridge is not compared in this paper, but the age and bathymetry of sediments and volcanic rocks suggestive of shallow-water tend to be concentrated, which suggests they are not related to the distance from the mid-ocean ridge.

Regarding (3), the oldest shallow-water sediments known from the DSDP to the ODP are, in the Atlantic Ocean, the Late Triassic (Rhaetian-Hettangian) sandy mudstones or alluvial fan deposits of the Mazagan Escarpment in western Morocco. In the Indian Ocean, it is the Late Triassic (Carnian-Norian) carbonate reef deposit at the Wombat Plateau in the western Australia, or the Permian fluvial deposit at the Prydz Bay in the eastern Antarctica. In the Pacific Ocean, the Aptian-Albian shallow-water reef limestones of the Guyot and other areas.

Regarding (4), as for the chronological bias in the distribution of shallow-water indicating rocks on the deep-sea floor, as shown in Figs. 4 and 5, the shallow-water indicator such as reef limestones are concentrated in Jurassic, Late Jurassic-Early Cretaceous, Aptian-Albian, Early to Late Eocene, and Miocene. The reef limestones and other rocks found in these areas are often formed by submergence immediately after terrestrial volcanic activity, and the timing of these volcanic activities is just before or about the same time as the major sea-level rise period. The volcanic activity is thought to coincide with the period of large-scale volcanism in the Large Igneous Provinces (LIPs) on the sea floor that occurred at the same time as or just before these volcanic events.

As for the cause of the change in the present distribution depth of the rocks indicating shallow-water in (5), as already mentioned by Hanada (1998), it may be related to the amount of uplift and sea-level rise in the area.

The depth of distribution of shallow-water indicator on the deep-sea floor tends to become shallower from the oldest to the newest (Fig. 5). And from their distribution, assuming that they are not subducted, we can estimate the position of the sea-level at the respective epochs. Based on the results for each of the ages in the previous chapters, we can estimate that Late Jurassic sea-level was about 6,000 m lower than the present sea-level, about 5,200 m in Cretaceous Barremian, about 4,100 m in Late Albian, about 3,800 m in Early Eocene, about 3,400 m in Late Oligocene, about 3,400 m in Middle Miocene and about 3,000 m or more in Late Miocene, respectively.

Hoshino (2019) argued that the essence of the Earth is its micro-expansion, that the phenomena corresponding to its uplift are non-uplift, and that the Earth's surface does not sink unless there is volcanic activity or an ejection of water due to strata compression, and that since Jurassic the crust has been uplifted by the intrusion of tholeiitic basaltic magma from the upper mantle into the crust, and sea-levels have risen due to uplift of the sea floor. The author also believes that there was little crustal subsidence and that sea-levels have risen in stages over time since the Jurassic period. The periods of rapid sea-level rise since the end of Jurassic are also seen in Jurassic-Early Cretaceous, Aptian-Albian, Late Cretaceous, Early to Middle Eocene, Middle Miocene and Pliocene and later, based on deep-sea drilling results.

The dotted line shown in Fig. 5 is the estimated sea-level position from the deepest depth at which shallow-water indicating rocks were recovered for each age. However, this dotted line (sea-level rise curve) does not reflect the amount of sea-level rise inferred from carbonate reef thicknesses, such as >183 m in Late Cretaceous (Late Campanian-Maastrichtian), >540 m in Eocene

and >630 m in Miocene at the Eniwetok Atoll, nor the gradual and rapid sea-level rise since Jurassic. The actual sea-level rise during these ages would therefore have been greater, and the pre-Miocene sea-level position would have been lower than the respective chronological positions given here.

Sea-level rise curve based on the coastal onlap of the Haq's curve

Vail et al. (1977) proposed the seismic stratigraphy to assemble and analyses temporal stratigraphy from seismic sections of petroleum exploration, and Haq et al. (1987) constructed the third-order stratigraphic sequence deposition model based on it and proposed a sea-level curve for the post-Triassic period. A sedimentary sequence is a package of sedimentary layers bounded by a sequence boundary (Sequence boundary; Mitchum et al., 1977), defined as 'an unconformity surface and a contiguous offshore conformity surface', which is considered the most important stratigraphic model to reconstruct stratigraphic processes created from the practices of 20th century petroleum geologists. And at the same time, it provides important data for estimating the transgressive stage and the amount of sea-level rise.

The sedimentary sequence consists of the Lowstand Systems Tract (LST), which formed on submarine fans consisting mainly of the channel-levee complex as the sea-level fall from below, the Transgressive Systems Tract (TST), which formed on the land shelf as the sea-level rise, and the Highstand Systems Tract (HST), which accumulated offshore after the maximum sea-level rise of the transgression. The sedimentary sequence, a package of three sedimentary bodies (the systems tracts), is formed by the global sea-level change and can therefore be used to correlate with the global stratigraphy.

Haq et al. (1987) explained the mechanism of stratigraphic formation represented by the stratigraphic sequence deposition model by sea-level fluctuation and crustal subsidence. However, the author believes that the mechanism responsible for the formation of the strata is not sea-level fluctuation and crustal subsidence as described by Haq et al. (1987), but crustal uplift and consequent sea-level rise as described by Hoshino (1983, 1991). In this context, Shiba (1992) converted the Vail curve (coastal onlap curve) of Vail et al. (1977) into a sea-level rise curve and an uplift curve and estimated the sea-level rise since Jurassic to be 5,000 m. In the Vail curve, the Cretaceous part was only outlined and the details of the curve were unpublished.

In this paper, a sea-level rise and an uplift curve after the post-Jurassic are constructed using the coastal onlap curve of Haq et al. (1988) for the Mesozoic and Haq (1991) for the Cenozoic in the same way as Shiba (1992) (Fig. 23). The ages and age values in Fig. 23 follow Haq et al. (1988) and Haq (1991).

The sea-level rise curve presented in this paper (Fig. 23-ii) are directly integrated with the amount of sea-level rise in the coastal onlap curve (Fig. 23-i), while the uplift curve (which is itself not a curve but a staircase lines, Fig. 23-iii) interprets the sea-level fall in the coastal onlap curve as crustal uplift and changes the amount of fall into the amount of uplift, which is then integrated.

According to the sea-level rise curve (Fig. 23-ii), the sea-level rise since the end of Jurassic is estimated to be about 10,000 m, and from the boundary between Albian and Cenomanian at the end of Early Cretaceous about 7,500 m. On the other hand, the position of the sea-level at the end of Miocene is at 3,000 m according to the deep-sea drilling results (Fig. 5), whereas the sea-level rise curve (Fig. 23-ii) differs at 1,000 m. The values of the sea-level rise curve transformed from the Haq's coastal onlap curve (Fig. 23-ii) for each age are smaller after Oligocene and larger before Eocene than the sea-level positions for each age estimated from the deep-sea drilling results (Fig. 5) in this paper.

However, the sea-level rise curve (Fig. 23-ii) shows a sea-level rise of 1,000 m in Aptian-Albian (Early Cretaceous), which is consistent with the value estimated from the thickness of the coral reefs at Guyot. Sea-level rise estimated from reef-bearing limestone thicknesses such as >183 m in Late Campanian-Maastrichtian (Late Cretaceous) and >540 m in Eocene and >630 m in Miocene at the Eniwetok Atoll is also in agreement with the sea-level rise curve (Fig. 23-ii) of the Haq's coastal onlap better reflect the sea-level rise values.

In this paper, the sea-level rise curve (Fig. 23-ii) is assumed to be 3,000 m lower than at present during Late Miocene, and the dashed red line (Fig. 23-iv) is produced by moving the sea-level rise curve downwards by 2,000 m. This sea-level rise curves (Fig. 23-iv) show that the sea-level positions at the end of Jurassic and the end of Early Cretaceous are about 12,000 m and 9,500 m,

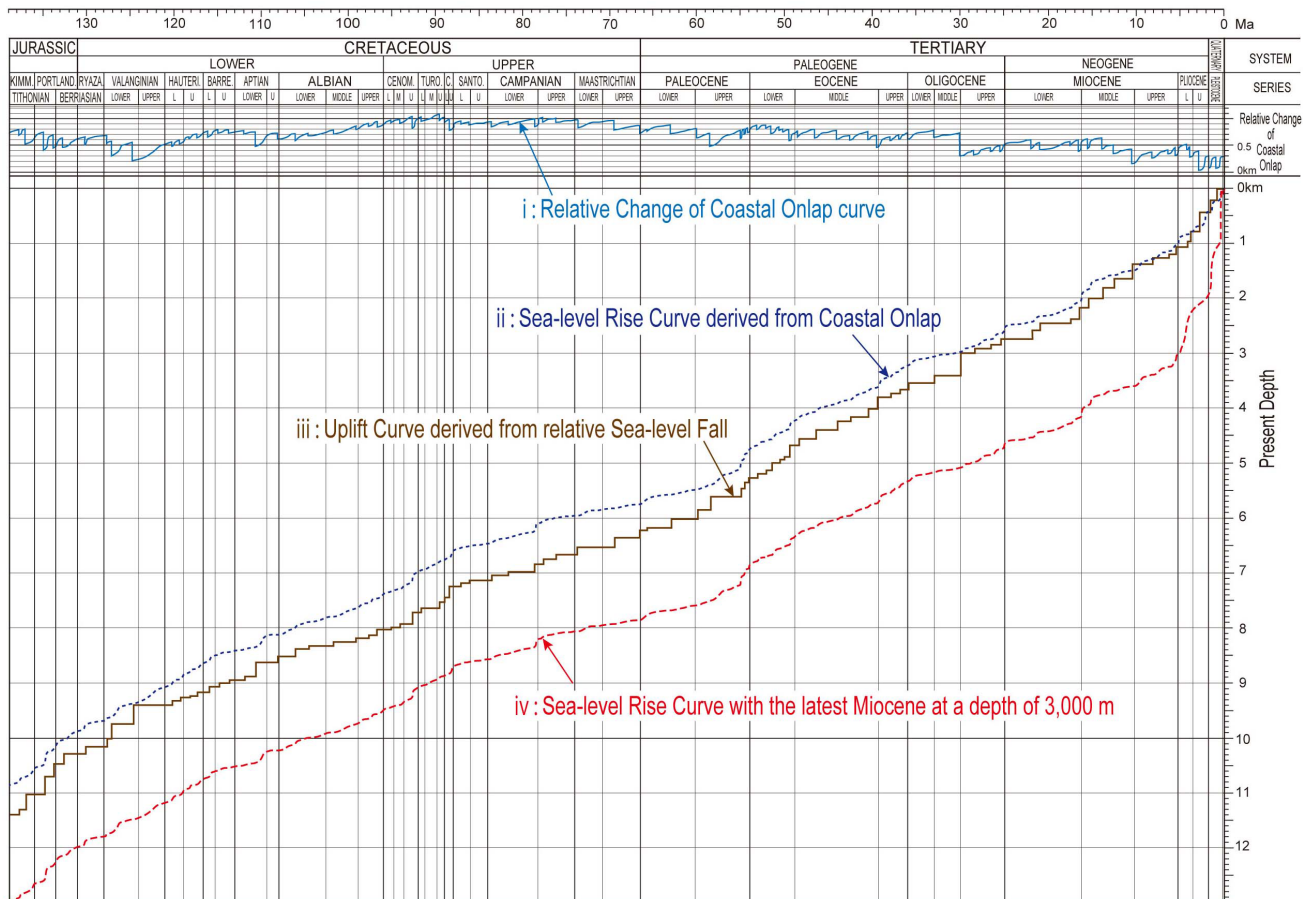


Fig. 23 Post-Jurassic sea-level rise (ii: dotted blue line) and uplift curves (iii: solid brown line) based on the relative sea-level curves from the relative change of coastal onlap (i) by Haq et al. (1988) and Haq (1991). The fourth curve (iv: dashed red line) is a sea-level rise curve with a depth of 3,000 m at the latest Miocene.

respectively. In particular, the location of Late Jurassic sea-level is consistent with the depth estimated by Sheridan et al. (1981) in the Gulf of Mexico-the Greater Bahamas Reef area (Fig. 7). Based on the newly proposed sea-level rise curve, the past shallow-water sediments and onshore volcanic rocks on the deep-sea floor considered in this paper may have moved vertically to a higher position (shallower sea floor) due to crustal uplift. On the other hand, it can be inferred that area that have been land since Jurassic have been uplifted to an even greater extent than those that have been ocean floor.

Deep-sea floor basement and its formation

According to Mullins and Lynts (1977), the Gulf of Mexico-the Greater Bahamas Reef area in the Atlantic Ocean consists of the pre-Triassic continental crust, which formed horsts and grabens in Late Triassic-Early Jurassic, and subsided thereafter, continuing that structure. In the southeast Greenland margin, the continental margin strata and continental basement are continuous to the ocean floor, where marine shales were deposited during Eocene, uplifted by west-trending faults, flattened by onshore erosion, and flattened by onshore basalt eruption, followed by erosion and eastward trending during Early Eocene and relative subsidence on the ocean floor (Larsen et al., 1994).

Devonian arkose sandstones recovered from the Goban Spur to the west of Britain are rocks that comprise the Hercynian Orogenic belt, and although not sedimentary rocks, serpentinites or serpentinitised peridotites of the western Iberian margin are also considered extensions of the terrestrial Hercynian Orogenic belt (Pinheiro et al, 1996). The Rio Grande Rise is a huge volcanic island of unconformable basaltic lava from mid-Late Cretaceous (90-80 Ma) overlying Proterozoic granites and metamorphic rocks, with a shoreline fringed by limestone reefs, which submerged during Eocene to form the middle bathyal zone, and then

uplifted into a dome shape during Eocene with igneous activity and flattened by land erosion at the top of the swelling, which was subsequently submerged (Yano, 2021). The Guatemalan margin is also composed of an ophiolitic base of the Central American continental skeleton belonging to the Laramie Orogeny (SSP, 1985f).

Other areas where pre-Jurassic basement rocks have been recovered include the Falklands Plateau, the Wombat Plateau and Tasman Rise around Australia in the Indian Ocean, and the Prydz Bay in the eastern Antarctica, where the continental margin and its extension are considered to be essentially submerged continental crust. The area of continental basement revealed in the north Atlantic extends to the Goban Spur, and the continental margin, including the Continental Rise on the east coast of North America and the southeast Greenland margin, as well as the Mid-Atlantic Ridge region, may be continental crust. It is also possible that parts of the deep-sea floor in the north Atlantic Ocean that are considered to be oceanic crust may also be continental crust.

The distribution of the basement rocks recovered by deep-sea drilling in the Atlantic and Indian Oceans suggests that the deep-sea floor of the Atlantic and Indian Oceans was, until the end of Paleozoic Era, a terrestrial area composed of basement rocks of the Proterozoic and the Hercynian Orogenic belt. The combination of active host-graben movements and tilted-blocks formation by rifting in Triassic, flood basalts on the continent or sea floor and consequent sea-level rise after Jurassic, and submergence of the rift areas (ocean basins) with low uplift, are considered to have resulted in deepening of the ocean by a large-scale sea-level rise after Cretaceous.

Hoshino (2014) inferred the presence of continental crust at the base of the Mid-Atlantic Ridge by showing a lot of xenoliths of continental rocks in the basaltic rocks of the islands of the Mid-Atlantic Ridge. Yano et al. (2009, 2011) reported continental rocks and rocks with geochemical features derived from continental lithospheric material from the deep-sea floor of the continental margins, ridges and basin wings in the Atlantic and Indian Oceans. Based on this, Yano et al. (2009, 2011) described the possibility of a widespread distribution of continental crust beneath the deep-sea floor of the Atlantic and Indian Oceans (Fig. 24).

These facts suggest that what was previously regarded as oceanic crust on the deep-sea floor of the Atlantic and Indian Oceans may be the Proterozoic or the Paleozoic Orogenic belts. It was submerged from Jurassic onwards and at the same time became sites of large-scale basalt volcanism (LIPs). The basaltic lava then erupted and overlapped thickly, and the sea-level rise caused by the deposition of basaltic lava on the sea floor is thought to have deepened the sea floor and made it a deep-sea floor.

Regarding the Pacific Ocean, Yano et al. (2011) stated that reports of continental rocks on the ocean floor indicate that few continental rocks have been found on the Pacific floor, even taking into account differences in survey density. Vasiliev (2006, 2009) attributed this to the fact that the Pacific Ocean crust is different from the Atlantic and Indian Oceans, reflecting its inherently

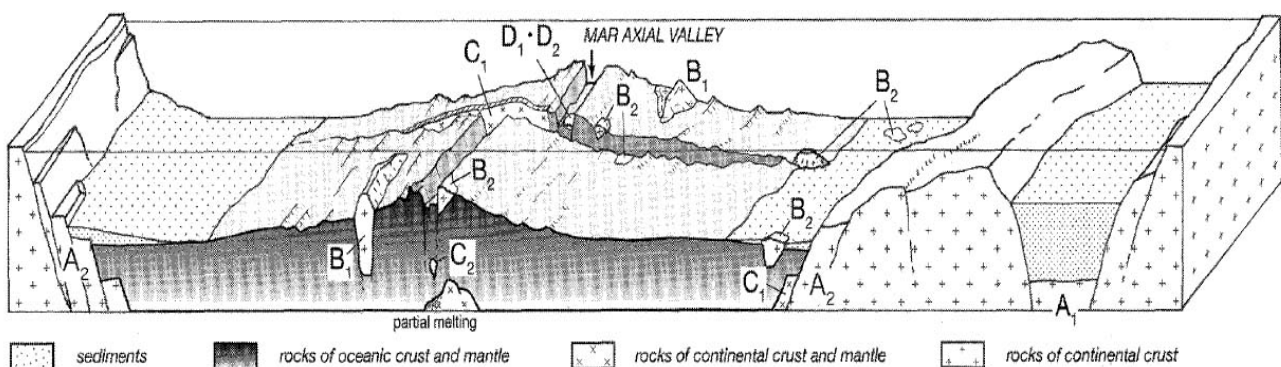


Fig. 24 Schematic diagram showing the classification of ancient and continental rocks in the Atlantic Ocean (after Yano et al., 2011). Ancient and continental rocks exaggerated due to their small spatial extents. Type A: continental blocks in ocean/continent transition zones, submerging deeper than ocean floor (A1: beneath sedimentary basins in continental margins, A2: in ocean margins), B: continental materials in ocean floor (B1: block, B2: rock masse to mineral in size), C: crust and upper mantle materials geochemical of continental nature (C1) and volcanics derived from their partial melting (C2), D: fossiliferous sediments (D1) and mafic rocks (D2) significantly older than estimated ages of adjacent oceanic plates. MAR: Mid-Atlantic Ridge.

Geological-structural stage	Geologic age	Lithologic structure	Constituent	Component rocks	Remarks
THIRD	Cenozoic	reef limestone seamount, plateau & rise	sea water		forming the present topographic-geologic structure of the mega-basin block subsidence of the Pacific mega-basin (≈ 6 km)
		horst graben	sediments volcanics	pillow basalt, hyaloclastite, tuff	
SECOND	Jurassic		volcanics & intrusives	pillow basalt, tuff, breccia, tuffaceous sediments, intrusions	accumulated in shallow marine environments
			massive plutonics	olivine gabbro-norite, gabbro, gabbro-diabase, metagabbro, epidote amphibolite (originated from diabase)	underlying most part of the Pacific mega-basin
FIRST	Triassic		layered basic intrusions	plagioclase wehrlite, websterite, orthopyroxenite, troctolite	structural unconformity
			cumulates		
FIRST	Archean (3.5 Ga)		acidic rocks	epidote-amphibolite schist, amphibolite schist, epidote amphibolite, pyroxene-plagioclase metamorphic rock, chlorite-talc rock, serpentinite (garnite, gneiss, granulite)	outcropping at trenches, fracture zones and plateaus
			metamorphics		
			ultrabasics	dunite, lherzollite, wehrlite, garnet peridotite, garnet pyroxenite	occurring as nodules in volcanic rocks on oceanic islands

Fig. 25 Basic structure of the Pacific Giant Basin (after Vasiliev, 2006).

mafic composition.

Vasiliev (2006) identified the following three geological-structural stages in the uppermost mantle-crustal structure of the Pacific basin floor (Fig. 25). The first stage consists of metamorphic rocks such as serpentinite, hornblende and glaucophane hornblende schist of harzburgite origin, the oldest of which date back to the Archean Eon, and the mantle host rock from which these ejecta magmas were separated is estimated to be about 3.5 billion years old. The second stage consists of layered basic intrusive rocks, such as olivine-hanleyite-norite, and is found without exception in major topographic uplifts. The upper part consists of pillow lava, tuff and conglomerate, almost completely covering the bottom of the Pacific megabasin, and together with the volcanic rocks of the third stage, constitutes the second layer of the oceanic crust, which is 2-3 km thick over most of this vast area. The majority of the ejecta rocks show a tholeiite-subalkaline basalt composition, formed in a shallow-water environment and similar to continental flood basalt in chemical composition. The third stage is Late Jurassic-Cenozoic volcanism and sedimentary action, the duration of which varies from region to region. Sedimentary layers are generally 200-500 m thick, but can reach up to 1,200 m in rift valleys. The Pacific Ocean has subsided significantly since the Late Jurassic period. This sedimentation takes the form of block movements, with the timing and rate of sedimentation differing from one block to another. The earliest sedimentation events occurred in the western equatorial area of the Giant Basin, where the base of the sedimentary layer consists of Middle Jurassic sediments, with an accumulated sedimentation volume reaches 6 km.

In other words, according to the view of Vasiliev (2006), the rocks of the first stage of the Pacific Basin are the Archean basement, the rocks of the second stage may span the Proterozoic to Paleozoic, the rocks of the third stage consist of volcanic rocks and sediments from Late Jurassic onwards and what is considered oceanic crust consists of the volcanic rocks of the upper second and third stages. In the Pacific Ocean, the eruption of basaltic lava of the Large Igneous Provinces (LIPs) in the Pacific Basin after Late Jurassic caused significant submergence of the Pacific Basin due to sea-level rise. The total sedimentation rate since Middle Jurassic is estimated to have reached 6,000 m.

Note that in the southern part of the northwest Pacific Basin, the northern part of the Central Basin and the vast area between 20°N and 45°N in the northeast Pacific Basin, Neogene-Quaternary sediments are almost completely absent (Vasiliev, 2006). This suggests that there was large-scale flood basalt activity in these areas of the Pacific Basin during Neogene-Quaternary. This widespread flood basalt activity during Neogene-Quaternary may have contributed significantly to the large-scale sea-level rise since Neogene.

Supplementary table

This table shows the sites where shallow-water sediments and volcanic rocks of subaerial eruption were found in the drilling records from DSDP to ODP. This table lists the location (latitude and longitude), water depth (Depth), penetration depth (Penetr.), depth below sea floor of finding shallow-water indicator rocks (Dep. F), depth below sea-level (Dep. Sl), and age (Age) and content (Sediments and rocks) where shallow-water indicator rocks have been recovered from deep-sea drilling. Sites marked with * are those already listed in Hanada (1998). Neog.: Neogene, Paleog.: Paleogene, Creta.: Cretaceous, Jura.: Jurassic, Trias.: Triassic, Perm.: Permian, Devon.: Devonian, Mediter.: Mediterranean Sea.

Leg	Site	Ocean	Area or Position	Lat.	Long.	Depth	Penetr.	Dep.F	Dep.Sl	Period	Age	Sediments and rocks
3	21 *	Atrantic	Rio Grande Rise	28°35.10'S	30°35.85'W	2,102.0	133.0	105.9	2,207.9	Creta.	Maastrichtian	Algal limestone
3	21 *	Atrantic	Rio Grande Rise	28°35.10'S	30°35.85'W	2,102.0	133.0	38.0	2,140.0	Neog.		L. Pliocene/M. Eocene unconformity
4	25 *	Atrantic	NE. of Brazil	0°31.00'S	39°14.40'W	1,916.0	66.0	54.9	1,970.9	Neog.	Pre-M. Miocene	Shallow algal limestone
10	86 *	Mexico	Champeche Bank	22°52.48'N	90°57.75'W	1,462.0	686.0	610.0	2,072.0	Creta.	Albian	Shallow-water limestone
10	94 *	Mexico	Champeche Bank	24°31.64'N	88°28.16'W	1,793.0	660.0	635.0	2,428.0	Creta.	Albian	Shallow-water limestone
10	94 *	Mexico	Champeche Bank	24°31.64'N	88°28.16'W	1,793.0	660.0	425.0	2,218.0	Paleog.		L. Eocene/M. Eocene unconformity
10	94 *	Mexico	Champeche Bank	24°31.64'N	88°28.16'W	1,793.0	660.0	290.0	2,083.0	Neog.		L. Miocene/E. Miocene unconformity
10	94 *	Mexico	Champeche Bank	24°31.64'N	88°28.16'W	1,793.0	660.0	52.0	1,845.0	Neog.		L. Pleistocene/L. Pliocene unconformity
10	95 *	Mexico	Champeche Bank	24°09.00'N	86°23.85'W	1,633.0	463.0	438.0	2,071.0	Creta.	Albian	Shallow-water dolomite
12	111 *	Atrantic	Orphan Knoll	50°25.57'N	46°22.05'W	1,797.0	250.0	189.0	1,986.0	Creta.	Albian-Cenomanian	Calcareneite, shelly limestone
12	117 *	Atrantic	Rockall Bank	57° 20.17'N	15° 23.97'W	1,038.0	313.0	303.0	1,341.0	Paleog.	L. Paleocene	Basaltic sandstone
14	144 *	Atrantic	Demerara Rise	9° 27.23'N	54° 20.52'W	2,957.0	327.0	280.0	3,237.0	Creta.	E. Aptian-L. Albian	Marlstone with shelly limestone
17	171 *	Pacific	Horizon Guyot	19°07.9'N	169°27.6'W	2,295.0	479.0	345.0	2,640.0	Creta.	Aptian-Albian	Reef limestone
19	192 *	Pacific	Meiji Guyot	53°00.57'N	164°42.81'E	3,014.0	1,057.0	1,044.0	4,058.0	Creta.	Pre-Maastrichtian	Subaerial erupted basalt and trachyte lava
20	202 *	Pacific	Ita Mai Tai Guyot	12°48.9'N	156°57.2'E	1,015.0	153.5	74.0	1,579.0	Paleog.	Pre-Eocene	Ooid limestone
21	207 *	Pacific	Lord Howe Rise	36°57.75'S	165°26.06'E	1,389.0	513.0	309.0	1,698.0	Creta.	Maastrichtian	Glauconitic sandstone
21	207 *	Pacific	Lord Howe Rise	36°57.75'S	165°26.06'E	1,389.0	513.0	357.0	1,746.0	Creta.	Maastrichtian	Subaerial erupted rhyolite
21	209 *	Pacific	Queensland Plateau	15°56.19'S	152°11.27'E	1,428.0	344.0	275.0	1,703.0	Paleog.	M. Eocene	Shallow-water foraminifer limestone
21	209 *	Pacific	Queensland Plateau	15°56.19'S	152°11.27'E	1,428.0	344.0	357.0	1,785.0	Paleog.	M. Eocene	Shallow-water foraminifer limestone
22	214 *	Indian	Ninety east Ridge	11°20.21'S	88°43.08'E	1,665.0	494.5	390.0	2,055.0	Paleog.	Paleocene	Pyroclastic rock
22	216 *	Indian	Ninety east Ridge	1°27.73'N	90°12.48'E	2,247.0	477.5	457.0	2,704.0	Creta.	L. Maastrichtian	Tuff, Chalk, Clay
22	217 *	Indian	Ninety east Ridge	8°55.57'N	90°32.33'E	3,020.0	663.5	600.0	3,620.0	Creta.	L. Campanian	Dolomite
23	219 *	Indian	Laccadive-Chagos Ridge	9°01.75'N	72°52.07'E	1,764.0	411.0	280.0	2,044.0	Paleog.	L. Paleocene	Limestone, Sandstone, Siltstone
23	225 *	Indian	Red Sea	21°18.58'N	38°15.11'E	1,228.0	230.0	176.0	1,404.0	Neog.	L. Miocene	Evaporite
23	227 *	Indian	Red Sea	21°19.86'N	38°07.97'E	1,795.0	359.0	229.0	2,024.0	Neog.	L. Miocene	Evaporite
23	228 *	Indian	Red Sea	19°05.10'N	39°00.20'E	1,038.0	325.0	287.0	1,325.0	Neog.	L. Miocene	Anhydrite and siltstone
24	237 *	Indian	Mascarene Plateau	07°04.99'S	58°07.48'E	1,623.0	693.5	402.0	2,025.0	Paleog.	L. Paleocene	Calcareous nannofossils dominate
25	246 *	Indian	Madeagascar Ridge	33°37.21'S	45°09.60'E	1,030.0	203.0	125.0	1,155.0	Paleog.	E. Eocene	Calcareous volcanic sandstone
26	253 *	Indian	Ninety east Ridge	24°52.65'S	87°21.97'E	1,962.0	559.0	405.0	2,367.0	Paleog.	M. Eocene	Volcanic ash
26	254 *	Indian	Ninety east Ridge	30°58.15'S	87°53.72'E	1,253.0	343.5	200.0	1,453.0	Paleog.	L. Eocene-E. Oligocene	Basaltic sandstone
26	255 *	Indian	Broken ridge	31°07.87'S	93°43.72'E	1,144.0	108.5	75.0	1,219.0	Creta.	Santonian	Limestone
26	255 *	Indian	Broken ridge	31°07.87'S	93°43.72'E	1,144.0	108.5	75.0	1,219.0			M. Eocene/Santonian unconformity
27	262 *	Indian	Timor Trough	10°52.19'S	123°50.78'E	2,298.0	442.0	427.0	2,725.0	Neog.	Pliocene	Dolomite and calcareous sandstone
28	264 *	Indian	Naturaliste Plateau	34°58.13'S	112°02.68'E	2,873.0	215.5	171.0	3,044.0	Creta.	Cenomanian or older	Volcaniclastic conglomerate
28	270 *	Southern	Ross Sea	77°26.48'S	178°30.19'W	634.0	427.5	383.3	1,017.3	Paleog.	L. Oligocene	Glauconitic sandstone
28	273 *	Pacific	Ross Sea	74°32.29'S	174°37.57'E	495.0	346.5	42.5	537.5	Neog.	L. -M. Miocene	Semifossilified pebbly sand-silt
29	277 *	Pacific	Campbell Plateau	52°13.43'S	166°11.48'E	1,232.0	472.5	10.0	1,242.0			Pliocene/E. Oligocene unconformity
29	281 *	Indian	Tasman Rise	47°59.84'S	147°45.85'E	1,591.0	169.0	160.0	1,751.0	Paleog.	L. Eocene	Glauconitic sandstone
30	289 *	Pacific	Ontong-Java Plateau	00°29.92'S	158°30.69'E	2,224.0	1,271.0	1,262.0	3,486.0	Creta.	Pre-Aptian	Limestone
31	296 *	Pacific	Palau-Kyushu Ridge	29°20.41'N	133°31.52'E	2,958.0	1,087.0	453.0	3,411.0	Paleog.	L. Oligocene	Shallow-water pyroclastic rock
32	308 *	Pacific	Koko Guyot	34°58.94'N	172°08.98'E	1,346.0	68.5	0.0	1,346.0	Paleog.	E. Eocene	Biogenic volcanic sandstone
32	309 *	Pacific	Koko Guyot	34°54.32'N	171°33.67'E	1,470.0	12.0	0.0	1,470.0	Paleog.	L. Oligocene-E. Miocene	Biogenic volcanic sandstone
33	317 *	Pacific	Manihiki Plateau	11°00.09'S	162°15.78'W	2,613.8	943.5	910.0	3,523.8	Creta.	Pre-Barremian-Aptian?	Basalt
36	327 *	Atrantic	Falkland Plateau	50°52.28'S	46°47.02'W	2,411.0	469.5	324.0	2,735.0	Creta.	Neocomian?-Aptian	Sapropelic claystone
36	330 *	Atrantic	Falkland Plateau	50°55.19'S	46°53.00'W	2,636.0	575.5	271.5	2,907.5	Jura.-Creta.	Oxfordian-Aptian	Sapropelic claystone
38	336 *	Atrantic	Iceland-Faeroe Ridge	63°21.06'N	7°47.27'W	830.0	515.0	484.5	1,314.5	Paleog.	Pre-M. Eocene	Subaerial erupted basalt
38	338 *	Atrantic	Vøring Plateau	67°47.11'N	5°23.26'E	1,297.0	427.5	285.0	1,582.0	Paleog.	E. Eocene	Glauconitic sandstone
38	349 *	Atrantic	Jan Mayen ridge	69°12.41'N	8°05.80'W	928.0	319.5	119.6	1,047.6	Paleog.	L. Eocene	Sandstone
39	356 *	Atrantic	São Paulo Plateau	28°17.22'S	41°05.28'W	3,175.0	741.0	708.0	3,883.0	Creta.	Albian	Dolomitic and calcareous mudstone
39	357 *	Atrantic	Rio Grande Rise	30°00.25'S	35°33.59'W	2,086.0	796.5	358.0	2,444.0	Paleog.	M. Eocene	Fossil bearing volcanic breccia
40	363 *	Atrantic	Walvis ridge	19°38.75'S	9°02.80'E	2,247.0	715.0	696.0	2,943.0	Creta.	E. Aptian	Shallow-water limestone
40	364 *	Atrantic	Angora Continental Margin	11°34.32'S	11°58.30'E	2,439.0	427.5	427.5	2,866.5	Creta.	L. Aptian-E. Albian	Dolomitic limestone and sapropels
42-1	374 *	Mediter.	Messina Abyssal Plain	35°50.87'N	18°11.78'E	4,088.0	457.0	381.5	4,469.5	Neog.	L. Miocene	Dolomitic mudstone and Gypsum
42-1	375 *	Mediter.	Florence Rise	34°45.74'N	31°45.58'E	1,914.0	821.5	137.5	2,051.5	Neog.	L. Miocene	Gypsum and marlstone
42-1	376 *	Mediter.	Florence Rise	34°52.32'N	31°48.45'E	2,117.0	216.5	140.5	2,257.5	Neog.	L. Miocene	Gypsum and marlstone
42-1	378 *	Mediter.	North Creta basion	35°55.67'N	25°06.97'E	1,445.0	343.5	308.0	2,153.0	Neog.	L. Miocene	Gypsum
43	384 *	Atrantic	J-Anomaly ridge	40°21.65'N	51°39.80'W	3,919.0	330.3	202.0	4,121.0	Creta.	Barremian-Aptian/Albian	Shallow-water bioclastic limestone
44	390 *	Atrantic	Blake Nose	30°08.54'N	76°06.74'W	2,656.5	206.0	161.4	2,817.9	Creta.	Barremian	Shallow-water limestone
44	392 *	Atrantic	Blake Nose	29°54.63'N	76°10.68'W	2,606.5	349.0	99.0	2,705.5	Creta.	E. Barremian	Shallow-water limestone
48	401 *	Atrantic	Biscay Margin	47°25.65'N	8°48.62'W	2,555.5	341.0	247.0	2,802.5	Creta.	L. Aptian-Tithonian	Bioclastic limestone
48	402 *	Atrantic	Biscay Bay	47°52.48'N	8°50.44'W	2,355.5	469.5	175.0	2,530.5	Creta.	Aptian-Albian	Shallow-water limestone
48	403 *	Atrantic	Rockall Bank	56°08.31'N	23°17.64'W	2,317.0	489.0	260.0	2,577.0	Paleog.	L. Paleocene-M. Eocene	Volcaniclastics and mudstones
48	404 *	Atrantic	Rockall Bank	56°03.13'N	23°14.95'W	2,322.0	389.0	294.0	2,616.0	Paleog.	L. Paleocene-M. Eocene	Volcaniclastics and mudstones

Leg	Site	Ocean	Area or Position	Lat.	Long.	Depth	Penetr.	Dep.F	Dep.SI	Period	Age	Sediments and rocks
55	430A *	Pacific	Ojin Seamount	37°59.29'N	170°35.86'E	1,485.5	118.0	0.0	1,485.5	Paleog.	L. Paleocene -E. Eocene	Shallow-reef calcareous ooze and sand
55	430A *	Pacific	Ojin Seamount	37°59.29'N	170°35.86'E	1,485.5	118.0	59.3	1,544.8	Paleog.	L. Paleocene or older	Subaerially erupted basalt lava
55	432 *	Pacific	Nintoku Seamount	41°20.03'N	170°22.74'E	1,320.0	74.0	42.5	1,362.5	Paleog.	L. Paleocene or older	Subaerially erupted basalt lava
55	433 *	Pacific	Suiko Seamount	44°46.60'N	170°01.26'E	1,874.0	174.0	52.5	1,926.5	Paleog.	Paleocene	Reef limestone
56/57	439 *	Pacific	Japan Trench	40°37.61'N	143°18.63'E	1,666.0	1,157.5	1,098.0	2,764.0	Paleog.	L. Oligocene	Subaerial conglomerate
59	451 *	Pacific	West Mariana Ridge	18°00.88'N	143°16.57'E	2,070.0	930.5	36.0	2,106.0	Neog.	L. Miocene	Vitic tuff
62	465 *	Pacific	Southern Hess Rise	33°49.23'N	178°55.14'E	2,165.5	476.0	411.7	2,577.2	Creta.	L. Aptian or older	Subaerially erupted trachyte lava
66	489 *	Pacific	Middle America Trench	16°16.19'N	99°01.13'W	1,266.5	327.0	300.0	1,566.5	Neog.	E. Miocene	Calcareous sandstone
66	493 *	Pacific	Middle America Trench	16°22.86'N	98°55.53'W	675.0	670.5	365.0	1,040.0	Neog.		L. Miocene/E. Miocene unconformity
66	494 *	Pacific	Middle America Trench	16°22.86'N	98°55.53'W	675.0	670.5	652.0	1,327.0	Neog.		E. Miocene/Dioltite unconformity
67	496 *	Pacific	Middle America Trench	13°03.82'N	90°47.71'W	2,064.0	378.0	283.0	2,347.0	Neog.	E. Miocene	Shallow-water conglomerate
71	511 *	Atrantc	Fotland Plateau	51°00.28'S	46°58.30'W	2,602.0	632.0	432.5	3,034.5	Jura.-Creta.	L. Jurassic-Albian	Shallow-water black shale
72	516 *	Atrantc	Rio Grande Rise	30°16.59'S	35°17.10'W	1,327.9	1,270.6	1,248.6	2,576.5	Creta.	Campanian	Skeletal grainstone
74	525 *	Atrantc	Walvis Ridge	29°04.24'S	2°59.12'E	2,478.9	678.1	575.0	3,053.9	Creta.	Campanian	Basalt lava and marl limestone
74	526 *	Atrantc	Walvis Ridge	30°07.36'S	3°08.28'E	1,065.5	356.0	221.6	1,287.1	Paleog.	L. Paleocene-M. Eocene	Fossiliferous limestone
77	540	Mexico	Straits of Florida	23°49.73'N	84°22.25'W	2,940.5	745.4	417.0	3,357.5	Creta.	Senonian	Limestone
79	544 *	Atrantc	Mazagan Escarpment	33°46.0'N	9°24.3'W	3,617.0	235.0	103.8	3,720.8	Jura.	Oxfordian	Shallow-water Limestone
79	545 *	Atrantc	Mazagan Escarpment	33°39.86'N	9°21.88'W	3,160.0	701.0	530.7	3,690.7	Creta.	Neocomian?	Dolomitic shallow-water limestone
79	546 *	Atrantc	Mazagan Escarpment	33°46.71'N	9°33.86'W	4,002.0	192.0	155.5	4,157.5	Jura.-Trias.	Rhaetian-Hettangian	Layered salt rock
79	547 *	Atrantc	Mazagan Escarpment	33°46.84'N	9°20.98'W	3,951.0	1,030.0	923.5	4,874.5	Jura.-Trias.	Rhaetian-Hettangian	Sandy mudstone
80	548 *	Atrantc	Goban Spur	48°54.93'N	12°09.87'W	1,256.0	551.5	535.5	1,791.5	Devon.	M. Devonian	Quartzitic sandstone
80	549 *	Atrantc	Goban Spur	49°05.28'N	13°05.88'W	2,533.0	1,001.5	964.5	3,497.5	Devon.	M.-L. Devonian	Sandstone
80	549 *	Atrantc	Goban Spur	49°05.28'N	13°05.88'W	2,533.0	1,001.5	673.9	3,206.9	Creta.	E. Barremian	Shallow-water limestone
81	552 *	Atrantc	Rockall Plateau	56°02.56'N	23°13.88'W	2,315.0	314.0	193.5	2,508.5	Paleog.	E. Eocene	Tuff
81	553 *	Atrantc	Rockall Plateau	56°05.32'N	23°20.61'W	2,339.0	682.5	261.5	2,600.5	Paleog.	E. Eocene	Tuff
81	554 *	Atrantc	Rockall Plateau	56°17.4'N	23°31.69'W	2,584.0	209.0	118.8	2,702.8	Paleog.	E. Eocene	Zeolitic tuffaceous marlstone
81	555 *	Atrantc	Hatton Bank	56°33.70'N	20°46.93'W	1,669.0	964.0	320.0	1,989.0	Paleog.	E. Eocene	Tuffaceous glauconitic sandstone
84	566	Pacific	Middle America Trench	12°48.84'N	90°41.53'W	3,673.0	136.6	109.1	3,782.1		Pre-Late Miocene	Serpentinized peridotite
84	567	Pacific	Middle America Trench	12°42.96'N	90°55.99'W	5,529.0	501.0	368.0	5,897.0		Pre-Campanian	Ophiolite complex
84	569	Pacific	Middle America Trench	12°56.22'N	90°50.81'W	2,814.0	364.9	351.0	3,165.0		Pre-Eocene	Metamorphosed gabbro and diabase
84	570	Pacific	Middle America Trench	13°17.12'N	91°23.57'W	1,718.2	401.9	374.0	2,092.2		Pre-E. Eocene	Serpentinized peridotites
93	605	Atrantc	Continental Rise	38°44.53'N	72°36.55'W	2,207.0	816.7	152.0	2,359.0	Neog.		Pleistocene/M. Eocene unconformity
95	612	Atrantc	Continental Rise	38°49.21'N	72°46.43'W	1,414.3	675.3	36.9	1,451.2	Neog.		U. Pleistocene/U. Pliocene unconformity
95	612	Atrantc	Continental Rise	38°49.21'N	72°46.43'W	1,414.3	675.3	88.1	1,502.4	Neog.		L. Pliocene/U. Miocene unconformity
95	612	Atrantc	Continental Rise	38°49.21'N	72°46.43'W	1,414.3	675.3	136.2	1,550.5	Neog.		U. Miocene/E. Oligocene unconformity
95	612	Atrantc	Continental Rise	38°49.21'N	72°46.43'W	1,414.3	675.3	181.4	1,595.7	Neog.		U. Eocene/M. Eocene unconformity
95	612	Atrantc	Continental Rise	38°49.21'N	72°46.43'W	1,414.3	675.3	323.4	1,737.7	Neog.		M. Eocene/L. Eocene unconformity
95	612	Atrantc	Continental Rise	38°49.21'N	72°46.43'W	1,414.3	675.3	559.4	1,973.7	Creta.		L. Eocene/M. Maestrichtian unconformity
95	612	Atrantc	Continental Rise	38°49.21'N	72°46.43'W	1,414.3	675.3	639.6	2,053.9	Creta.		L. Maestrichtian/U. Campanian unconformity
95	613	Atrantc	Continental Rise	38°46.26'N	72°30.43'W	2,333.2	581.9	268.3	2,601.5	Neog.		Pliocene/Miocene unconformity
95	613	Atrantc	Continental Rise	38°46.26'N	72°30.43'W	2,333.2	581.9	278.0	2,611.2	Neog.		Miocene/M. Eocene unconformity
101	627	Atrantc	Southern Blake Plateau	27°38.1'N	78°17.65'W	1,036.0	1,572.0	468.0	1,504.0	Creta.	L. Albian	Dolomites, limestones, and gypsum
103	637	Atrantc	Galicja Bank	42°05.3'N	12°51.8'W	5,321.0	285.6	212.0	5,533.0		Pre-L. Miocene	Serpentinized peridotite
103	639 *	Atrantc	Galicja margin	42°08.6'N	12°15.3'W	4,753.0	293.1	196.8	4,949.8	Jura.	Tithonian	Dolomite (Shallow-water limestone)
107	654	Mediter.	Upper Sardinian Margin	40°34.76'N	10°41.80'E	2,218.4	483.4	416.0	2,634.4	Neog.	L. Miocene	Conglomerate
106/109	670	Atrantc	Mid-Atlantic Ridge	23°09.995'N	45°01.930'W	3,625.0	92.5	0.0	3,625.0			Serpentinized harzburgite
112	686 *	Pacific	Outer Peru shelf	13°28.81'S	76°53.49'W	658.3	303.0	284.8	743.1	Neog.	Quaternary	Diatomaceous mud
112	687 *	Pacific	Outer Peru shelf	12°51.78'W	76°59.43'W	317.3	207.0	74.0	391.3	Neog.	Quaternary	Diatomaceous mud
112	688	Pacific	Peru Trench	11°32.28'S	78°56.65'W	3,836.3	779.0	678.0	4,514.3	Neog.	E. Eocene	Calcareous mudstones and sandstone
113	693 *	Atrantc	Weddell Sea margin	70°49.892'S	14°34.410'W	2,359.0	483.9	409.0	2,768.0	Creta.	M. Albian	Clayey mudstone
113	696 *	Atrantc	Orkney microcontinent	61°50.959'S	42°55.996'W	650.0	645.6	606.9	1,256.9	Neog.	E. Paleocene-Eocene	Sandy mudstone
114	698	Atrantc	Northeast Georgia Rise	51°27.51'S	33°05.96'W	2,138.0	237.0	219.3	2,357.3	Creta.	Pre-Campanian	Extremely weathered basalt
115	707 *	Indian	Mascarene Plateau	07°32.72'S	59°01.01'E	1,551.9	443.2	358.2	1,910.1	Neog.	M. Paleocene	Dolomitized shelly shallow water limestone
115	715 *	Indian	Maldives Ridge	05°04.89'N	73°49.88'E	2,272.8	287.8	104.6	2,377.4	Neog.	E. Eocene	Reef limestone
117	724 *	Indian	Oman Continental Margin	18°27.713'N	57°47.147'E	602.0	257.7	248.0	850.0	Neog.	E. Pliocene	Clayey Silt
117	726 *	Indian	Oman Continental Margin	17°48.965'N	57°22.290'E	340.1	186.3	131.1	471.2	Neog.	Eocene	Shallow-water nummulitic limestone
117	728	Indian	Oman Continental Margin	17°40.790'N	57°49.553'E	1,435.8	347.7	163.0	1,598.8	Neog.	E. Pliocene	Shallow-water benthic foraminifera
117	729	Indian	Oman Continental Margin	17°38.715'N	57°57.221'E	1,403.8	109.1	28.4	1,432.2	Neog.	Eocene?	Shallow-water limestone
118	732	Indian	Southwest Indian Ridge	32°32.81'S	57°03.289'E	4,920.5	24.0	0.0	4,920.5			Subangular of Basalt, diabase, sandstone
118	733	Indian	Southwest Indian Ridge	33°04.92'S	56°59.39'E	5,242.5	23.5	0.0	5,242.5			Subangular of Metagabbro and amphibolite
118	734	Indian	Southwest Indian Ridge	32°06.87'S	57°08.24'E	3,417.4	31.0	23.5	3,440.9			Breccia of serpentinite, amphibolite
118	735	Indian	Southwest Indian Ridge	32°43.395'S	57°15.959'E	719.9	500.7	0.0	719.9			Gabbro
119	738 *	Indian	Kerguelen Plateau	62°42.54'S	82°47.25'E	2,252.5	533.8	379.9	2,632.4	Creta.	L. Maestrichtian	Limestone
119	740	Southern	Inner part of Prydz Bay	68°41.22'S	76°43.25'E	807.5	225.5	56.6	864.1	Perm.?		Red sandstone
119	741 *	Southern	Inner part of Prydz Bay	68°23.16'S	76°23.02'E	551.4	128.1	24.1	575.5	Creta.	Albian?	Sandstone
119	742	Southern	Inner part of Prydz Bay	67°32.98'S	75°24.27'E	415.7	316.0	304.3	720.0	Neog.	E. Eocene?-Oligocene	Claystone and sandstone
120	747 *	Indian	Kerguelen Plateau	54°48.68'S	76°47.64'E	1,695.2	350.5	296.6	1,991.8	Creta.	E. Santonian	Bioclast grainstone with glauconite
120	748 *	Indian	Kerguelen Plateau	58°26.45'S	78°58.89'E	1,290.5	935.0	389.1	1,679.6	Paleog.	Turonian-L. Paleocene	Shallow-water limestone
120	748 *	Indian	Kerguelen Plateau	58°26.45'S	78°58.89'E	1,290.5	935.0	897.6	2,188.1	Creta.	L. Albian or older	Subaerially erupted basalt lava
120	750 *	Indian	Kerguelen Plateau	57°35.52'S	81°14.37'E	2,030.5	709.7	675.5	2,706.0	Creta.	Albian or older	Subaerially erupted basalt lava
121	752 *	Indian	Broken Ridg	30°53.483'S	93°34.652'E	1,086.3	435.6	113.0	1,199.3	Neog.		M. Eocene/E. Eocene unconformity
121	753	Indian	Broken Ridg	30°50.310'S	93°35.394'E	1,176.1	100.2	43.6	1,219.7	Neog.		E. Miocene/M. Eocene unconformity
121	754 *	Indian	Broken Ridg	30°56.439'S	93°33.954'E	1,065.5	354.7	151.0	1,216.5			L. Eocene/E. Maestrichtian unconformity
121	755 *	Indian	Broken Ridg	31°01.786'S	93°32.803'E	1,057.9	208.4	65.5	1,123.4			M. Miocene/Turonian-Santonian unconformity
121	756 *	Indian	Ninetyeast Ridge.	27°21.288'S	87°35.843'E	1,513.1	221.0	139.0	1,652.1	Neog.	L. Eocene or older	Subaerially erupted basalt

Leg	Site	Ocean	Area or Position	Lat.	Long.	Depth	Penetr.	Dep.F	Dep.SI	Period	Age	Sediments and rocks
121	757 *	Indian	Ninetyeast Ridge.	17°01.389'S	88°10.812'E	1,643.6	420.7	212.0	1,855.6	Neog.	L. Paleocene	Volcanic clastics
122	759 *	Indian	Wombat Plateau	16°55.24'S	115°33.63'E	2,091.6	308.0	40.5	2,132.1	Trias.	Norian	Shallow-water limestone
122	760 *	Indian	Wombat Plateau	16°55.32'S	115°32.48'E	1,969.7	506.0	84.9	2,054.6	Trias.	Norian	marsh to lagoon? Siltstones
122	761 *	Indian	Wombat Plateau	16°44.23'S	115°32.10'E	2,167.9	436.7	259.5	2,427.4	Trias.	Rhaetian	Shallow-water limestone
122	762 *	Indian	Exmouth Plateau	19°53.23'S	112°15.24'E	1,360.0	940.0	848.5	2,208.5	Creta.	Berriasian- E. Valanginian	Prodelta deposits on 200-500 m
122	763 *	Indian	Exmouth Plateau	20°35.21'S	112°12.51'E	1,367.5	1,036.6	570.0	1,937.5	Creta.	L. Albian	Glauconite-rich silty claystone
122	764 *	Indian	Wombat Plateau	16°33.96'S	115°27.43'E	2,698.6	294.5	49.6	2,748.2	Trias.	Rhaetian	Reef limestone
125	778	Pacific	Conical Seamount	19°29.93'N	146°39.94'E	3,913.7	107.6	29.8	3,943.5		Pre-E. Pleistocene	Sheared serpentine
125	779	Pacific	Conical Seamount	19°30.75'N	146°41.75'E	2,809.3	653.7	520.6	3,957.8		Pre-E. Pleistocene	Blocks of serpentized harzburgite, dunite
125	780	Pacific	Conical Seamount	19°32.53'N	146°39.21'E	3,083.4	163.5	14.0	3,097.4		Pre-Pleistocene	Harzburgite and dunite
125	783	Pacific	Izu-Bonin forearc	30°57.86'N	141°47.27'E	4,648.8	168.2	120.0	4,768.8		Pre-M. Miocene	Sheared serpentine
125	784	Pacific	Izu-Bonin Trench	30°54.49'N	141°44.27'E	4,900.8	425.3	321.1	5,221.9		Pre-M. Miocene	Sheared serpentine microbreccia
127	794	Japan	Northern Yamato Basin	40°11.40'N	138°13.86'E	2,809.3	653.7	520.6	3,329.9	Neog.	M. Miocene	Claystone (Upper middle bathyal)
127	795	Japan	Northern Yamato Basin	43.987°N	138.965°E	3,299.0	762.2	596.7	3,895.7	Neog.	M. Miocene	Claystone (Upper middle bathyal)
127	796	Japan	Okushiri Ridge	42°84900'N	139°41400'E	2,622.6	464.9	416.5	3,039.1	Neog.	M. Miocene	Claystone (Upper middle bathyal)
127	797	Japan	Southern Yamato Basin	38.616°N	134.536°E	2,864.6	900.1	646.9	3,511.5	Neog.	E. Miocene	Volcaniclastic sandstone on delta slope
133	811 *	Pacific	Queensland Plateau	16°30.948'S	148°9.454'E	937.0	392.5	269.5	1,206.5	Neog.	M. Miocene-E. Eocene	Shallow-water biogenic limestone
133	812 *	Pacific	Queensland Plateau	17°48.842'S	149°36.306'E	461.6	300.0	141.6	603.2	Neog.	M. Miocene	Shallow-water limestone
133	813 *	Pacific	Queensland Plateau	17°49.959'S	149°29.669'E	539.1	231.5	195.0	734.1	Neog.	M. Miocene or older	Dolomitized reef limestone
133	814 *	Pacific	Queensland Plateau	17°49.985'S	149°30.831'E	520.4	300.0	136.0	656.4	Neog.	M. Miocene	Dolomitized reef limestone
133	815 *	Pacific	Marion Plateau	19°9.034'S	149°59.508'E	465.5	950.2	425.3	890.8	Neog.	E.-L. Miocene	Reef limestone
133	816 *	Pacific	Marion Plateau	19°11.911'S	150°0.608'E	437.8	250.0	93.0	530.8	Neog.	M. Miocene	Dolomitized reef limestone
133	824 *	Pacific	Queensland Plateau	16°26.690'S	147°45.753'E	1,001.9	431.0	242.3	1,244.2	Neog.	M.-L. Miocene	Reef limestone
133	825	Pacific	Queensland Plateau	16°30.961'S	148°9.457'E	939.3	466.3	305.4	1,244.7	Neog.	M. Miocene-E. Eocene	Shallow-water biogenic limestone
133	826 *	Pacific	Marion Plateau	19°13.530'S	150°0.597'E	425.3	250.0	98.5	523.8	Neog.	M. Miocene	Dolomitized reef limestone
134	828	Pacific	d'Entrecasteaux Ridge	15°17.26'S	166°16.96'E	3,082.0	129.0	100.0	3,182.0	Neog.	M. Eocene?	Subaerial soil and brecciated basalt/dolerite
134	831	Pacific	Bougainville Guyot	16°00.56'S	166°40.36'E	1,066.4	852.0	102.4	1,168.8	Neog.	Pleistocene	Reef limestone
134	831	Pacific	Bougainville Guyot	16°00.56'S	166°40.36'E	1,066.4	852.0	429.6	1,496.0	Neog.	L. Oligocene-E. Miocene	Reef limestone and red soil
143	865 *	Pacific	Allison Guyot	18°26.410'N	179°33.339'W	1,518.4	870.9	139.7	1,658.1	Creta.	L. Albian	Reef limestone
143	866 *	Pacific	Resolution Guyot	21°19.953'N	174°18.844'E	1,361.8	1,743.6	19.6	1,381.4	Creta.	Albian	Reef limestone
143	867 *	Pacific	Resolution Guyot	21°20.959'N	174°18.561'E	1,352.2	76.8	0.3	1,352.5	Creta.	Albian	Phosphatized reef limestone
143	868 *	Pacific	Resolution Guyot	21°21.171'N	174°18.564'E	1,385.0	20.3	0.0	1,385.0	Creta.	Albian	Reef limestone
144	871 *	Pacific	Limalok (Harrie) Guyot	5°33.438'N	172°20.658'E	1,254.6	500.0	133.7	1,388.3	Neog.	L. Paleocene-M. Eocene	Reef limestone
144	871 *	Pacific	Limalok (Harrie) Guyot	5°33.438'N	172°20.658'E	1,254.6	500.0	451.6	1,706.2	Neog.	L. Paleocene or older	Subaerial erupted nepheline basalt lava
144	872 *	Pacific	Lo-En Guyot	10°05.808'N	162°51.996'E	1,083.6	192.5	135.4	1,219.0	Creta.	Pre-L. Turonian	Subaerial erupted basalt lava
144	873 *	Pacific	Wodejebato Guyot	11°53.796'N	164°55.188'E	1,335.0	232.3	58.0	1,393.0	Creta.	Campanian-Maastrichtian	Reef limestone
144	873 *	Pacific	Wodejebato Guyot	11°53.796'N	164°55.188'E	1,335.0	232.3	151.4	1,486.4	Creta.	Campanian or older	Subaerial weathered clay of basalt lava
144	874 *	Pacific	Wodejebato Guyot	12°00.228'N	164°56.388'E	1,335.0	193.5	0.1	1,335.1	Creta.	Campanian-Maastrichtian	Reef limestone
144	874 *	Pacific	Wodejebato Guyot	12°00.228'N	164°56.388'E	1,335.0	193.5	162.8	1,497.8	Creta.	Campanian or older	Subaerial weathered alkali basalt lava
144	875 *	Pacific	Wodejebato Guyot	12°00.756'N	164°56.466'E	1,408.8	133.0	0.1	1,408.9	Creta.	M.-L. Maastrichtian	Reef limestone
144	876 *	Pacific	Wodejebato Guyot	12°14.796'N	164°55.908'E	1,398.8	154.0	0.8	1,399.6	Creta.	M.-L. Maastrichtian	Reef limestone
144	877 *	Pacific	Wodejebato Guyot	12°01.146'N	164°55.326'E	1,354.8	190.5	0.2	1,355.0	Creta.	Maastrichtian	Reef limestone
144	877 *	Pacific	Wodejebato Guyot	12°01.146'N	164°55.326'E	1,354.8	190.5	183.0	1,537.8	Creta.	L. Campanian	Subaerial weathered clay
144	878 *	Pacific	MIT Guyo	27°19.143'N	151°53.028'E	1,323.2	910.0	3.2	1,326.4	Creta.	E. Aptian-Albian	Reef limestone
144	879 *	Pacific	Seiko Guyot	34° 10.46'N	144°18.56'E	1,500.8	226.5	0.0	1,500.8	Creta.	L. Aptian-Albian?	Reef limestone
147	894	Pacific	Hess Deep	2°18.059'N	101°31.526'W	3,013.7	28.7	0.0	3,013.7			Gabbro
147	895	Pacific	Hess Deep	2°16.635'N	101°26.777'W	3,820.7	93.7	0.0	3,820.7			Serpentinized peridotite and gabbro
149	897	Atrantc	West Iberia Margin	40°50.31'N	12°28.51'W	5,315.8	837.2	693.8	6,009.6		Pre-Hauterivian	Serpentinized peridotite
149	899	Atrantc	West Iberia Margin	40°46.347'N	12°16.063'W	5,291.0	562.5	484.2	5,775.2		Pre-Barremian	Serpentinized peridotite and gabbro
149	900	Atrantc	West Iberia Margin	46°40.994'N	11°36.252'W	5,036.8	805.0	748.9	5,785.7		Pre-Paleocene	Metamorphic microgabbro
149	901	Atrantc	West Iberia Margin	40°40.477'N	11°03.587'W	4,718.5	247.8	182.0	4,900.5	Jura.	E. Tithonian	Silty claystone
150	902	Atrantc	New Jersey shore	38°56.079'N	72°46.375'W	808.0	740.1	121.1	929.1	Neog.		M. Pleistocene/L. Miocene unconformity
150	902	Atrantc	New Jersey shore	38°56.079'N	72°46.375'W	808.0	740.1	680.9	1,488.9	Neog.		E. Oligocene/L. Eocene unconformity
151	908	Atrantc	Hovgaard Ridge	78°23.112'N	1°21.637'E	1,273.6	344.6	185.0	1,458.6	Neog.		Pliocene/L. Oligocene unconformity
152	914	Atrantc	East Greenland Shelf	63°27.736'N	39°43.479'W	533.2	224.0	187.2	720.4	Neog.	L. Eocene-E. Oligocene	Volcaniclastic sandy siltstone
152	915	Atrantc	East Greenland Shelf	63°28.285'N	39°46.909'W	533.1	209.4	84.8	617.9	Neog.	M.-L. Eocene	Volcaniclastic sandy siltstone
152	916	Atrantc	East Greenland Shelf	63°29.137'N	39°48.400'W	513.7	78.6	97.0	610.7	Neog.	E.-M. Eocene	Volcaniclastic sandy siltstone
152	917	Atrantc	East Greenland Shelf	63°29.500'N	39°49.665'W	508.1	874.9	28.7	536.8	Neog.	M. Eocene	Volcaniclastic sandy siltstone
152	918 *	Atrantc	Greenland Margin	63°05.572'N	38°38.334'W	1,868.2	1,310.1	1,157.9	3,026.1	Neog.	E. Eocene	Glauconitic sandy silt
153	920	Atrantc	Mid-Atlantic Ridge	23°20.322'N	45°01.044'W	3,327.5	200.8	0.0	3,327.5			Massive serpentized peridotite
153	921	Atrantc	Mid-Atlantic Ridge	23°32.328'N	45°01.878'W	2,444.9	82.6	0.0	2,444.9			Olivine gabbro, gabbro, trondjemite
153	922	Atrantc	Mid-Atlantic Ridge	23°31.368'N	45°01.926'W	2,600.8	37.4	0.0	2,600.8			Troctolite, metatroctolite, gabbro
153	923	Atrantc	Mid-Atlantic Ridge	23°32.556'N	45°01.896'W	2,428.7	70.0	0.0	2,428.7			Olivine gabbro, gabbro, troctolite
153	924	Atrantc	Mid-Atlantic Ridge	23°32.496'N	45°00.864'W	3,165.7	48.5	0.0	3,165.7			Olivine gabbro, gabbro, troctolite
159	959	Atrantc	Ghana Marginal Ridge	3°37.656'N	2°44.149'W	2,090.7	1,158.9	1,081.7	3,172.4	Creta.	L. Albian	Shallow-water sandstone
159	960	Atrantc	Ghana Marginal Ridge	3°34.979'N	2°44.009'W	2,048.3	451.2	329.0	2,377.3	Creta.	Turonian and older	Reef limestone
159	961	Atrantc	Deep Ivorian Basin	3°26.556'N	3°03.560'W	3,292.0	374.6	188.5	3,480.5	Creta.	Bajocian-Maastrichtian	Reef limestone
160	965	Mediter.	Eratosthenes Seamount	33°55.080'N	32°42.785'E	1,506.6	250.4	29.3	1,535.9	Neog.	Miocene?	Reef limestone
160	966	Mediter.	Eratosthenes Seamount	33°47.858'N	32°42.093'E	922.9	356.0	96.2	1,019.1	Neog.	Miocene?	Reef limestone
160	967	Mediter.	Eratosthenes Seamount	34°04.106'N	32°43.525'E	5,522.7	600.3	427.0	2,979.7	Creta.	L. Cretaceous	Reef limestone
160	969	Mediter.	Mediterranean Ridge	33°50.399'N	24°53.065'E	2,200.3	111.4	102.8	2,303.1	Neog.	Pre-Pliocene	Brackish water calcareous silty clay
161	975	Mediter.	South Balearic Margin	38°53.786'N	4°30.596'E	2,415.5	317.1	307.0	2,722.5	Neog.	Miocene	Gypsum
161	976	Mediter.	Spanish Margin	36°12.313'N	4°18.763'W	1,108.0	928.7	669.7	1,777.7	Neog.	E. Miocene	High-grade metamorphic rocks
163	988	Atrantc	East Greenland Coast	65°42.255'N	34°52.262'W	262.6	32.0	10.0	272.6	Neog.	Pre-Quaternary	Subaerial erupted basalt lava

Leg	Site	Ocean	Area or Position	Lat.	Long.	Depth	Penetr.	Dep.F	Dep.SI	Period	Age	Sediments and rocks
163	989	Atrantic	East Greenland Coast	63°31.355'N	39°54.110'W	459.5	84.2	4.0	463.5	Neog.	Pre-Quaternary	Subaerial erupted basalt lava
163	990	Atrantic	East Greenland Coast	63°28.372'N	39°46.808'W	541.5	342.7	192.4	733.9	Neog.	E. Eocene?	Cobble conglomerate
165	1001	Atrantic	Lower Nicaragua Rise	15°45.427'N	74°54.627'W	3,259.6	522.8	485.4	3,745.0	Creta.	M. Campanian	Basalt lava and limestone
166	1003	Atrantic	Great Bahama Bank	24°32.763'N	79°15.65'W	483.3	1,300.0	0.0	483.3	Neog.	M. Miocene-Holocene	Limestone (upper bathyal)
166	1004	Atrantic	Great Bahama Bank	24°33.283'N	79°14.95'W	418.9	200.0	0.0	418.9	Neog.	E. Pliocene-Pleistocene	Limestone (upper bathyal)
166	1005	Atrantic	Great Bahama Bank	24°33.755'N	79°14.141'W	351.6	700.0	0.0	351.6	Neog.	M. Miocene-Pleistocene	Limestone (upper bathyal)
166	1008	Atrantic	Great Bahama Bank	23°36.64'N	79°05.01'W	437.1	134.5	0.0	437.1	Neog.	L. Pleistocene-Holocene	Limestone (upper bathyal)
166	1009	Atrantic	Great Bahama Bank	23°36.84'N	79°03.00'W	307.9	226.1	0.0	307.9	Neog.	L. Pleistocene-Holocene	Limestone (upper bathyal)
170	1039	Pacific	Costa Rica Margin	9°38.383'N	86°12.002'W	4,351.4	448.7	422.0	4,773.4		Pre-M. Miocene	Gabbro
170	1040	Pacific	Costa Rica Margin	9°39.697'N	86°10.735'W	4,177.9	665.0	422.0	4,599.9		Pre-M. Miocene	Gabbro
171B	1052	Atrantic	Blake Nose	29°57.0794'N	76°37.6094'W	1,343.5	684.8	633.2	1,976.7	Creta.	L. Albian	Clayey siltstone
173	1065	Atrantic	Galicía Bank	40°43.447'N	11°17.724'W	4,770.1	631.4	308.8	5,078.9	Jura.	Tithonian	Claystone (offshore shelf)
173	1067	Atrantic	Iberia Abyssal Plain	40°40.950'N	11°35.750'W	5,020.9	855.6	763.8	5,784.7		Pre-L. Paleocene	Amphibolite, tonalite gneiss
173	1068	Atrantic	Iberia Abyssal Plain	40°40.955'N	11°36.720'W	5,043.9	955.8	893.1	5,937.0		Pre-Berriasian	Serpentinized plagioclase peridotite
173	1069	Atrantic	Iberia Abyssal Plain	40°43.612'N	11°46.633'W	5,074.8	959.3	867.8	5,942.6	Jura.	Tithonian?	Limestone Conglomerate
173	1070	Atrantic	Iberia Abyssal Plain	40°47.779'N	12°43.430'W	5,321.8	718.8	658.4	5,980.2		Pre-L. Albian	Breccia with serpentinite clasts
174A	1071	Atrantic	New Jersey Shelf	39°22.9321'N	72°42.9398'W	90.0	424.2	60.9	150.9	Neog.		Four unconformity-bounded sequences
174A	1072	Atrantic	New Jersey Shelf	39°21.9305'N	72°41.6647'W	98.0	358.6	57.5	155.5	Neog.		Three unconformity-bounded sequences
174A	1073	Atrantic	New Jersey Shelf	39°13.5214'N	72°16.5461'W	639.4	663.6	519.8	1,159.2	Neog.		Four unconformity-bounded sequences
175	1087	Atrantic	Cape Basin	31°27.9137'S	15°18.6541'E	1,374.2	491.9	424.8	1,799.0	Neog.		L. Miocene/M. Miocene unconformity
179	1105	Indian	Southwest Indian Ridge	32°43.1346'S	57°16.6518'E	702.9	158.0	15.0	717.9			Gabbro
180	1109	Pacific	Woodlark Rise	9°30.380'S	151°34.355'E	2,211.0	802.0	570.4	2,781.4	Neog.	M-E. Pliocene	Shallow marine sandstone and limestone
180	1114	Pacific	Moresby Seamount	9°47.613'S	151°34.504'E	406.5	352.8	295.4	701.9		Pre-M. Pliocene	Metadolerite (greenschist facies)
180	1115	Pacific	Woodlark Rise	9°11.383'S	151°34.422'E	1,148.7	802.5	513.4	1,662.1	Neog.	L. Miocene	Siltstone, bioclastic limestone
180	1117	Pacific	Moresby Seamount	9°46.526'S	151°32.945'E	1,663.2	111.1	0.0	1,663.2			Brecciated gabbro
180	1118	Pacific	Woodlark Basin	9°35.110'S	151°34.421'E	2,303.6	926.6	857.1	3,160.7			Reef limestone
182	1129	Indian	Great Australian Bight	33°17.7887'S	128°28.8675'E	202.1	604.2	0.0	202.1	Neog.	Pleistocene	Bryozoan limestone
182	1130	Indian	Great Australian Bight	33°25.1988'S	127°36.1248'E	488.1	395.2	369.5	857.6	Neog.	L. Eocene	Shallow-water calcareous sandstone
182	1131	Indian	Great Australian Bight	33°19.5655'S	128°28.8721'E	333.6	616.9	0.0	333.6	Neog.	Pleistocene	Bryozoan limestone
182	1132	Indian	Great Australian Bight	33°18.9624'S	127°36.1235'E	218.5	603.2	517.7	736.2	Neog.	L-M. Eocene	Shallow-water limestone
183	1136	Indian	Kerguelen Plateau	59°39.1'S	84°50.1'E	1,930.6	161.4	89.5	2,020.1	Creta.	L. Albian	Carbonate-bearing zeolitic silty clay
183	1136	Indian	Kerguelen Plateau	59°39.1'S	84°50.1'E	1,930.6	161.4	128.1	2,058.7	Creta.	Pre-L. Albian	Subaerial erupted basalt lava
183	1137	Indian	Kerguelen Plateau	56°50.0'S	68°05.6'E	1,004.5	371.2	199.5	1,204.0	Creta.	Campanian	Glauconite-bearing sandy limestone
183	1137	Indian	Kerguelen Plateau	56°50.0'S	68°05.6'E	1,004.5	371.2	219.5	1,224.0	Creta.	Campanian or older	Subaerial erupted basalt lava
183	1138	Indian	Kerguelen Plateau	53°33.1'S	75°58.5'E	1,141.4	842.7	655.6	1,797.0	Creta.	Turonian-Santonian	Glauconitic calcareous sandstone
183	1138	Indian	Kerguelen Plateau	53°33.1'S	75°58.5'E	1,141.4	842.7	698.2	1,839.6	Creta.	Turonian or older	Subaerial erupted basalt lava
183	1139	Indian	Kerguelen Plateau	50°11.1'S	63°56.2'E	1,415.3	694.2	383.5	1,798.8	Neog.	Eocene or older	Sandy shallow limestone
183	1139	Indian	Kerguelen Plateau	50°11.1'S	63°56.2'E	1,415.3	694.2	461.7	1,877.0	Neog.	Eocene or older	Subaerial erupted rhyolite-trachyte lava
188	1166	Southern	Prydz Bay Shelf	67°41.8'S	74°47.2'E	475.4	381.3	156.5	631.9	Neog.	Eocene	Albual coarse sand
189	1168	Indian	Tasmania margin	42°36.5809'S	144°24.7620'E	2,463.3	883.5	762.0	3,225.3	Neog.	L. Eocene	Brackish silty claystone
189	1170	Indian	South Tasman Rise	47°09.0107'S	146°02.9829'E	2,704.7	779.8	497.0	3,201.7	Neog.	M. Eocene	Neritic siltstone
189	1171	Indian	South Tasman Rise	48°29.9975'S	149°06.7222'E	2,147.8	958.8	343.5	2,491.3	Neog.	M. Eocene	Neritic siltstone
189	1172	Pacific	East Tasman Plateau	43°57.5545'S	149°55.7169'E	2,621.7	766.5	361.1	2,982.8	Neog.	L.-M. Eocene	Neritic claystone
192	1183	Pacific	Ontong Java Plateau	01°10.6189'S	157°00.8988'E	1,804.7	1,211.1	1,088.8	2,893.5	Creta.	Aptian-Albian	Limestone
192	1184	Pacific	Ontong Java Plateau	05°00.6653'S	164°13.9771'E	1,661.5	538.8	380.5	2,042.0	Neog.	M. Eocene	Lapilli tuff with inclined layers
194	1193	Pacific	Marion Plateau	20°14.495'S	151°47.538'E	348.3	548.5	35.0	383.3	Neog.	M.-L. Miocene	Reef limestone
194	1194	Pacific	Marion Plateau	20°14.554'S	151°58.991'E	373.9	427.1	117.4	491.3	Neog.	M. Miocene	Bryozoan-dominated limestone
194	1195	Pacific	Marion Plateau	20°24.283'S	152°40.243'E	419.2	521.2	517.5	936.7	Neog.	E. Eocene	Nummulitids reef limestone
194	1196	Pacific	Marion Plateau	21°00.371'S	152°51.512'E	304.2	672.2	0.0	304.2	Neog.	L. Miocene	Dolomitic reef limestone
194	1197	Pacific	Marion Plateau	21°04.574'S	153°03.943'E	348.3	674.9	601.7	950.0	Neog.	E. Miocene	Shallow-water limestone
194	1197	Pacific	Marion Plateau	21°04.574'S	153°03.943'E	348.3	674.9	656.1	1,004.4	Neog.	E. Miocene or older	Basalt breccia on subaerial alluvium fan
194	1198	Pacific	Marion Plateau	20°57.930'S	152°44.005'E	319.4	522.6	503.6	823.0	Neog.	E. Miocene	Shallow-water limestone
194	1199	Pacific	Marion Plateau	20°58.692'S	152°54.947'E	315.7	419.5	0.0	315.7	Neog.	L. Miocene	Dolomitic reef limestone
195	1200	Pacific	Chamorro Seamount	13°47.0724'N	146°00.1717'E	2,932.0	56.4	0.0	2,932.0		Pre-L. Pleistocene	Serpentine mud with dispersed clasts
197	1203	Pacific	Detroit Seamount	50°56.9976'N	167°44.3969'E	2,604.4	914.6	457.5	3,061.9	Creta.	Campanian	Subaerial erupted basalt lava
197	1204	Pacific	Detroit Seamount	51°11.6406'N	167°46.4217'E	2,381.0	954.5	814.0	3,195.0	Creta.	Campanian	Subaerial erupted basalt lava
197	1205	Pacific	Nintoku Seamount	41°19.9986'N	170°22.6992'E	1,321.0	326.0	0.0	1,321.0	Neog.	E. Eocene	Shallow-water calcareous conglomerate
197	1205	Pacific	Nintoku Seamount	41°19.9986'N	170°22.6992'E	1,321.0	326.0	35.2	1,356.2	Neog.	E. Eocene or older	Subaerial erupted basalt lava
197	1206	Pacific	Koko Seamount	34°55.5485'N	172°08.7536'E	1,557.0	335.2	57.0	1,614.0	Neog.	Pre-M. Eocene	Subaerial erupted basalt lava
198	1213	Pacific	Shatsky Rise	31°34.649'N	157°17.861'E	3,883.0	494.4	447.8	4,330.8		Pre-Berriasian	Diabase
202	1236	Pacific	Nazca Ridge	21°21.539'S	81°26.165'W	1,323.0	207.7	181.0	1,504.0	Neog.	L. Oligocene	Shallow-water limestone
202	1242	Pacific	Cocos Ridge	7°51.35'N	83°36.42'W	1,364.0	256.0	250.7	1,614.7	Neog.		L. Pliocene/M. Miocene hiatus
207	1258	Atrantic	Demerara Rise	9°26.000'N	54°43.966'W	3,192.2	485.0	449.6	3,641.8	Creta.	E. Albian	Phosphatic calcareous claystone
207	1259	Atrantic	Demerara Rise	9°17.999'N	54°11.998'W	2,353.8	558.8	549.1	2,902.9		Pre-Cenomanian	Shallow-water sandstone
207	1260	Atrantic	Demerara Rise	9°15.931'N	54°32.652'W	2,548.8	509.0	483.6	3,032.4	Creta.	E.-L. Albian	Clayey limestone with quartz
207	1261	Atrantic	Demerara Rise	9°2.918'N	54°19.049'W	1,899.7	674.1	650.2	2,549.9	Creta.	Albian	Shallow-water quartz sandstone
208	1263	Atrantic	Walvis Ridge	28°31.970'S	2°46.769'E	2,717.1	345.6	50.0	2,767.1	Neog.		Miocene/E. Oligocene unconformity
209	1268	Atrantic	Mid-Atlantic Ridge	14°50.7552'N	45°4.6409'W	3,007.0	147.6	0.0	3,007.0			Harzburgite/dunite
209	1270	Atrantic	Mid-Atlantic Ridge	14°43.2702'N	44°53.0839'W	1,816.9	57.3	0.0	1,816.9			Harzburgite/dunite and oxide gabbro
209	1271	Atrantic	Mid-Atlantic Ridge	15°2.1888'N	44°56.9119'W	3,584.9	103.8	0.0	3,584.9			Dunite/gabbro
209	1272	Atrantic	Mid-Atlantic Ridge	15°5.6665'N	44°58.3003'W	2,559.8	131.0	0.0	2,559.8			Diabase
209	1274	Atrantic	Mid-Atlantic Ridge	15°38.8669'N	46°40.5824'W	3,939.8	155.8	0.0	3,939.8			Harzburgite
209	1275	Atrantic	Mid-Atlantic Ridge	15°44.4396'N	46°54.2173'W	1,553.6	209.0	0.0	1,553.6			Troctolite and diabase/oxide gabbro
210	1277	Atrantic	Newfoundland Basin	45°11.8002'N	44°25.5999'W	4,639.4	180.3	142.1	4,781.5			Gabbro and serpentinized peridotites

Reference

- Barber, P. M. (1981): Messinian subaerial erosion of the proto-Nile Delta. *Marine Geology*, 44, 253-272.
- Belousov, V. V. and E. E. Milanovsky (1977): On tectonics and tectonic position of Iceland. *Tectonophys.*, 37, 25-40.
- Bott, M. H. P. (1968): Deep structure and geodynamics of the Greenland-Scotland Ridge: An introductory review. 3-9, in Bott, M. H. P. et al. eds.: *Structure and Development of the Greenland-Scotland Ridge*, Plenum Press, N. Y.
- Dai-Ichi Kashima Seamount Research Group (1976): Topography and Geology of the Dai-Ichi Kashima Seamount. *Earth Science*, 30, 222-240.
- Feary D. A. and N. P. James (1998): Seismic Stratigraphy and Geological Evolution of the Cenozoic, Cool-Water Eucla Platform, Great Australian Bight. *Am. Assoc. Petrol. Geol. Bulletin*, 82(5A), 792-816.
- Fioravanti, C. (2020): Revelations from a submerged archipelago-Beaches, river, and mangroves covered a mountain range that was above sea level 40 million years ago. *Oceanografia*, 282, 56-59.
- Hamilton, E. L. (1956): Sunken islands of the Mid-Pacific Mountains. *Geol. Soc. Amer. Mem.* 64, 1-97.
- Hanada, M. (1998): Study on distribution of shallow water sediments and volcanic rocks on deep sea floor in relation to sealevel changes. *Jour. Sch. Mar. Sci. Tech., Tokai Univ.*, (45), 137-166. (In Japanese with English abstract)
- Haq, B. U. (1991): Sequence stratigraphy, sea-level change, and significance for the deep sea. 3-39, in Macdonald, D. I. M. ed., *Sedimentation, Tectonics and Eustasy, Sea-level Changes at Active Margins*, Spec. Pub. int. Ass. Sediment., 12.
- Haq, B. U., J. Hardenbol and P. R. Vail (1987): Chronology of fluctuating sea levels since the Triassic. *Science*, 235, 1156-1166.
- Haq, B. U., J. Hardenbol and P. R. Vail (1988): Mesozoic and Cenozoic chronostratigraphy and cycles of sea-level change. 71-108, in Wilgus, C. K., B. S. Hastings, C. G. Kendall, H. W. Posamentier, C. A. Ross and J. C. Van Wagoner eds., *Sea Level Changes: An Integrated Approach*. SEPM Spec. Publ., 42.
- Heezen, B. C., J. L. Matthews, R. Catalano, J. Natland, A., Coogan, M. Tharp and M. Rawson (1973): Western Pacific Guyots. doi:10.2973/dsdp.proc.20.132.1973
- Hoshino, M. (1962): Pacific Ocean. *Assoc. Geol. Collab. Japan*, Tokyo, 136pp. (In Japanese)
- Hoshino, M. (1970): Latest Tertiary sea-level change and trench formation. 155-177, in Hoshino, M. and H. Aoki eds., *Island-arc and Ocean*, Tokai Univ. Press, Tokyo. (In Japanese with English abstract)
- Hoshino, M. (1983): *Marine Geology*. *Assoc. Geol. Collab. Japan.*, 373pp. (in Japanese)
- Hoshino, M. (1991): *The Basaltic Stage - Basic Concepts of Geological Science*. Tokai Univ. Press, Tokyo, 456pp. (in Japanese with English abstract)
- Hoshino, M. (2014): *The History of Micro-Expanding Earth -The History of the Earth from viewpoint of Sea Level Rise-*. E. G. Service Press, Sapporo, 234pp.
- Hoshino, M. (2019): *Upheaval of the Earth Crust - Why is the mountain high? -*. E. G. Service Press, Sapporo, 188pp. (in Japanese)
- Hsü, K. J., L. Montadert, D. Bernoulli, M. B. Cita, A. Erickson, R. E. Garrison, R. B. Kidd, F. Mélières, C. Müller, and R. Wright (1978a): History of the Mediterranean Salinity Crisis. doi:10.2973/dsdp.proc.42.155.1978
- Hsü, K. J., Montadert, L., Bernoulli, D. Cita, M. B. Erickson, A. Garrison, R. E. Kidd, R. B. Mélières, F. Moeller, C. and R. Wright (1978b): History of the Mediterranean salinity crisis. *Nature*, 267, 399-403.
- Kitasato, H. (2014): *Deep-Sea, Another Universe - The birthplace of life as seen by the Shinkai 6500*. Iwanami, Tokyo, 176pp.
- Konishi, K. (1985): Cretaceous reefal fossils dredged from two seamount of the Ogasawara Plateau. 169-180, in Kobayashi, K. ed.: *Preliminary Rept. Hakuho-maru cruise, KH-84-1*, 169-180.
- Kuroda, J., T. Yoshimura, H. Kawahata, Francisco J. Jimenez-Espejo, Stefano Lugli, Vinicio Manzi, Marco Roveri (2014): Evaporation of marine basins: a review of evaporite formation and Messinian Salinity Crisis. *Jour. Geol. Soc. Japan*, 120, 181-200. (In Japanese with English abstract)
- Ladd, H. S., W. A. Newman and N. F. Sohl (1974): Darwin guyot, the Pacific's oldest atoll. *Preceding Second. International Coral Reef Symposium*, 2, 513-522.

- Ladd, H. S. and S. O. Schlanger (1960): Drilling operations on Eniwetok Atoll: U.S. Geol. Survey Prof. Paper 260-Y, 863-905.
- Larsen, H. C., A. D. Saunders, P. D. Clift, and the Shipboard Scientific Party (1994): Introduction: Breakup of the Southeast Greenland Margin and the Formation of the Irminger Basin: Background and Scientific Objectives. doi:10.2973/odp.proc.ir.152.101.1994
- Lorenzo, J. M. and S. P. Hesselbo (1996): Seismic-to-Well Correlation of Seismic Unconformities at Leg 150 Continental Slope Sites. doi:10.2973/odp.proc.sr.150.031.1996
- Matthews, J. L., B. C. Heezen, R. Catalano, M. Tharp, A. Coogan, J. Natland, and M. Rawson (1974) Cretaceous drowning of reefs on Mid-Pacific and Japanese guyots. *Science*, 184, 462-464.
- McKenzie, J., Bernoulli, D. and Schlanger, S. O. (1980): Shallow-water carbonate sediments from the Emperor Seamounts, their diagenesis and paleogeographic significance. doi:10.2973/dsdp.proc.55.115.1980
- Mitchum, R. M., P. R. Vail and J. B. Sangree (1977): Stratigraphic interpretation of seismic reflection patterns in depositional sequence. 213-248, in Payton, C. E. ed., *Seismic Stratigraphy - Application to Hydrocarbon Exploration*, Amer. Assoc. Petrol. Geol. Mem., 26.
- Mullins, H. T. and G. W. Lynts (1977): Origin of the northwestern Bahama platform: review and reinterpretation. *Geol. Soc. Am. Bull.*, 88:1447-1461.
- Ovenshine A., T., B. Csejty Jr., J. G. Smith and P. B. Andrews (1975): Petrography and Age of the Quartz-Muscovite-Chlorite Semischist, Site 281, South Tasman Rise. doi:10.2973/dsdp.proc.29.140.1975
- Paulus F. J. (1972): The Geology of Site 98 and the Bahama Platform. doi:10.2973/dsdp.proc.11.130.1972
- Pinheiro, L. M., R. C. L. Wilson, R. Pena dos Reis, R. B. Whitmarsh and A. Ribeiro (1996): The Western Iberia Margin: A Geophysical and Geological Overview. doi:10.2973/odp.proc.sr.149.246.1996
- Roberts, D. G. (1975): Evaporite deposition in the Aptian South Atlantic Ocean. *Marine Geology*, 18, M65-M72.
- Sager, W. W., T. Sano, J. Geldmacher and the Expedition 324 Scientists (2010): Site U1349. doi:10.2204/iodp.proc.324.106.2010
- Santos, R. V., C. E. Ganade, C. M. Lacasse, I. S. L. Costa, I. Pessanha, E. P. Frazao, E. L. Dantas and J. A. Cavalcante (2019): Dating Gondwanan continental crust at the Rio Grande Rise, South Atlantic. *Terra Nova*, 31, 424-429.
- Schlanger, S. O. (1981): Shallow-water limestones in Oceanic basins as tectonic and Palaeoceanographic indications. *SEPM. Special Publication*, 32, 209-226.
- Schlanger, S. O. and K. Konishi (1975): The geographic boundary between the Coral-Algal and Bryozoan-Algal facies: A paleolatitude indicator: Theme I, IX Int. Cong. Sedimentology, Nice, 189-190.
- Sheridan, R. E., J. T. Crosby, G. M. Bryan and P. L. Stoffa (1981): Stratigraphy and structure of southern Blake Plateau, northern Florida Straits, and northern Bahama Platform from multichannel seismic reflection data. *AAPG Bull.*, 65, 2571-2593.
- Shiba, M. (1979): Geological history of the Yabe guyot to the east of the Ogasawara Islands. *Jour. Geol. Soc. Japan*, 85, 209-220. (In Japanese with English abstract)
- Shiba, M. (1988): Geohistory of the Daiichi-Kashima Seamount and the Middle Cretaceous Eustasy. *Sci. Rep. Nat. Hist. Mus., Tokai Univ.*, (2), 1-69.
- Shiba, M. (1992) Eustatic rise of sea-level since Jurassic modified from Vail's curve. *Abstracts, 29th IGC*, I-3-17, 95.
- Shiba, M. (1993): Middle Cretaceous Carbonate Bank on the Daiichi-Kashima Seamount at the junction of the Japan and Izu-Bonin Trenches. 465-471, in Simo, T., B. Scott and J-P. Masse eds., *Cretaceous Carbonate Platform*, Am. Assoc. Petrol. Geol. Mem., 56.
- Shiba, M. (2017) Formation of Suruga Bay - Large-scale uplift and sea level rise. *Tokai Univ. Press, Hiratsuka*, 406p. (in Japanese)
- Shiba, M. (2021a) Characteristic of crustal uplift since the Pliocene in central Honshu, Japan and sea level rise. *Earth Science*, 75, 37-55. (In Japanese with English abstract)
- Shiba, M. (2021b): Distribution of island endemic animals and the late Middle Pleistocene land bridges as evidence of sea level rise of 1,000 m since 430 ka. *NCGT Journal*, 9 (2), 60-78.
- Shipboard Scientific Party (1978): Sites 389 and 390: North Rim of Blake Nose. doi:10.2973/dsdp.proc.44.104.1978SSP.1978a

- Shipboard Scientific Party (1980a): Site 430: Ojin Seamount. doi:10.2973/dsdp.proc.55.103.1980
- Shipboard Scientific Party (1980b): Site 433: Suiko Seamount. doi:10.2973/dsdp.proc.55.106.1980
- Shipboard Scientific Party (1980c): Sites 438 and 439: Japan Deep Sea Terrace, Leg 57. doi:10.2973/dsdp.proc.5657.102.1980
- Shipboard Scientific Party (1981): Site 451: East Edge of the West Mariana Ridge. doi:10.2973/dsdp.proc.59.105.1981
- Shipboard Scientific Party (1982a): Site 489. doi:10.2973/dsdp.proc.66.105.1982
- Shipboard Scientific Party (1982b): Site 493. doi:10.2973/dsdp.proc.66.109.1982
- Shipboard Scientific Party (1982c): Site 496: Middle America Trench Upper Slope. doi:10.2973/dsdp.proc.67.104.1982
- Shipboard Scientific Party (1984a): Site 544. doi:10.2973/dsdp.proc.79.102.1984
- Shipboard Scientific Party (1984b): Site 545. doi:10.2973/dsdp.proc.79.103.1984
- Shipboard Scientific Party (1984c): Site 546. doi:10.2973/dsdp.proc.79.104.1984
- Shipboard Scientific Party (1984d): Site 547. doi:10.2973/dsdp.proc.79.105.1984
- Shipboard Scientific Party (1984e): Sites 535, 539, and 540. doi:10.2973/dsdp.proc.77.102.1984
- Shipboard Scientific Party (1985a): Site 548. doi:10.2973/dsdp.proc.80.103.1985
- Shipboard Scientific Party (1985b): Site 549. doi:10.2973/dsdp.proc.80.104.1985
- Shipboard Scientific Party (1985c): Site 566. doi:10.2973/dsdp.proc.84.103.1985
- Shipboard Scientific Party (1985d): Site 567. doi:10.2973/dsdp.proc.84.104.1985
- Shipboard Scientific Party (1985e): Site 569. doi:10.2973/dsdp.proc.84.106.1985
- Shipboard Scientific Party (1985f): Site 570. doi:10.2973/dsdp.proc.84.107.1985
- Shipboard Scientific Party (1987a): Site 639. doi:10.2973/odp.proc.ir.103.110.1987
- Shipboard Scientific Party (1987b): Sites 604 and 605. doi:10.2973/odp.proc.93.103.1987
- Shipboard Scientific Party (1987c): Site 654: Upper Sardinian Margin. doi:10.2973/odp.proc.ir.107.110.1987
- Shipboard Scientific Party (1987d): Site 613. doi:10.2973/dsdp.proc.95.104.1987
- Shipboard Scientific Party (1987e): Site 637. doi:10.2973/odp.proc.ir.103.108.1987
- Shipboard Scientific Party (1988a): Site 698. doi:10.2973/odp.proc.ir.114.105.1988
- Shipboard Scientific Party (1988b): Site 702. doi:10.2973/odp.proc.ir.114.109.1988
- Shipboard Scientific Party (1988c): Site 702. doi:10.2973/odp.proc.ir.114.109.1988
- Shipboard Scientific Party (1988d): Site 715. doi:10.2973/odp.proc.ir.115.113.1988
- Shipboard Scientific Party (1988e): Site 707. doi:10.2973/odp.proc.ir.115.106.1988
- Shipboard Scientific Party (1988f): Site 696. doi:10.2973/odp.proc.ir.113.112.1988
- Shipboard Scientific Party (1988g): Site 688. doi:10.2973/odp.proc.ir.112.119.1988
- Shipboard Scientific Party (1988h): Site 686. doi:10.2973/odp.proc.ir.112.117.1988
- Shipboard Scientific Party (1988i): Site 687. doi:10.2973/odp.proc.ir.112.119.1988
- Shipboard Scientific Party (1989a): Site 740. doi:10.2973/odp.proc.ir.119.108.1989
- Shipboard Scientific Party (1989b): Site 748. doi:10.2973/odp.proc.ir.120.110.1989
- Shipboard Scientific Party (1989c): Site 741. doi:10.2973/odp.proc.ir.119.109.1989
- Shipboard Scientific Party (1989d): Site 742. doi:10.2973/odp.proc.ir.119.110.1989
- Shipboard Scientific Party (1989e): Site 752. doi:10.2973/odp.proc.ir.121.106.1989
- Shipboard Scientific Party (1989f): Site 753. doi:10.2973/odp.proc.ir.121.107.1989
- Shipboard Scientific Party (1989g): Site 754. doi:10.2973/odp.proc.ir.121.108.1989
- Shipboard Scientific Party (1989h): Site 755. doi:10.2973/odp.proc.ir.121.109.1989
- Shipboard Scientific Party (1989i): Site 724. doi:10.2973/odp.proc.ir.117.111.1989

Shipboard Scientific Party (1989j): Site 726. doi:10.2973/odp.proc.ir.117.113.1989
Shipboard Scientific Party (1989k): Site 728. doi:10.2973/odp.proc.ir.117.115.1989
Shipboard Scientific Party (1989l): Site 729. doi:10.2973/odp.proc.ir.117.116.1989
Shipboard Scientific Party (1990a): Site 760. doi:10.2973/odp.proc.ir.122.106.1990
Shipboard Scientific Party (1990b): Site 761. doi:10.2973/odp.proc.ir.122.107.1990
Shipboard Scientific Party (1990c): Site 762. doi:10.2973/odp.proc.ir.122.108.1990
Shipboard Scientific Party (1990d): Site 763. doi:10.2973/odp.proc.ir.122.109.1990
Shipboard Scientific Party (1990e): Site 794. doi:10.2973/odp.proc.ir.127.104.1990
Shipboard Scientific Party (1990f): Site 795. doi:10.2973/odp.proc.ir.127.105.1990
Shipboard Scientific Party (1990g): Site 796. doi:10.2973/odp.proc.ir.127.106.1990
Shipboard Scientific Party (1990h): Site 797. doi:10.2973/odp.proc.ir.127.107.1990
Shipboard Scientific Party (1991a): Site 811/825. doi:10.2973/odp.proc.ir.133.104.1991
Shipboard Scientific Party (1991b): Site 812. doi:10.2973/odp.proc.ir.133.105.1991
Shipboard Scientific Party (1991c): Site 813. doi:10.2973/odp.proc.ir.133.106.1991
Shipboard Scientific Party (1991d): Site 814. doi:10.2973/odp.proc.ir.133.107.1991
Shipboard Scientific Party (1991e): Site 824. doi:10.2973/odp.proc.ir.133.117.1991
Shipboard Scientific Party (1991f): Site 826. doi:10.2973/odp.proc.ir.133.118.1991
Shipboard Scientific Party (1991g): Site 816. doi:10.2973/odp.proc.ir.133.109.1991
Shipboard Scientific Party (1992a): Site 828. doi:10.2973/odp.proc.ir.134.108.1992
Shipboard Scientific Party (1992b): Site 831. doi:10.2973/odp.proc.ir.134.111.1992
Shipboard Scientific Party (1993a): Site 866. doi:10.2973/odp.proc.ir.143.107.1993
Shipboard Scientific Party (1993b): Site 873. doi:10.2973/odp.proc.ir.144.106.1993
Shipboard Scientific Party (1993c): Site 874. doi:10.2973/odp.proc.ir.144.107.1993
Shipboard Scientific Party (1993d): Site 875/876. doi:10.2973/odp.proc.ir.144.108.1993
Shipboard Scientific Party (1993e): Site 877. doi:10.2973/odp.proc.ir.144.109.1993
Shipboard Scientific Party (1993f): Site 867/868. doi:10.2973/odp.proc.ir.143.108.1993
Shipboard Scientific Party (1993g): Site 871. doi:10.2973/odp.proc.ir.144.104.1993
Shipboard Scientific Party (1994a): Site 914. doi:10.2973/odp.proc.ir.152.106.1994
Shipboard Scientific Party (1994b): Site 915. doi:10.2973/odp.proc.ir.152.107.1994
Shipboard Scientific Party (1994c): Site 916. doi:10.2973/odp.proc.ir.152.108.1994
Shipboard Scientific Party (1994d): Site 917. doi:10.2973/odp.proc.ir.152.109.1994
Shipboard Scientific Party (1994e): Site 918. doi:10.2973/odp.proc.ir.152.111.1994
Shipboard Scientific Party (1994f): Summary and Principal Results. doi:10.2973/odp.proc.ir.152.113.1994
Shipboard Scientific Party (1996a): Site 959. doi:10.2973/odp.proc.ir.159.105.1996
Shipboard Scientific Party (1996b): Site 967. doi:10.2973/odp.proc.ir.160.108.1996
Shipboard Scientific Party (1996c): Site 988. doi:10.2973/odp.proc.ir.163.103.1996
Shipboard Scientific Party (1996d): Site 989. doi:10.2973/odp.proc.ir.163.104.1996
Shipboard Scientific Party (1996e): Site 990. doi:10.2973/odp.proc.ir.163.105.1996
Shipboard Scientific Party (1996f): Site 969. doi:10.2973/odp.proc.ir.160.110.1996
Shipboard Scientific Party (1996g): Site 975. doi:10.2973/odp.proc.ir.161.105.1996
Shipboard Scientific Party (1997a): Site 1039. doi:10.2973/odp.proc.ir.170.103.1997

Shipboard Scientific Party (1997b): Site 1040. doi:10.2973/odp.proc.ir.170.104.1997
Shipboard Scientific Party (1997c): Introduction. doi:10.2973/odp.proc.ir.170.101.1997
Shipboard Scientific Party (1998a): Site 1065. doi:10.2973/odp.proc.ir.173.103.1998
Shipboard Scientific Party (1998b): Site 1069. doi:10.2973/odp.proc.ir.173.107.1998
Shipboard Scientific Party (1998c): Site 1068. doi:10.2973/odp.proc.ir.173.106.1998
Shipboard Scientific Party (1998d): Site 1070. doi:10.2973/odp.proc.ir.173.108.1998
Shipboard Scientific Party (1998e) Site 1067. doi:10.2973/odp.proc.ir.173.105.1998
Shipboard Scientific Party (1998f): Site 1087. doi:10.2973/odp.proc.ir.175. 115.1998
Shipboard Scientific Party (2000a): Site 1139. doi:10.2973/odp.proc.ir.183.107.2000
Shipboard Scientific Party (2000b): Site 1130. doi:10.2973/odp.proc.ir.182.108.2000
Shipboard Scientific Party (2000c): Site 1132. doi:10.2973/odp.proc.ir.182.110.2000
Shipboard Scientific Party (2000d): Site 1129. doi:10.2973/odp.proc.ir.182.107.2000
Shipboard Scientific Party (2000e): Site 1131. doi:10.2973/odp.proc.ir.182.109.2000
Shipboard Scientific Party (2000f): Site 1109. doi:10.2973/odp.proc.ir.180.106.2000
Shipboard Scientific Party (2000g): Site 1118. doi:10.2973/odp.proc.ir.180.112.2000
Shipboard Scientific Party (2000h): Site 1115. doi:10.2973/odp.proc.ir.180.105.2000
Shipboard Scientific Party (2001a): Site 1183. doi:10.2973/odp.proc.ir.192.103.2001
Shipboard Scientific Party (2001b): Site 1184. doi:10.2973/odp.proc.ir.192.104.2001
Shipboard Scientific Party (2001c): Site 1168. doi:10.2973/odp.proc.ir.189.103.2001
Shipboard Scientific Party (2001d): Site 1170. doi:10.2973/odp.proc.ir.189.105.2001
Shipboard Scientific Party (2001f): Leg 189 Summary. doi:10.2973/odp.proc.ir.189.101.2001
Shipboard Scientific Party (2001g): Site 1166. doi:10.2973/odp.proc.ir.188.104.2001
Shipboard Scientific Party (2002a): Site 1203. doi:10.2973/odp.proc.ir.197.103.2002
Shipboard Scientific Party (2002b): Site 1204. doi:10.2973/odp.proc.ir.197.104.2002
Shipboard Scientific Party (2002c): Site 1205. doi:10.2973/odp.proc.ir.197.105.2002
Shipboard Scientific Party (2002d): Site 1206. doi:10.2973/odp.proc.ir.197.106.2002
Shipboard Scientific Party (2002e): Site 1193. doi:10.2973/odp.proc.ir.194.104.2002
Shipboard Scientific Party (2002f): Site 1194. doi:10.2973/odp.proc.ir.194.105.2002
Shipboard Scientific Party (2002g): Site 1195. doi:10.2973/odp.proc.ir.194.106.2002
Shipboard Scientific Party (2002h): Sites 1196 and 1199. doi:10.2973/odp.proc.ir.194.107.2002
Shipboard Scientific Party (2002i): Leg 194 Summary. doi:10.2973/odp.proc.ir.194.101.2002
Shipboard Scientific Party (2003a) Site 1242. doi:10.2973/odp.proc.ir.202.113.2003
Shipboard Scientific Party (2003b): Site 1238. doi:10.2973/odp.proc.ir.202.109.2003
Shipboard Scientific Party (2003c): Site 1239. doi:10.2973/odp.proc.ir.202.110.2003
Shipboard Scientific Party (2004a): Site 1277. doi:10.2973/odp.proc.ir.210.104.2004
Shipboard Scientific Party (2004b): Site 1258. doi:10.2973/odp.proc.ir.207.105.2004
Shipboard Scientific Party (2004c): Site 1259. doi:10.2973/odp.proc.ir.207.106.2004
Shipboard Scientific Party (2004d): Site 1261. doi:10.2973/odp.proc.ir.207.108.2004
Shipboard Scientific Party (2004e): Leg 207 Summary. doi:10.2973/odp.proc.ir.207.101.2004
The Shipboard Scientific Party (1969a): Site 1. doi:10.2973/dsdp.proc.1.101.1969
The Shipboard Scientific Party (1969b): Site 2. doi:10.2973/dsdp.proc.1.102.1969

- The Shipboard Scientific Party (1970): Site 21. doi:10.2973/dsdp.proc.3.111.1970
- The Shipboard Scientific Party (1972): Sites 143 and 144. doi:10.2973/dsdp.proc.14.110.1972
- The Shipboard Scientific Party (1973a): Site 86. doi:10.2973/dsdp.proc.10.103.1973
- The Shipboard Scientific Party (1973b): Site 94. doi:10.2973/dsdp.proc.10.111.1973
- The Shipboard Scientific Party (1973c): Site 95. doi:10.2973/dsdp.proc.10.112.1973
- The Shipboard Scientific Party (1973d): Site 192. doi:10.2973/dsdp.proc.19.111.1973
- The Shipboard Scientific Party (1973e): Oolitic limestone on the Ita Maitai Guyot, Equatorial Pacific: DSDP Site 202. doi:10.2973/dsdp.proc.20.108.1973
- The Shipboard Scientific Party (1974a): Site 225. doi:10.2973/dsdp.proc.23.115.1974
- The Shipboard Scientific Party (1974b): Site 214. doi:10.2973/dsdp.proc.22.105.1974
- The Shipboard Scientific Party (1974c): Site 237. doi:10.2973/dsdp.proc.24.108.1974
- The Shipboard Scientific Party (1974d): Sites 246 and 247. doi:10.2973/dsdp.proc.25.108.1974
- The Shipboard Scientific Party (1974e): Site 227. doi:10.2973/dsdp.proc.23.117.1974
- The Shipboard Scientific Party (1975a): Site 264. doi:10.2973/dsdp.proc.28.102.1975
- The Shipboard Scientific Party (1975b): Site 289. doi:10.2973/dsdp.proc.30.107.1975
- The Shipboard Scientific Party (1975c): Site 308: Kōko Guyot. doi:10.2973/dsdp.proc.32.107.1975
- The Shipboard Scientific Party (1975d): Site 309: Kōko Guyot. doi:10.2973/dsdp.proc.32.108.1975
- The Shipboard Scientific Party (1975e): Site 296. doi:10.2973/dsdp.proc.31.107.1975
- The Shipboard Scientific Party (1975f): Site 277. doi:10.2973/dsdp.proc.29.104.1975
- The Shipboard Scientific Party (1976): Site 317. doi:10.2973/dsdp.proc.33.105. 1976
- The Shipboard Scientific Party (1977): Site 357: Rio Grande Rise. doi:10.2973/dsdp.proc.39.106.1977
- The Shipboard Scientific Party (1978a): Angola Continental Margin - Site 364 and 365. doi:10.2973/dsdp.proc.40.104.1978
- The Shipboard Scientific Party (1978b): Walvis Ridge - Sites 362 and 363. doi:10.2973/dsdp.proc.40.183.1978
- The Shipboard Scientific Party (1978c): Sites 375 and 376: Florence Rise. doi:10.2973/dsdp.proc.42-1.106.1978
- The Shipboard Scientific Party (1978d) Site 374; Messina Abyssal Plain. doi:10.2973/dsdp.proc.42-1.105.1978
- The Shipboard Scientific Party (1979): Site 384: The Cretaceous/Tertiary Boundary, Aptian Reefs, and the J-Anomaly Ridge. doi:10.2973/dsdp.proc.43.104.1979
- The Shipboard Scientific Party, M. Bourbon, D. N. Lumsden and D. Mann (1979): Site 401. doi:10.2973/dsdp.proc.48.104.1979
- The Shipboard Scientific Party and D. Burns (1973): Site 209. doi:10.2973/dsdp.proc.21.109.1973
- The Shipboard Scientific Party, D. Burns, W. A. Watters and P. N. Webb (1973): Site 207. doi:10.2973/dsdp.proc.21.107.1973
- The Shipboard Scientific Party and W. G. Deuser, M. H. Delevaux, and B. R. Doe (1974b) Site 228. doi:10.2973/dsdp.proc.23.118.1974
- The Shipboard Scientific Party and A. J. Erickson (1974): Site 262. doi:10.2973/dsdp.proc.27.105.1974
- The Shipboard Scientific Party, N. Hamilton, J. Hunziker and Paleontological Laboratories of the Geological Survey of India (1974a): Site 219. doi:10.2973/dsdp.proc.23.103.1974
- The Shipboard Scientific Party, W. K. Harris and W. V. Sliter (1977): Site 330. doi:10.2973/dsdp.proc.36.106.1977
- The Shipboard Scientific Party, R. Løvlie, S. B. Manum, H. Raschka, F.-J. Eckhardt and H.-J. Schrader (1976a): Sites 336 and 352. doi:10.2973/dsdp.proc.38.102.1976
- The Shipboard Scientific Party and D. Mann (1979): Site 402/Hole 402A. doi:10.2973/dsdp.proc.48.105.1979
- The Shipboard Scientific Party, S. B. Manum, H. Raschka, F.-J. Eckhardt and H.-J. Schrader (1976b): Sites 338-343. doi:10.2973/dsdp.proc.38.104.1976
- The Shipboard Scientific Party, S. B. Manum and H.-J. Schrader (1976c): Sites 346, 347 and 349,

doi:10.2973/dsdp.proc.38.108.1976

- The Shipboard Scientific Party, H. Nelson, P. A. Hacquebard, T. W. Bloxam, G. Kelling, N. P. James, J. C. Hopkin, S. A. J. Pocock, J. A. Jeletzky, E. A. Pessagno, Jr. and J. F. Longoria T (1972a): Site 111. doi:10.2973/dsdp.proc.12.103.1972
- The Shipboard Scientific Party and G. J. Wilson (1975): Site 281. doi:10.2973/dsdp.proc.29.108.1975
- Tsuchi and Kagami (1967): Discovery of nerineid gastropoda from seamount Susoev (Erimo) at the junction of Japan and Kuril-Kamchatka Trenches. *Rec. Ocean. Works Japan*, 9, 1-6.
- Udintsev, G. B. (1987): Topography and structure of the oceans. Nedra, Moscow, 239pp. (in Russian)
- Vail, P. R., R. M. Michum, Jr. and S. Thompson. III (1977): Global cycle of relative changes of sea level. 83-97, in Payton, C. E. ed., *Seismic Stratigraphy - Application to Hydrocarbon Exploration*, Amer. Assoc. Petrol. Geol. Mem., 26.
- Vasiliev, B. I. (2006): Geological structure and origin of the Pacific Ocean. *Earth Science*, 60, 185-196. (in Japanese)
- Vasiliev, B. I. (2009): Geological Structure and Origin of the Pacific Ocean. Dalnauka, Vladjvostok, 559pp. (in Russian)
- Winterer, E. L. and C. V. Metzler (1984): Origin and subsidence of Guyots in Mid-Pacific Mountain. *Jour. Geophysics. Res.*, 89, 9969-9979.
- Yano, T., A. A. Gavrilov, S. Miyagi and B. I. Vasiliev (2009): Ancient and continental rocks in Atlantic. *Earth Science*, 63, 119-140. (In Japanese with English abstract)
- Yano, T., B. I. Vasiliev, D. R. Choi, A. A. Gavrilov, S. Miyagi and H. Adachi (2011): Continental rocks from Indian Ocean floor - Significance of the continental rocks distributed in oceans -. *Earth Science*, 65, 199-215. (In Japanese with English abstract)
- Yano, T. (2021): Submerged continental mass at the bottom of the Atlantic Ocean - Rio Grande Rise. *Chigakukyoiku and Kagaku-undo*, (87), 37-46. (In Japanese)